A Reference Equation of State for Heavy Water

Stefan Herrig and Monika Thol

Lehrstuhl für Thermodynamik, Ruhr-Universität Bochum, Universitätsstraße 150, 44801 Bochum, Germany

Allan H. Harvey[a] and Eric W. Lemmon[b]

Applied Chemicals and Materials Division, National Institute of Standards and Technology, 325 Broadway, Boulder, Colorado 80305, USA

(Received 28 August 2018; accepted 2 October 2018; published online 3 December 2018)

An empirical fundamental equation of state (EOS) is presented for fluid heavy water (deuterium oxide, D_2O). The equation is explicit in the reduced Helmholtz energy and allows the calculation of all thermodynamic properties over the whole fluid surface. It is valid from the melting-pressure curve up to a temperature of 825 K at pressures up to 1200 MPa. Overall, the formulation represents the most accurate measured values and almost all other available data within their experimental uncertainty. In the homogeneous liquid and vapor phase, the expanded relative uncertainties of densities calculated from the EOS are mostly 0.1% or less; liquid-phase densities at atmospheric pressure can be calculated with an uncertainty of 0.01%. The speed of sound in the liquid phase is described with a maximum uncertainty of 0.1%; the most accurate experimental sound speeds are represented within their uncertainties ranging from 0.015% to 0.02%. In a large part of the liquid region, the isobaric heat capacity is represented with an uncertainty of 1%. The uncertainty in vapor pressure is mostly within 0.05%. In the critical region, the uncertainties of calculated properties are in most cases higher than the values above, but the EOS enables a reasonable description of this region. The equation matches available data for the metastable subcooled liquid, and it extrapolates in a qualitatively correct way to extreme values of temperature and pressure. This formulation is the result of an effort to establish a new standard for the thermodynamic properties of heavy water by the International Association for the Properties of Water and Steam. https://doi.org/10.1063/1.5053993

Key words: D_2O; deuterium oxide; equation of state; fundamental equation; heavy water; thermodynamic properties.

CONTENTS

[a]Electronic mail: allan.harvey@nist.gov.
[b]Electronic mail: eric.lemmon@nist.gov.

List of Tables

List of Figures

1. Introduction

Heavy water or deuterium oxide (D_2O, CAS no. 7789-20-0) is a liquid at ambient conditions. It is not radioactive and, if not taken in unreasonably large amounts, nontoxic. It differs from ordinary, light water in its hydrogen isotopes. The heavy water molecule contains two deuterium atoms instead of two ordinary hydrogen atoms. The nucleus of ordinary hydrogen, also called "protium" (^{1}H), consists of only one proton. The isotope deuterium (^{2}H, D) has one additional neutron. As a result, the molecular mass of heavy water is higher than that of ordinary water by a factor of roughly 20/18. The resulting higher density is vividly presented in Fig. 1, which shows a photograph of heavy-water ice cubes that sink in ordinary water due to their higher density, whereas the ordinary-water ice cubes float due to the well-known expansion of water upon freezing.

Heavy water should not be confused with other heavier forms of water such as "super-heavy water" (tritium oxide, T_2O) containing the hydrogen isotope tritium (^{3}H, T), "semi-heavy water" (deuterium hydrogen oxide, HDO), or "heavy-oxygen water" ($H_2{}^{17}O$ or $H_2{}^{18}O$) enriched in heavier oxygen isotopes. The equation of state (EOS) presented here was developed to describe the properties of deuterium oxide with the oxygen isotopes ^{16}O, ^{17}O, and ^{18}O in the standard proportions as defined by "Vienna Standard Mean Ocean Water" (V-SMOW), discussed by Kell,[1] and adopted by the International Association for the Properties of Water and Steam (IAPWS).[2] These standard (molar) proportions are $x_{16O} = 0.997\,620\,6$, $x_{17O} = 0.000\,379$, and $x_{18O} = 0.002\,000\,4$. However, experimentally investigated samples of heavy water never contain 100% D_2O but are contaminated by a varying amount of H_2O and HDO. Since the EOS was fitted to

FIG. 1. Ice cubes made from heavy and ordinary water in ordinary liquid water. Photo courtesy of Christopher Tietz, Ruhr-Universität Bochum.

experimental data, the D_2O content of the samples investigated within the corresponding references was considered in order to estimate the experimental uncertainty of the data.

In 1932, Urey *et al.*[3] were the first to prove the existence of deuterium and thus of heavy water. Soon after this discovery, heavy water became a target for many nuclear physicists and played an important role in the first research on nuclear fission. It was therefore regarded as a compound of high commercial and military potential. Consequently, interest in the production of D_2O increased significantly during World War II. A summary of the interesting history of this almost mystical substance is given within the essay of Waltham.[4]

Over the past decades, D_2O has mostly been used as a neutron moderator in nuclear reactors. It slows free neutrons down to thermal energies, which is necessary for a self-sustaining chain reaction. The process of moderation can also be done with light water, but due to the additional neutrons in its hydrogen atoms, heavy water absorbs significantly fewer free neutrons.[5] Nowadays, the interest in heavy water is as much scientific as commercial. In biological and medical research, heavy water is used in the ''doubly labeled water method'' to measure the average daily metabolic rate of an organism.[6,7] Another application is ''boron neutron capture therapy'' for the treatment of brain tumors, in which the ability of heavy water to moderate neutrons is useful (see, for instance, the work of Fairchild *et al.*[8]).

The equilibrium geometry of the D_2O molecule is almost identical to that of H_2O.[9] While normally isotopic substitution has little effect on the thermal properties of fluids, this is not the case when hydrogen bonding is important. Quantum delocalization has a net weakening effect on water's hydrogen bonds,[10] so the heavier deuterium atoms make the hydrogen bonding stronger in D_2O than in H_2O. The effect is large enough that a separate EOS for D_2O must be developed, rather than a small perturbation to the H_2O EOS. The differences in thermodynamic behavior between H_2O and D_2O as quantified by their EOS therefore provide useful insights into quantum effects and hydrogen bonding.

The previous reference EOS for the thermodynamic properties of D_2O was published in 1982 by Hill *et al.*[11] and became a standard of the International Association for the Properties of Steam (IAPS, now IAPWS) in 1984. This formulation was later adjusted to the International Temperature Scale of 1990 (ITS-90)[12] as discussed in the corresponding Release of IAPWS.[13] It is explicit in the specific Helmholtz energy with temperature T and density ρ as independent variables. The equation is valid from the triple-point temperature up to 800 K and for pressures up to 100 MPa. The equation is not recommended for calculations in the critical region bordered by $|T - T_c| \leq 10$ K and $|\rho/\rho_c - 1| \leq 0.3$, with the critical temperature T_c and critical density ρ_c. For calculations within this region, IAPWS[13] refers to the much more complex crossover EOS by Kostrowicka Wyczalkowska *et al.*,[14] which is only valid in a small region around the critical point and is therefore not discussed in this article. In comparison to modern EOS for other fluids, the formulation by Hill *et al.*[11] has a quite long functional form with a total of 50 terms. This relatively complex mathematical structure frequently leads to numerical problems. Due to both the great advances in the development of EOS and modern computer technology, it is now possible to develop equations with a reduced number of terms without loss of accuracy. Based on these factors, IAPWS initiated the development of a new EOS for heavy water in 2013, although at that point new experimental data since the publication of Hill *et al.* were relatively few. During the development of the EOS, additional accurate data were contributed by various groups associated with IAPWS. Thus, the new formulation is based on the most up-to-date thermodynamic database. A preliminary version of this formulation was adopted as an IAPWS Release in 2017,[15] and a Revised Release based on the formulation presented in this paper is expected to be adopted by IAPWS in 2018.

2. Physical Constants and Characteristic Properties

An overview of the most important physical constants and characteristic properties of D_2O as relevant for the EOS presented here is given in Table 1. Aside from the information taken from literature references, Table 1 contains values determined from the new equation.

In the development of an EOS, the critical temperature and density are essential thermodynamic properties. With regard to the structure of modern equations, the reason for this is obvious. Most of these formulations are explicit in the reduced Helmholtz energy with the critical temperature and density as the reducing parameters of the independent variables. However, measurements of the critical point are difficult and thus rare and with wide variation between sources. The experimental determination of the critical density poses a special challenge because of the extreme sensitivity of density to changes in temperature and pressure near the critical point. For the critical point of heavy water, only four references are available and only two of them include information about the critical density. The available critical parameters are listed in Table 2. All temperature values were converted to ITS-90. The critical temperature and density used to develop the new EOS are recommended in the IAPWS Release on the critical values of ordinary and heavy water.[17] The critical temperature in Ref. 17 corresponds to the measurement of Blank[19] converted to ITS-90. The critical pressure and density were obtained numerically by Levelt Sengers *et al.*[20] by a scaled analysis of $p\rho T$ data measured by Rivkin and Akhundov.[21] The recommended critical parameters and their corresponding uncertainties (reflecting the correlation between errors in critical temperature and critical pressure) are $T_{c,IAPWS}/K = 643.847 + \delta$ with $\delta = 0.000 \pm 0.200$, $p_{c,IAPWS}/MPa = 21.671 + 0.27\delta \pm 0.01$, and $\rho_{c,IAPWS}/(kg\ m^{-3}) = 356 \pm 5$ or $\rho_{c,IAPWS}/(mol\ dm^{-3}) = 17.775\ 55 \pm 0.25$ on a molar basis. We note that the critical pressure recommended by IAPWS slightly differs (by 0.0092 MPa) from the value obtained from the new EOS as given in Table 1. However, this deviation is within the uncertainty of the IAPWS value, which is 0.01 MPa at the chosen critical temperature.

TABLE 1. Physical constants and characteristic properties of heavy water (D_2O)

Quantity	Symbol	Value	Reference
Molar gas constant	R	8.314 459 8 J mol^{-1} K^{-1}	Mohr *et al.*[16]
Molar mass	M	20.027 508 g mol^{-1}	IAPWS[2]
Critical temperature	T_c	643.847 K	IAPWS[17]
Critical pressure	p_c	21.6618 MPa	This work
Critical density	ρ_c	17.775 55 mol dm^{-3}	IAPWS[17]
Triple-point temperature	T_{tp}	276.969 K	Markó *et al.*[18]
Triple-point pressure	p_{tp}	0.661 59 kPa	This work
Vapor density at triple point	ρ_{tpv}	0.000 287 mol dm^{-3}	This work
Liquid density at triple point	ρ_{tpl}	55.188 mol dm^{-3}	This work
Normal-boiling-point temperature	T_{nbp}	374.549 K	This work
Vapor density at the normal boiling point	ρ_{nbpv}	0.033 043 mol dm^{-3}	This work
Liquid density at the normal boiling point	ρ_{nbpl}	53.039 mol dm^{-3}	This work
Maximum density temperature at atmospheric pressure	$T_{\rho max,atm}$	284.748 K	This work
Maximum density at atmospheric pressure	$\rho_{max,atm}$	55.221 mol dm^{-3}	This work
Acentric factor	ω	0.364	This work

TABLE 2. Critical and triple-point parameters of D_2O. See Table 1 for the values from this work

Reference	Year	Temperature T (K)	Pressure p (MPa)	Density ρ (mol dm^{-3})
		Triple-point parameters		
Bartholomé and Clusius[24 a]	1935	276.967	0.000 674 6	...
Jones[23]	1952	276.957	...	...
Markó *et al.*[18]	1989	276.969	0.000 659 3	...
		Critical-point parameters		
Riesenfeld and Chang[25]	1935	644.684	22.150	18.125 07
Eck[26]	1939	644.684	21.722	18.223 11
Oliver and Grisard[27]	1956	644.084	21.856	...
Blank[19]	1969	643.847	21.659	...
IAPWS[17 b]	1992	643.847	21.671	17.775 55

[a]Reference 24 presents triple-point parameters without describing a triple-point experiment or giving a reference for these values. Nevertheless, it is included here since no earlier reference for the triple-point parameters was found.
[b]Recommended critical point parameters: Critical temperature taken from the work of Blank[19] and critical pressure and density determined from the $p\rho T$ measurements of Rivkin and Akhundov.[21]

Equations of state as presented here cannot be used to calculate the properties of solid phases. Thus, separate knowledge of the melting and sublimation curves is needed to set the lower temperature limit of the range of validity of such formulations. For (heavy) water, the triple point is not the lowest temperature at which the substance remains liquid due to the anomalous shape of its melting curve, which exhibits a negative initial slope (dp/dT). Nevertheless, the triple-point parameters are important natural constants, which are known extremely accurately for ordinary water[22] but less satisfactorily for heavy water. Although triple-point parameters of D_2O can be found in a number of publications, almost all of these studies obtained the triple-point pressure by extrapolating vapor-pressure data measured at higher temperatures down to a given triple-point temperature. Furthermore, the triple point is frequently equated with the melting point at atmospheric pressure. Only Jones[23] and Markó *et al.*[18] carried out ''real'' triple-point experiments. The data from these studies are given in Table 2 with temperatures converted to ITS-90. In addition to these references, the data of Bartholomé and Clusius[24] are included in Table 2. This reference is given since no earlier work providing triple-point parameters of heavy water was found. However, the authors do not describe a direct experimental investigation of the triple point; thus, the source of the given values is unclear. For the development of the new EOS, the most recent value for the triple-point temperature by Markó *et al.*[18] was adopted. The triple-point pressure given in Table 1 was calculated at this temperature from the final EOS, since the pressure reported by Markó *et al.*[18] deviates by about 0.35% from the most accurate vapor-pressure data at slightly higher temperatures.

3. Auxiliary Equations for Phase-Equilibrium Calculations

Within the scope of this work, auxiliary equations for the vapor pressure, the saturated-liquid and saturated-vapor densities, the melting pressure, and the sublimation pressure were developed. The first three equations can be used to quickly obtain good estimates for the thermal properties along the phase boundaries of the vapor–liquid equilibrium region. However, the results calculated from these correlations are not identical to the saturation properties obtained from our reference EOS. In order to determine such reference-quality properties, iterations based on the Maxwell criterion are

required. Fulfilling this criterion ensures that at any fixed temperature bubble- and dew-point pressures as well as the Gibbs energies of both coexisting phases are equal. Since accurate saturation properties are obtained by this iterative procedure, auxiliary equations for the saturated liquid and vapor are not necessarily needed but provide excellent starting values for phase-equilibrium calculations in typical engineering applications such as process simulations. With the purpose of achieving high consistency between the reference equation and the corresponding auxiliary equations, the latter were fitted to values calculated at 1 K intervals from our EOS between 238 K (which corresponds to an extrapolation far below the triple point) and the critical point.

As discussed in Sec. 2, the lower temperature limit of the EOS is not defined by the triple-point temperature, but by the lowest temperature along the melting curve. Additional auxiliary equations for the melting pressure of the relevant ice structures of heavy water were developed. The description of fluid-solid boundaries is completed by an auxiliary equation for the sublimation pressure. The correlations for the solid–fluid equilibria were fitted to experimental results available in the literature. The complete phase diagram, as calculated with the new EOS and the auxiliary equations for the melting and sublimation curves, is presented in Fig. 2.

3.1. Vapor-pressure equation

The auxiliary equation for the vapor pressure p_v is given by

$$\ln\left(\frac{p_v}{p_c}\right)=\frac{T_c}{T}\left(n_1\theta+n_2\theta^{1.5}+n_3\theta^{2.44}+n_4\theta^{5.3}+n_5\theta^{14}+n_6\theta^{20}\right), \tag{1}$$

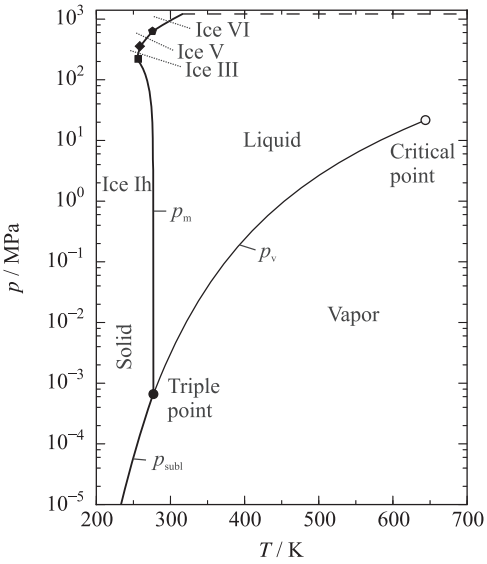

FIG. 2. The phase-boundary curves of heavy water in a p, T diagram. The vapor-pressure curve p_v is calculated with the EOS. The sublimation- and melting-pressure curves p_{subl} and p_m are obtained from the corresponding auxiliary equations. The dashed line indicates the upper pressure limit of the EOS. The sublimation curves and the melting curves define the lower temperature limit of the range of validity.

with $\theta=(1-T/T_c)$ and the coefficients n_1–n_6 as given in Table 3. The critical parameters are discussed in Sec. 2 and listed in Table 1. The first two temperature exponents were not included in the fitting process but set to 1 and 1.5, respectively. In addition, the coefficient n_1 was kept negative and n_2 positive. A detailed explanation of these constraints for the first two exponents and coefficients is given by Lemmon and Goodwin.[28] Deviations between the calculated values from Eq. (1) and values obtained from the reference EOS by means of the Maxwell criterion are below 0.01% over the entire temperature range. However, these deviations (and the ones given for the auxiliary equations for the saturated-liquid and -vapor density) must not be equated with uncertainties of saturation properties calculated from our EOS, which are discussed in Sec. 5.1. For checking computer implementations, at 293.15 K Eq. (1) gives a vapor pressure of $0.199\,914\,326\times10^{-2}$ MPa.

3.2. Saturated-liquid density equation

The saturated-liquid density equation is

$$\frac{\rho'}{\rho_c}=1+n_1\theta^{0.29}+n_2\theta^{1}+n_3\theta^{1.3}+n_4\theta^{1.77}+n_5\theta^{2.5}+n_6\theta^{16}, \tag{2}$$

with the saturated density ρ' and the critical density ρ_c as given in Table 1. The coefficients n_1–n_6 are given in Table 3. In order to ensure the correct behavior of the correlation and its derivatives at the critical point, the first temperature exponent must be between zero and one, with a positive coefficient n_1.[29,30] The calculated values from Eq. (2) deviate from the results obtained from our EOS by less than 0.03% at temperatures up to 641 K. In the vicinity of the critical point, deviations increase to a maximum of 0.06%. For checking computer implementations, at 293.15 K Eq. (2) gives a saturated-liquid density of $0.551\,959\,089\times10^{2}$ mol dm^{-3}.

3.3. Saturated-vapor density equation

For the saturated-vapor density ρ'', the auxiliary equation reads

$$\ln\left(\frac{\rho''}{\rho_c}\right)=n_1\theta^{0.33}+n_2\theta^{1.29}+n_3\theta^{1.68}+n_4\theta^{2.09}+n_5\theta^{6.1}+n_6\theta^{17}, \tag{3}$$

TABLE 3. Coefficients of the auxiliary equations for the vapor pressure p_v, the saturated-liquid density ρ', and the saturated-vapor density ρ'' as given by Eqs. (1)–(3)

Coefficient	p_v [Eq. (1)]	ρ' [Eq. (2)]	ρ'' [Eq. (3)]
n_1	$-0.794\,440\times10^{1}$	$0.166\,200\times10^{1}$	$-0.247\,140\times10^{1}$
n_2	$0.194\,340\times10^{1}$	$0.901\,130\times10^{1}$	$-0.266\,744\times10^{2}$
n_3	$-0.243\,530\times10^{1}$	$-0.154\,210\times10^{2}$	$0.531\,080\times10^{2}$
n_4	$-0.342\,000\times10^{1}$	$0.115\,760\times10^{2}$	$-0.480\,150\times10^{2}$
n_5	$0.355\,000\times10^{2}$	$-0.516\,940\times10^{1}$	$-0.576\,230\times10^{2}$
n_6	$-0.302\,000\times10^{3}$	$-0.236\,240\times10^{3}$	$-0.371\,720\times10^{3}$

with the coefficients n_1–n_6 as listed in Table 3. In fitting Eq. (3), the first temperature exponent was kept between zero and one with a negative coefficient n_1, ensuring a correct description of the critical region.[29] Deviations between calculated values from Eq. (3) and our EOS are below 0.03% at temperatures up to 590 K. The deviations increase at higher temperatures with a maximum of 0.07% in the vicinity of the critical point. For checking computer implementations, at 293.15 K Eq. (3) gives a saturated-vapor density of $0.821\,136\,767 \times 10^{-3}$ mol dm^{-3}.

3.4. Melting-pressure equations

Solid water forms different crystalline structures depending on the temperature and pressure. For ordinary water, five ice structures are known that are bordered by the liquid phase (ice Ih, III, V, VI, VII). The corresponding melting-pressure curves are limited by triple points, in which two ice structures and the liquid phase are in thermodynamic equilibrium. An exception to this is the lower pressure limit of the melting curve of ice Ih, which is the ''normal'' solid–vapor–liquid triple point. The five ice structures are described by equations that were developed by Wagner *et al.*[31] and also included in the IAPWS-95 publication by Wagner and Pruß.[32] The correlation for ice Ih was later updated by Wagner *et al.*[33] For heavy water, the same ice structures are believed to exist, although to our knowledge the high-pressure structure VII has not been experimentally observed. We adopted the structures of the original correlations and refitted them to the available experimental melting-pressure data by Bridgman[34] (for ice structures Ih, III, V, and VI) and Henderson and Speedy[35] (only for ice structure Ih). The triple-point data required to define the range of validity for each ice-structure correlation were taken from the work of Bridgman[34] for the solid-solid-liquid triple points and from Table 1 for the ''normal'' triple point. All applied triple-point parameters of the different ice structures are listed in Table 4. Since no data are available along the ice-VII melting curve, it was ensured that the equation for ice VI yields reasonable results up to the upper pressure limit of the new EOS, $p_{max} = 1200$ MPa. All experimental pressure values of Bridgman[34] were multiplied by a correction factor of 1.0102. This factor corresponds to the ratio between the melting pressure of mercury at 0 °C obtained by Bridgman[36] (749.2 MPa), which was used to calibrate the apparatus for his light and heavy water melting-pressure measurements, and the reference value reported by Molinar *et al.*[37] (756.84 MPa).

TABLE 4. Triple-point parameters limiting the melting-pressure correlations for the different ice structures of heavy water

Reference	T_{tp} (K)	p_{tp} (MPa)	Coexisting phases
Table 1	276.969	0.000 661 59	ice Ih-V-L
Bridgman[34 a]	254.415	222.41	ice Ih-ice III-L
Bridgman[34 a]	258.661	352.19	ice III-ice V-L
Bridgman[34 a]	275.748	634.53	ice V-ice VI-L

[a]All pressures reported by Bridgman[34] were multiplied by 1.0102, since the apparatus used was calibrated by means of an obsolete melting pressure of mercury at 0 °C.

The four melting-pressure equations developed within this work are as follows:

The melting-pressure equation for ice Ih (temperature range from 276.969 K *to 254.415* K*) is*

$$\frac{p_{m,\text{ice Ih}}}{p_n} = 1 - 0.301\,53 \times 10^5\left(1-\theta^{5.5}\right) + 0.692\,503 \times 10^6\left(1-\theta^{8.2}\right), \quad (4)$$

with reduced temperature $\theta = T/T_n$ and the reducing parameters $T_n = 276.969$ K and $p_n = 0.000\,661\,59$ MPa. For checking computer implementations, at 270 K Eq. (4) gives a melting pressure of $0.837\,888\,413 \times 10^2$ MPa.

The melting-pressure equation for ice III (temperature range from 254.415 K *to 258.661* K*) is*

$$\frac{p_{m,\text{ice III}}}{p_n} = 1 - 0.802\,871\left(1-\theta^{33}\right), \quad (5)$$

with $\theta = T/T_n$, $T_n = 254.415$ K, and $p_n = 222.41$ MPa. For checking computer implementations, at 255 K Eq. (5) gives a melting pressure of $0.236\,470\,168 \times 10^3$ MPa.

The melting-pressure equation for ice V (temperature range from 258.661 K *to 275.748* K*) is*

$$\frac{p_{m,\text{ice V}}}{p_n} = 1 - 0.128\,038\,8 \times 10^1\left(1-\theta^{7.6}\right), \quad (6)$$

with $\theta = T/T_n$, $T_n = 258.661$ K, and $p_n = 352.19$ MPa. For checking computer implementations, at 275 K Eq. (6) gives a melting pressure of $0.619\,526\,971 \times 10^3$ MPa.

The melting-pressure equation for ice VI (temperature range from 275.748 K *to 315* K*) is*

$$\frac{p_{m,\text{ice VI}}}{p_n} = 1 - 0.127\,602\,6 \times 10^1\left(1-\theta^{4}\right), \quad (7)$$

with $\theta = T/T_n$, $T_n = 275.748$ K, and $p_n = 634.53$ MPa. For checking computer implementations, at 300 K Eq. (7) gives a melting pressure of $0.959\,203\,594 \times 10^3$ MPa.

Comparisons between the melting-pressure curves calculated from our correlations and the available experimental data are shown in Fig. 3. Especially for the ice structures III, V, and VI, the correlations are in very close agreement with the experimental data; the deviations are clearly below 1%. However, these low deviations are less meaningful because the correlations were exclusively fitted to the only available data by Bridgman.[34] Since these data are relatively self-consistent, quite low deviations can be achieved when fitting the correlations to these values. The melting-pressure equations for ordinary water of Wagner *et al.*[31] were also mainly fitted to Bridgman's data. The estimated uncertainty of melting pressures calculated from these equations is stated to be 3% for the ice structures III, V, and VI. Due to the comparable database and the same basic mathematical structure, this uncertainty estimate can reasonably be adopted for our melting-pressure equations for heavy water. Thus, the estimated uncertainty of melting pressures calculated from Eqs. (5)–(7) is 3%.

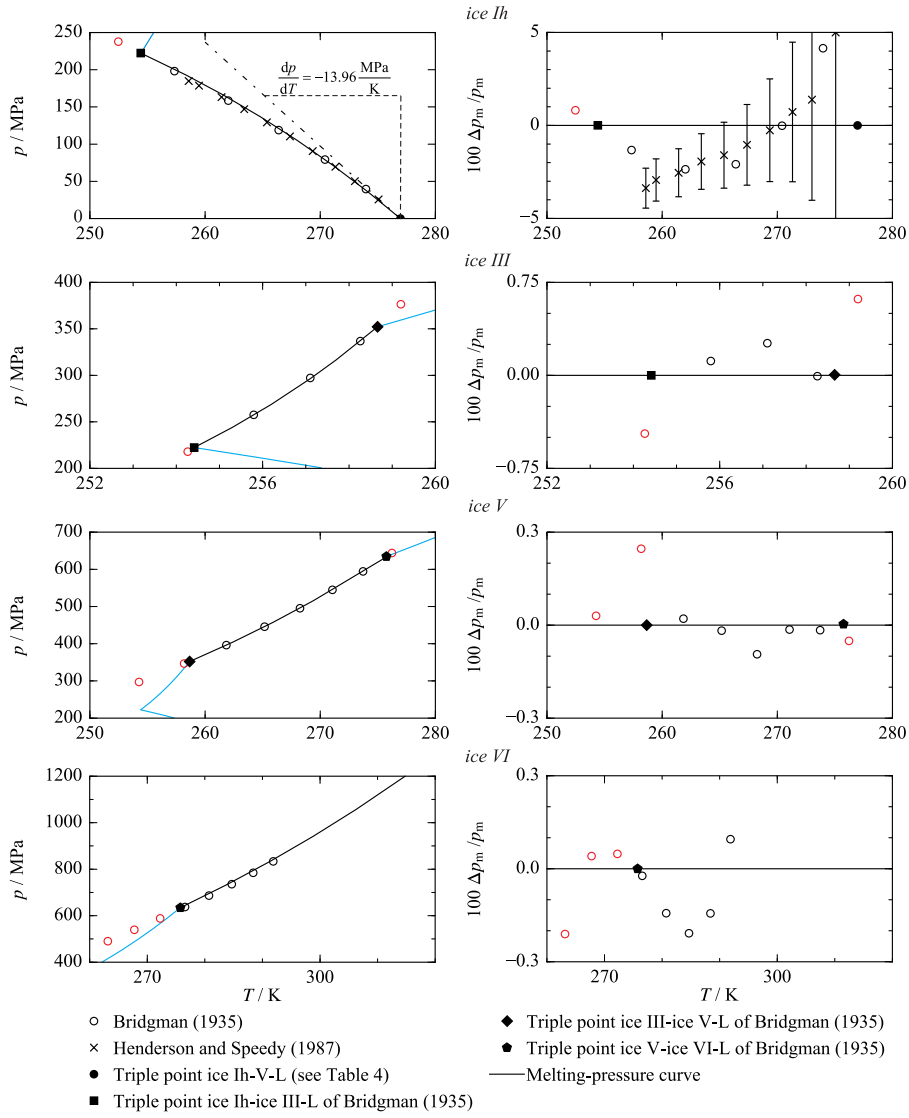

FIG. 3. Left: Melting-pressure curves of the different ice structures of heavy water in p, T diagrams. The curves are calculated from Eqs. (4)–(7). The lines shown in blue represent the melting-pressure curves of adjacent ice structures. The available experimental data including the triple points are shown for comparison. Right: Relative deviations $\Delta p_m/p_m = (p_{m,exp} - p_{m,calc})/p_{m,exp}$ of experimental melting-pressure data from the new correlations versus temperature. Metastable melting points from the work of Bridgman[34] above and/or below the triple points of the corresponding ice structure are shown in red.

Deviations between the experimental data and calculated melting pressures for ice Ih are considerably higher than those for the other ice structures. Two datasets are available for ice Ih, namely, the already discussed data by Bridgman[34] and also the data of Henderson and Speedy.[35] The authors of Ref. 35 state an uncertainty of 0.1 K in temperature and 0.5 MPa in pressure. Considering these uncertainties, the total combined expanded ($k = 2$) uncertainties in melting pressure range from approximately 1% at 258.6 K to 11% at 275.1 K, where uncertainties are higher due to the steep slope of the melting-pressure curve. The correlation describes the data within their uncertainty for temperatures above 265 K. For lower temperatures, the calculated melting curve represents a compromise between the best possible description of the datasets by Henderson and Speedy[35] and Bridgman.[34] Although the latter data are less accurate, they were used to fit the correlation in order to achieve a low deviation from the ice Ih-ice III-L triple point. An accurate description of this state point is necessary to ensure a continuously consistent description along the ice-Ih and ice-III melting curve. Attempts to fit the complete dataset of Henderson and Speedy[35] together with the upper triple point led to unreasonable changes in curvature along the saturation curve. Thus, the correlation was fitted to a carefully weighted selection of data points from both references. Additionally, the curvature and third derivative (d^3p_m/dT^3) were carefully constrained to avoid any unreasonable shape of the melting-pressure curve. The calculated initial slope of the melting curve at the ''normal'' solid–vapor–liquid triple point is -13.96 MPa K^{-1}. As a reliability check, this slope is compared to the result of the Clapeyron equation

$$\frac{dp_m}{dT} = \frac{\Delta h_m}{T(v_L - v_S)}, \tag{8}$$

with the enthalpy of fusion Δh_m and the liquid-solid volume change $(v_L - v_S)$. Considering the experimental results of

Long and Kemp[38] for $\Delta h_m = 1501$ cal mol^{-1} = 6280.2 J mol^{-1} and of Timmermans *et al.*[39] for $(v_L - v_S) = -1.62$ cm^3 mol^{-1}, Eq. (8) yields a slope of -13.96 MPa K^{-1} at $T = T_{tp}$ = 276.969 K. Thus, the initial slope calculated from the new melting-pressure equation is in perfect agreement with the result of the Clapeyron equation. With regard to the representation of the data of Henderson and Speedy,[35] the uncertainty of melting pressures of ice Ih calculated from Eq. (4) is conservatively estimated to be 4%.

3.5. Sublimation-pressure equation

To complete the description of the phase equilibria of heavy water, an auxiliary equation for the sublimation pressure of ice Ih is presented. The equation uses the structure of the correlation for ordinary water ice Ih as given in the work of Wagner *et al.*[31] and Wagner and Pruß.[32] The parameters were fitted to sublimation pressures obtained by Pupezin *et al.*[40] and Bottomley.[41] The data of Pupezin *et al.*[40] range from the triple-point temperature down to about 210 K, whereas Bottomley's measurements do not cover temperatures below 261 K. Thus, the lower temperature limit of the equation is defined only by the dataset of Pupezin *et al.*[40] The pressure and temperature are reduced by the "normal" triple-point parameters discussed in Sec. 2.

The sublimation-pressure equation for ice Ih (temperature range from 210 K *to 276.969* K*) is*

$$\ln\left(\frac{p_{sub}}{p_n}\right) = -0.131\,422\,6\times10^2\left(1-\theta^{-1.73}\right) + 0.321\,296\,9\times10^2\left(1-\theta^{-1.42}\right), \qquad (9)$$

with $\theta = T/T_n$, $T_n = 276.969$ K, and $p_n = 0.000\,661\,59$ MPa. For checking computer implementations, at 245 K Eq. (9) gives a sublimation pressure of $0.327\,390\,934\times10^{-4}$ MPa.

Comparisons between sublimation pressures calculated from Eq. (9) and the experimental data are shown in Fig. 4. For the sake of completeness, the data of Niwa and Shimazaki[42] are shown in addition to the datasets mentioned above, although they comprise only three data points of lower accuracy. Within the deviation plot in the bottom panel (as in all other deviation plots in this article), data points shown at the upper or lower vertical limits of the diagram indicate that the points are off scale.

At temperatures above 255 K, the data of Pupezin *et al.*[40] and Bottomley[41] are in agreement and are represented within 0.5% in sublimation pressure. At lower temperatures, where the sublimation pressures become quite low ($p_{sub} \le 10^{-4}$ MPa), the data exhibit significantly more scatter. Most of the data between 210 K and 255 K are described within 5%. The experimental uncertainty of the data of Bottomley[41] is not stated clearly and is difficult to estimate since the publication presents differences between the sublimation pressure and the vapor pressure of the metastable subcooled liquid. The data were calculated with vapor pressures obtained from our EOS extrapolated below the triple-point temperature. The experimental setup applied to measure the data of Pupezin *et al.*[40]

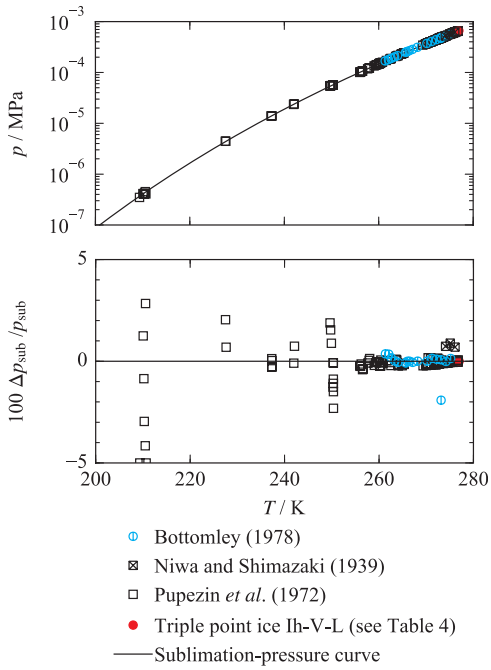

FIG. 4. Top: Sublimation-pressure curve of heavy water as calculated from Eq. (9). The available experimental data are shown for comparison. Bottom: Relative deviations $\Delta p_{sub}/p_{sub} = (p_{sub,exp} - p_{sub,calc})/p_{sub,exp}$ of experimental sublimation-pressure data from Eq. (9) versus temperature.

was presented by Jancsó *et al.*[43] together with experimental results for the sublimation pressure of ordinary water. These results deviate from the most accurate sublimation-pressure equation of Wagner *et al.*[33] (IAPWS standard correlation for the sublimation pressure of ordinary water[44]) by up to 0.5% at temperatures above 250 K. At lower temperatures, the deviations increase significantly to more than 10% at about 200 K. In this temperature range, the uncertainty of the sublimation-pressure equation for ordinary water is below 0.5%.[33,44] Thus, the experimental uncertainty of the data for D_2O of Pupezin *et al.*[40] can be reasonably estimated based on the deviations between the data for H_2O of Jancsó *et al.*[43] and the reference correlation by Wagner *et al.*[33] Considering these deviations, the estimated expanded ($k = 2$) uncertainties of sublimation pressures of D_2O calculated from Eq. (9) are 0.5% at temperatures above 255 K, 5% at $225 \le T/K \le 255$, and 10% at $210 \le T/K < 225$. Qualitative comparisons with the equation for H_2O show that Eq. (9) can be reasonably extrapolated down to temperatures of 150 K or lower.

4. Equation of State

The equation developed in this work is a fundamental EOS explicit in the Helmholtz energy as a function of density and temperature. A fundamental EOS enables calculations of all thermodynamic properties by combining derivatives of its functional form. Formulating the equation explicitly in the Helmholtz energy with the independent variables temperature and density yields the additional advantage of a clear description over the whole fluid surface, including the vapor–liquid equilibrium region. Thus, most modern

reference EOS were developed with the same basic mathematical structure as presented in this section. Excellent examples are the equations for R-125 of Lemmon and Jacobsen,[45] for propane of Lemmon *et al.*,[29] for R-1234ze(E) of Thol and Lemmon,[46] and for sulfur dioxide of Gao *et al.*[30]

In general, EOS in terms of the Helmholtz energy a can be formulated as

$$a(T,\rho) = a^{\mathrm{o}}(T,\rho) + a^{\mathrm{r}}(T,\rho). \tag{10}$$

The function a^{o} describes the behavior of the hypothetical ideal gas, whereas a^{r} represents the residual Helmholtz energy that results from molecular interactions in the real fluid. Since it is more convenient to work with dimensionless equations, density and temperature are reduced by their values at the critical point and the form of the resulting dimensionless function is

$$\alpha(\tau,\delta) = \frac{a(T,\rho)}{RT} = \frac{a^{\mathrm{o}}(T,\rho) + a^{\mathrm{r}}(T,\rho)}{RT} = \alpha^{\mathrm{o}}(\tau,\delta) + \alpha^{\mathrm{r}}(\tau,\delta), \tag{11}$$

where α is the reduced Helmholtz energy and R is the molar gas constant as given in Table 1. The reciprocal reduced temperature is $\tau = T_{\mathrm{c}}/T$, and the reduced density is $\delta = \rho/\rho_{\mathrm{c}}$. For D_2O, the critical-point parameters are given in Table 1.

4.1. Properties of the ideal gas

The ideal-gas part of the reduced Helmholtz energy can be written as

$$\alpha^{\mathrm{o}}(\tau,\delta) = \frac{a^{\mathrm{o}}(T,\rho)}{RT} = \frac{h_0^{\mathrm{o}}}{RT} - \frac{s_0^{\mathrm{o}}}{R} - 1 + \ln\frac{\delta\tau_0}{\delta_0\tau} - \frac{\tau}{R}\int_{\tau_0}^{\tau}\frac{c_p^{\mathrm{o}}}{\tau^2}\mathrm{d}\tau + \frac{1}{R}\int_{\tau_0}^{\tau}\frac{c_p^{\mathrm{o}}}{\tau}\mathrm{d}\tau, \tag{12}$$

where c_p^{o} is the isobaric heat capacity of the ideal gas and τ_0 and δ_0 are the reduced reciprocal temperature and reduced density at any arbitrary reference state defined by T_0 and ρ_0. For heavy water, this reference state was chosen following the conventions of IAPWS, where the internal energy u' and entropy s' of the real fluid at the saturated liquid state are set to zero at the triple point $T_{\mathrm{tp}} = 276.969$ K. A correlation for the ideal-gas heat capacity c_p^{o} is necessary in Eq. (12). The functional form used here is

$$\frac{c_p^{\mathrm{o}}(T)}{R} = c_0 + \sum_{k=1}^{4} v_k \left(\frac{u_k}{T}\right)^2 \frac{\exp(u_k/T)}{[\exp(u_k/T) - 1]^2}, \tag{13}$$

where $c_0 = 4.0$, $v_1 = 0.010\,633$, $v_2 = 0.997\,87$, $v_3 = 2.1483$, $v_4 = 0.354\,90$, $u_1 = 308$ K, $u_2 = 1695$ K, $u_3 = 3949$ K, and $u_4 = 10\,317$ K. The value of c_0 is physically meaningful, since it corresponds to the internal-energy contributions of translational and rotational motions of the molecule at low temperatures. A nonlinear triatomic molecule, such as D_2O, has three translational and three rotational degrees of freedom, leading to the isochoric ideal-gas heat capacity $c_v^{\mathrm{o}} = 6/2R$. From Eq. (13), this leads to the constant $c_0 = (c_v^{\mathrm{o}} + R)/R = 8/2 = 4$. As temperature increases, thermal energy additionally contributes to vibrational excitations that yield an increase in c_p^{o}. This temperature dependency is represented by four so-called "Planck-Einstein terms." Because this approach is empirical and only loosely based on physical considerations, the individual terms do not represent the contributions of specific vibrational frequencies. The adjustable coefficients v_k and exponents u_k were mainly fitted to the recently published ideal-gas heat capacities obtained from a highly accurate partition function by Simkó *et al.* [the temperature in these $c_p^{\mathrm{o}}(T)$ values is the thermodynamic temperature; for our purposes, this is negligibly different from temperatures on the ITS-90 scale].[47] However, since the ideal-gas part contributes to all caloric properties calculated from the EOS, it was simultaneously fitted with the residual part to additional experimental data for the speed of sound and heat capacity (c_p and c_v) of the real fluid. The ideal-gas part of the EOS, derived from Eqs. (12) and (13), is

$$\alpha^{\mathrm{o}}(\tau,\delta) = a_1 + a_2\tau + \ln\delta + (c_0 - 1)\ln\tau + \sum_{k=1}^{4} v_k \ln[1 - \exp(-u_k\tau/T_{\mathrm{c}})], \tag{14}$$

where a_1 and a_2 are defined to yield the above-discussed values of $u'(T_{\mathrm{tp}}) = s'(T_{\mathrm{tp}}) = 0$. The values of these constants are $a_1 = -8.670\,994\,022\,646\,00$ and $a_2 = 6.960\,335\,784\,587\,78$. All other parameters are the same as given for Eq. (13).

The data of Simkó *et al.*[47] are part of a comprehensive IAPWS-associated project in which thermochemical functions for the ideal-gas properties of water and its different isotopologues are being developed. The results for $H_2^{16}O$ were published by Furtenbacher *et al.*[48] Because the single-molecule partition functions developed in this project do not account for the dissociation that occurs in real water at high temperatures, they produced artificial maxima in the heat capacity. For heavy water, this maximum occurs near 4100 K. Since this is far beyond the upper temperature limit of the new EOS, the correlation given in Eq. (13) was only fitted, and is consequently only valid, up to this temperature. Comparisons between the new EOS and the available calculations[47,49,50] for the ideal-gas heat capacity are presented in Fig. 5. On the c_p^{o}, T-diagram, the maximum in c_p^{o} is quite distinct. The new equation yields reasonable information about the ideal-gas state over a much broader temperature range than the EOS of Hill *et al.*,[11] which was exclusively fitted to the old data of Friedman and Haar[49] up to about 1500 K.

Based on comparisons to the data of Simkó *et al.*,[47] the uncertainty of calculated ideal-gas heat capacities from the new EOS is estimated to be smaller than 0.01% at temperatures below 300 K and within 0.02% over the whole range of validity of the new EOS (with $T_{\mathrm{max}} = 825$ K). The uncertainty of calculated ideal-gas heat capacities from this correlation is still within a maximum uncertainty of 0.25% up to 4100 K. Our uncertainties do not match the standard uncertainties of the data as given by Simkó *et al.*,[47] which are stated to be below 0.01% up to 1800 K. However, since the present ideal-

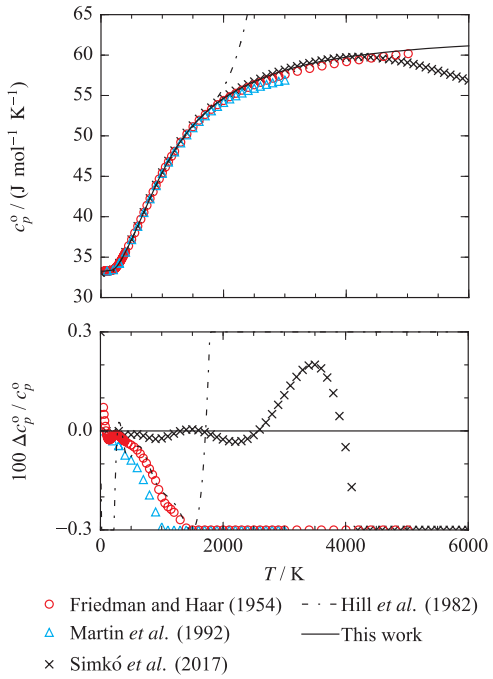

FIG. 5. Top: Ideal-gas heat capacity as a function of temperature as calculated with the new EOS and with the EOS of Hill *et al.*[11] The available data are included for comparison. The complete dataset of Simkó *et al.*[47] consists of 6000 points at intervals of 1 K. Only selected points are shown here. The ideal-gas correlation was fitted up to 4100 K, where the data of Simkó *et al.*[47] reach a maximum in c_p^o. Bottom: Relative deviations $\Delta c_p^o/c_p^o = (c_{p,\mathrm{data}}^o - c_{p,\mathrm{calc}}^o)/c_{p,\mathrm{data}}^o$ of ideal-gas heat-capacity data from Eq. (13) versus temperature. The equation of Hill *et al.*[11] is plotted for comparison.

gas correlation led to the best representation of the real-fluid properties, minor concessions were made in the description of the ideal-gas properties at elevated temperatures.

4.2. Properties of the real fluid

The residual part of our EOS for heavy water consists of six polynomial terms, six exponential terms, and 12 "Gaussian bell-shaped" terms. The complete equation with a total of 24 terms reads

$$\alpha^{\mathrm{r}}(\delta,\tau) = \sum_{i=1}^{6} n_i \delta^{d_i} \tau^{t_i} + \sum_{i=7}^{12} n_i \delta^{d_i} \tau^{t_i} \exp\left(-\delta^{l_i}\right) + \sum_{i=13}^{24} n_i \delta^{d_i} \tau^{t_i} \exp\left(-\eta_i(\delta-\varepsilon_i)^2 - \beta_i(\tau-\gamma_i)^2\right). \tag{15}$$

All parameters (coefficients n_i, temperature exponents t_i, density exponents d_i and l_i, and the parameters of the Gaussian bell-shaped terms η_i, ε_i, β_i, and γ_i) are listed in Table 5. The formulation is valid for all stable fluid states from $T_{\mathrm{min}} = 254.415$ K, which corresponds to the minimum temperature along the melting-pressure curve, to $T_{\mathrm{max}} = 825$ K at pressures up to 1200 MPa.

As previously mentioned, all thermodynamic properties can be calculated through the derivatives of Eqs. (14) and (15) with respect to the reduced density and reciprocal reduced temperature. Detailed explanations of the calculation of thermodynamic properties, including the required derivatives, are given by Span[51] and Lemmon *et al.*[29] To assist users in computer-program verification, three tables with test values are provided. Table 6 contains values of the ideal and residual part of the reduced Helmholtz energy together with values of their relevant derivatives. Table 7 gives various calculated single-phase properties at selected temperatures and densities, whereas Table 8 provides values of saturation properties at selected temperatures.

4.3. Fitting procedure

The essence of the fitting procedure can be described quite simply: The adjustable parameters of the ideal-gas correlation and of the residual part of the reduced Helmholtz energy [Eqs. (13) and (15)] are varied by a fitting algorithm to reach the best agreement between the input data and the properties calculated from the EOS. The mathematical structure of the ideal-gas part is relatively simple compared to the residual part. Because the residual part is fitted to a significantly more comprehensive database, most of the time required to fit an EOS is spent on the development of the residual part. The fitting algorithm used in this work was originally developed by Lemmon and Jacobsen[45] and is continuously improved at the National Institute of Standards and Technology (NIST). It is based on so-called "nonlinear fitting methods" that enable a simultaneous optimization of all parameters to different types of data. It is also possible to apply thermodynamic constraints to ensure that all properties behave correctly and extrapolate well even in regions beyond the data available. The EOS is fitted to a carefully chosen selection of points from the most accurate and consistent datasets. Each selected data point and constraint is weighted individually depending on the type, pressure and temperature region, target accuracy, and experimental uncertainty. Deviations of the calculated properties from the weighted data points and constraints contribute to an overall sum of squares that is minimized by varying the adjustable parameters of the EOS.

The number of each type of term in Eq. (15) is not varied by the fitting algorithm. The correlator has to find the optimum number and combination of terms to obtain a good fit. The number of terms should be as small as possible but as large as necessary. Equations with a large number of terms are very flexible and allow the correlator to find special terms to describe particular areas with high accuracy, but the extrapolation behavior of these equations can be unmanageable due to the many mathematical degrees of freedom. By contrast, short equations can be shaped more easily to extrapolate well and to exhibit smooth derivative behavior. However, it can be difficult to find a solution that covers the whole fluid region and yields a good compromise among all different data types. As discussed in Sec. 1, a short and thus numerically stable functional form was one of the main requirements for the new EOS for heavy water. In comparison to the equation of Hill *et al.*,[11] the new formulation has fewer than half the number of terms, 24 instead of 50 (excluding the ideal-gas correlations).

TABLE 5. Parameters of the residual part of the EOS given in Eq. (15)

i	n_i	t_i	d_i	l_i	η_i	β_i	γ_i	ε_i
1	$0.122\,082\,060 \times 10^{-1}$	1.0000	4	...				
2	$0.296\,956\,870 \times 10^{1}$	0.6555	1	...				
3	$-0.379\,004\,540 \times 10^{1}$	0.9369	1	...				
4	0.941 089 600	0.5610	2	...				
5	−0.922 466 250	0.7017	2	...				
6	$-0.139\,604\,190 \times 10^{-1}$	1.0672	3	...				
7	−0.125 203 570	3.9515	1	1				
8	$-0.555\,391\,500 \times 10^{1}$	4.6000	1	2				
9	$-0.493\,009\,740 \times 10^{1}$	5.1590	3	2				
10	$-0.359\,470\,240 \times 10^{-1}$	0.2000	2	1				
11	$-0.936\,172\,870 \times 10^{1}$	5.4644	2	2				
12	−0.691 835 150	2.3660	1	2				
13	$-0.456\,110\,600 \times 10^{-1}$	3.4553	1	...	0.6014	0.4200	1.5414	1.8663
14	$-0.224\,513\,300 \times 10^{1}$	1.4150	3	...	1.4723	2.4318	1.3794	0.2895
15	$0.860\,006\,070 \times 10^{1}$	1.5745	1	...	1.5305	1.2888	1.7385	0.5803
16	$-0.248\,410\,420 \times 10^{1}$	3.4540	3	...	2.4297	8.2710	1.3045	0.2236
17	$0.164\,476\,900 \times 10^{2}$	3.8106	1	...	1.3086	0.3673	2.7242	0.6815
18	$0.270\,393\,360 \times 10^{1}$	4.8950	1	...	1.3528	0.9504	3.5321	0.9495
19	$0.375\,637\,470 \times 10^{2}$	1.4300	2	...	3.4456	7.8318	2.4552	1.1158
20	$-0.177\,607\,760 \times 10^{1}$	1.5870	2	...	1.2645	3.3281	0.8319	0.1607
21	$0.220\,924\,640 \times 10^{1}$	3.7900	2	...	2.5547	7.1753	1.3500	0.4144
22	$0.519\,652\,000 \times 10^{1}$	2.6200	1	...	1.2148	0.9465	2.5617	0.9683
23	0.421 097 400	1.9000	1	...	18.738	1177.0	1.0491	0.9488
24	−0.391 921 100	4.3200	1	...	18.677	1167.0	1.0486	0.9487

TABLE 6. Values for the ideal-gas part α^{o}, Eq. (14), and for the residual part α^{r}, Eq. (15), of the reduced Helmholtz energy together with the corresponding derivatives[a] for $T = 500$ K and $\rho = 46.26$ mol dm^{-3}

Ideal-gas-part values	Residual-part values
$\alpha^{o} = 0.196\,352\,717 \times 10^{1}$	$\alpha^{r} = -0.342\,291\,092 \times 10^{1}$
$\alpha^{o}_{\delta} = 0.384\,253\,134$	$\alpha^{r}_{\delta} = -0.367\,562\,780$
$\alpha^{o}_{\delta\delta} = -0.147\,650\,471$	$\alpha^{r}_{\delta\delta} = 0.835\,183\,806$
$\alpha^{o}_{\tau} = 0.939\,259\,413 \times 10^{1}$	$\alpha^{r}_{\tau} = -0.589\,707\,436 \times 10^{1}$
$\alpha^{o}_{\tau\tau} = -0.209\,517\,144 \times 10^{1}$	$\alpha^{r}_{\tau\tau} = -0.245\,187\,285 \times 10^{1}$
$\alpha^{o}_{\delta\tau} = 0$	$\alpha^{r}_{\delta\tau} = -0.113\,178\,440 \times 10^{1}$

[a] $\alpha^{r}_{\delta} = \left[\frac{\partial \alpha^{r}}{\partial \delta}\right]_{\tau}$, $\alpha^{r}_{\delta\delta} = \left[\frac{\partial^2 \alpha^{r}}{\partial \delta^2}\right]_{\tau}$, $\alpha^{r}_{\tau} = \left[\frac{\partial \alpha^{r}}{\partial \tau}\right]_{\delta}$, $\alpha^{r}_{\tau\tau} = \left[\frac{\partial^2 \alpha^{r}}{\partial \tau^2}\right]_{\delta}$, $\alpha^{r}_{\delta\tau} = \left[\frac{\partial^2 \alpha^{r}}{\partial \delta\, \partial \tau}\right]$; the symbols α^{o}_{δ}, $\alpha^{o}_{\delta\delta}$, etc. for the ideal-gas part are analogous.

The 24 terms of the residual part of the present equation contain a total of 126 adjustable parameters as presented in Table 5. With regard to this number, it is apparent that during the fitting process the number of possible parameter sets is almost unmanageable. For this reason, some guidelines given by Lemmon and Jacobsen[45] were followed. The derivatives of the residual part of the equation must go to zero for small densities, because in this limit the fluid behaves like an ideal gas. Therefore, the density exponents d_i and l_i in Eq. (15) must be positive integers and are not adjusted in the fitting algorithm but are defined by the correlator while choosing the optimal set of terms. Special restrictions are defined for the first polynomial term, which should have a density exponent of $d_1 = 4$ and a corresponding temperature exponent of $t_1 = 1$.

TABLE 7. Thermodynamic property values in the single-phase region for selected values of T and ρ

T (K)	ρ (mol dm^{-3})	p (MPa)	c_v (J mol^{-1} K^{-1})	w (m s^{-1})	s (J mol^{-1} K^{-1})
300	$0.551\,26 \times 10^{2}$	$0.529\,123\,711 \times 10^{-1}$	$0.833\,839\,128 \times 10^{2}$	$0.140\,374\,625 \times 10^{4}$	$0.673\,910\,582 \times 10^{1}$
	$0.600\,00 \times 10^{2}$	$0.238\,222\,326 \times 10^{3}$	$0.738\,561\,038 \times 10^{2}$	$0.177\,279\,674 \times 10^{4}$	$0.540\,117\,148 \times 10^{1}$
	$0.650\,00 \times 10^{2}$	$0.626\,176\,781 \times 10^{3}$	$0.699\,125\,978 \times 10^{2}$	$0.229\,697\,942 \times 10^{4}$	$0.271\,566\,150 \times 10^{1}$
500	$0.500\,00 \times 10^{-1}$	0.206 052 588	$0.294\,298\,102 \times 10^{2}$	$0.514\,480\,413 \times 10^{3}$	$0.140\,879\,085 \times 10^{3}$
	0.500 00	$0.188\,967\,446 \times 10^{1}$	$0.366\,460\,545 \times 10^{2}$	$0.489\,633\,254 \times 10^{3}$	$0.120\,227\,024 \times 10^{3}$
	$0.462\,60 \times 10^{2}$	$0.835\,329\,492 \times 10^{1}$	$0.626\,885\,994 \times 10^{2}$	$0.117\,888\,631 \times 10^{4}$	$0.495\,587\,000 \times 10^{2}$
	$0.500\,00 \times 10^{2}$	$0.107\,462\,884 \times 10^{3}$	$0.617\,372\,286 \times 10^{2}$	$0.148\,374\,868 \times 10^{4}$	$0.469\,453\,826 \times 10^{2}$
	$0.600\,00 \times 10^{2}$	$0.721\,798\,322 \times 10^{3}$	$0.576\,860\,681 \times 10^{2}$	$0.241\,393\,520 \times 10^{4}$	$0.393\,599\,094 \times 10^{2}$
643.8	$0.200\,00 \times 10^{2}$	$0.216\,503\,820 \times 10^{2}$	$0.992\,661\,842 \times 10^{2}$	$0.256\,043\,612 \times 10^{3}$	$0.817\,656\,125 \times 10^{2}$
800	$0.100\,00 \times 10^{-1}$	$0.664\,864\,175 \times 10^{-1}$	$0.340\,033\,604 \times 10^{2}$	$0.642\,794\,634 \times 10^{3}$	$0.169\,067\,586 \times 10^{3}$
	0.250 00	$0.164\,466\,177 \times 10^{1}$	$0.344\,327\,932 \times 10^{2}$	$0.639\,281\,410 \times 10^{3}$	$0.142\,125\,615 \times 10^{3}$

TABLE 8. Thermodynamic property values for liquid-vapor saturation states for selected temperatures[a]

	$T = 280$ K	$T = 450$ K	$T = 625$ K
p_v (MPa)	$0.823\,054\,058 \times 10^{-3}$	0.921 212 105	$0.172\,118\,129 \times 10^{2}$
ρ' (mol dm^{-3})	$0.552\,072\,786 \times 10^{2}$	$0.492\,937\,575 \times 10^{2}$	$0.306\,770\,554 \times 10^{2}$
ρ'' (mol dm^{-3})	$0.353\,747\,143 \times 10^{-3}$	0.264 075 691	$0.694\,443\,339 \times 10^{1}$
h' (J mol^{-1})	$0.257\,444\,444 \times 10^{3}$	$0.145\,127\,149 \times 10^{5}$	$0.324\,533\,556 \times 10^{5}$
h'' (J mol^{-1})	$0.466\,106\,716 \times 10^{5}$	$0.515\,019\,146 \times 10^{5}$	$0.472\,460\,343 \times 10^{5}$
s' (J mol^{-1} K^{-1})	0.924 406 091	$0.406\,584\,121 \times 10^{2}$	$0.731\,042\,291 \times 10^{2}$
s'' (J mol^{-1} K^{-1})	$0.166\,471\,646 \times 10^{3}$	$0.122\,856\,634 \times 10^{3}$	$0.967\,725\,149 \times 10^{2}$

[a]All these test values were calculated from the Helmholtz energy, Eq. (11), by applying the phase-equilibrium condition (Maxwell criterion).

This ensures that the isotherms converge for high densities and do not cross or diverge. All other temperature exponents do not have to be integers but should be positive. Negative exponents might result in unreasonable extrapolation behavior at high temperatures. For low temperatures and in the vapor–liquid equilibrium region, the overall behavior of the equation is essentially defined by terms with high temperature exponents. In order to ensure proper behavior in these regions, the exponents t_i should be as small as possible. As discussed in Sec. 5.3, at low temperatures the slope of the second virial coefficient B with temperature is much steeper for (heavy) water than for most other fluids. The correct representation of this behavior and of the experimental data in the metastable subcooled-liquid region required some higher temperature exponents than are generally needed. Figure 6 shows that at low temperatures the derivative of the residual Helmholtz energy with respect to density α_δ^r, which in the zero-density limit yields the second virial coefficient B, is basically defined by the second exponential term of Eq. (15) ($i = 8$). The temperature exponent of this term is $t_8 = 4.6$. Thus, no unreasonably large exponent was needed to describe the special behavior of B. The highest temperature exponent is $t_{11} = 5.4644$, which is still relatively low compared to older reference equations such as those for ordinary water,[32] carbon dioxide,[52] or nitrogen.[53] In those equations, the highest temperature exponents range from 16 up to 50.

The description of the critical region is particularly challenging in the development of an EOS. The reference equations for ordinary water[32] and carbon dioxide[52] contain so-called "non-analytical" terms that were developed to model the special physical characteristics at the critical point such as the extreme increase in c_v or the global minimum of the speed of sound w. Since these terms frequently lead to numerical problems, especially when the particular equation is evaluated within mixture modeling, they are no longer used for the development of new EOS. The approximate description of the critical point is normally enabled by Gaussian bell-shaped terms. For heavy water, two such terms ($i = 23$ and $i = 24$) were set up, with similar parameters but one positive and one negative coefficient. Consequently, these two terms cancel each other out over most of the stable fluid region, except in the vicinity of the critical point, where they have their maximum contribution. The impact of these terms on properties calculated near the critical point is visualized in Fig. 7, where the residual part of the isochoric heat capacity is calculated first with all terms of Eq. (15) and then with all terms except for the two critical-region terms. Both resulting

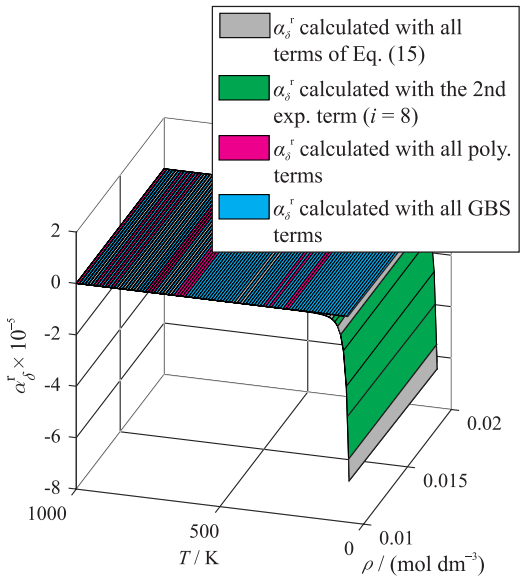

FIG. 6. First derivative of the residual Helmholtz energy with respect to density α_δ^r as a function of temperature and density. The derivative is calculated with all terms of Eq. (15), the sum of all polynomial terms, the sum of all Gaussian bell-shaped terms, and only by means of the second exponential term.

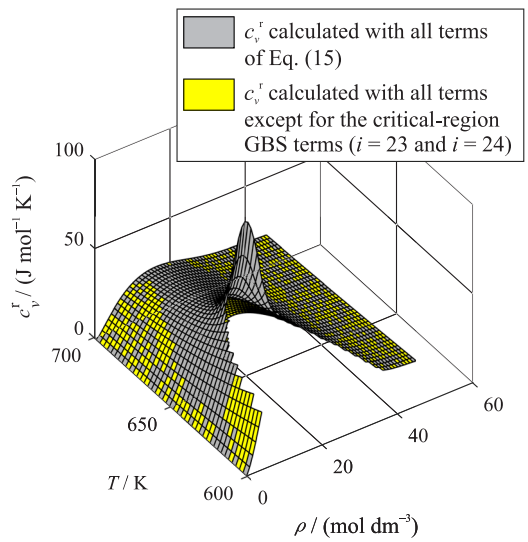

FIG. 7. Residual part of the isochoric heat capacity c_v^r versus temperature and density. The heat capacity is first calculated with all terms of Eq. (15) and then with all terms except for the two Gaussian bell-shaped terms that specifically contribute in the critical region. For parts of the surface shown with yellow and gray interspersed, the differences between the two surfaces are essentially zero.

surfaces are plotted over temperature and density. The steep increase in the isochoric heat capacity is modeled by the two Gaussian bell-shaped terms. However, as an analytic EOS, Eq. (15) is not capable of reproducing the nonclassical critical exponents that govern fluid behavior in the asymptotic limit of the critical point.

In general, Gaussian bell-shaped terms can be used to describe not only the critical region but also any region of the fluid surface. However, these terms need to be applied carefully, since they might lead to unreasonable results for derivatives of the reduced Helmholtz energy and thus to wrong qualitative behavior of certain properties. For heavy water, Gaussian bell-shaped terms were important to describe the anomalous behavior of the liquid at low temperatures, especially its density maximum. The final EOS was achieved by fitting its adjustable parameters to a representative selection of the reliable data from the literature and various mathematical and thermodynamic constraints. The fitting process was completed by carefully rounding all exponents and coefficients. This was done successively while refitting the equation. This guaranteed that the rounding off of each group of parameters was compensated by the coefficients and exponents that were still included in the fit.

5. Database and Validation of the EOS

As briefly discussed in Sec. 4, the EOS was fitted to a carefully weighted selection of the most reliable experimental data. Nevertheless, the fit was continuously evaluated by comparisons to all available data points. In this section, such comparisons to the final EOS are discussed in order to validate the EOS and to estimate the uncertainties of calculated values. The relative deviation of every data point from the value obtained from the EOS is calculated. This deviation for any property X can be written as

$$\frac{\Delta X}{X} = \left(\frac{X_{\text{exp}} - X_{\text{calc}}}{X_{\text{exp}}} \right). \tag{16}$$

Comparisons of the equation to complete datasets are based on the average absolute relative deviation (AAD). This property is defined as the arithmetic average of all percentage absolute deviations of a dataset (excluding clear outliers). It reads

$$\text{AAD} = \frac{1}{n} \sum_{i=1}^{n} \left| 100 \frac{\Delta X_i}{X_i} \right|, \tag{17}$$

where n is the number of data points used in the calculation. In many cases, calculating an overall AAD for one dataset would lead to false conclusions. For example, the AAD of a dataset including many excellent measurements in the liquid phase can be significantly affected by a small number of inaccurate data points in the vapor phase. Therefore, it is meaningful to separate the fluid range into parts and calculate the AAD for each region. This separation needs to be different for thermal saturation data than for other types of data and is discussed in Secs. 5.1 and 5.2. The relative deviation defined by Eq. (16) is not useful for properties such as virial coefficients whose values cross zero; see Sec. 5.3 for the discussion of deviations for virial coefficients.

All experimental values considered in the present work were converted to molar-based SI units, with temperatures on the ITS-90 scale.

5.1. Thermal saturation data

An overview of the available data for thermal saturation properties, namely, for the vapor pressure and the saturated-liquid and saturated-vapor densities, is given in Table 9 along with the AAD for each dataset. Aside from the overall AAD that was calculated for the complete dataset, separate values for the AAD for the low ($T/T_c \leq 0.6$), medium ($0.6 < T/T_c \leq 0.98$), and high ($T/T_c > 0.98$) temperature ranges are provided.

5.1.1. Vapor-pressure data

Most of the available saturation data for heavy water are measurements of the vapor pressure. In some cases, the vapor pressure was reported as a difference or ratio relative to that of ordinary water; in these cases, we used the IAPWS-95 formulation[32,73] to calculate the vapor pressure of ordinary water. Comparisons of the available data for D_2O with values calculated from the EOS are shown in Fig. 8. Figure 8 contains two deviation plots. The first one shows deviations of all available measurements and thus provides an overview of the entire database on this property. The second plot (with a smaller scale) illustrates comparisons with datasets included in the fitting process.

Most of the available data at temperatures higher than the triple-point temperature are represented within deviations of 0.2%. The database includes vapor pressures of the metastable subcooled liquid at temperatures below the triple-point temperature, published by Kraus and Greer[61] and Bottomley.[41] This scientifically interesting region is discussed in detail in Sec. 5.5. For the sake of completeness, deviations of these data are included in the top panel of Fig. 8. Most of the data of Bottomley[41] deviate from the EOS by less than 0.15%, although they were not used in the fitting process. Thus, these data demonstrate good extrapolation behavior of the vapor-pressure curve calculated from our EOS. The triple-point measurement of Markó *et al.*[18] is specifically highlighted in the top panel of Fig. 8. As noted in Sec. 2, the corresponding pressure value is less accurate than the available vapor-pressure data at slightly higher temperatures; the pressure deviates by −0.35% from the EOS. Therefore, the triple-point pressure provided in Table 1 was calculated from the EOS. Between the triple-point temperature ($T_{\text{tp}} = 276.969$ K) and about 300 K, the EOS was fitted to the experimental data of Besley and Bottomley,[54] which are the most accurate data available in this temperature range. The authors state uncertainties of 3 mK in temperature and about 2.7 Pa in pressure. Considering this information, we calculated relative combined expanded ($k = 2$) uncertainties in vapor pressure for every state point that range from 0.02% to 0.04%. Except

TABLE 9. Data summary and AADs of experimental vapor-pressure, saturated-liquid density, and saturated-vapor density data from the EOS

Reference[a]	Year	No. of data	Temperature range in K	Average absolute relative deviations in %			
				LT[b]	MT[b]	HT[b]	Overall
Vapor pressure p_v							
*Besley and Bottomley[54]	1973	37	277–299	0.024	...	...	0.024
Bottomley[41 c,d]	1978	17	261–276	0.088			0.088
Erokhin and Kompaniets[55]	1980	22	433–644	...	0.074	0.083	0.076
Jákli and Illy[56]	1980	157	280–362	0.068	...	...	0.068
Jákli and Markó[57 e]	1995	101	281–353	0.075	...	...	0.075
Jákli and Van Hook[58]	1981	57	280–363	0.068	...	...	0.068
Jones[59]	1968	32	361–388	0.303	0.108	...	0.289
Kirillin and Ulybin[60]	1959	4	573–645	...	0.035	0.042	0.039
Kraus and Greer[61 d]	1984	162	257–277	0.732	...	...	0.732
Lewis and MacDonald[62]	1933	10	293–389	0.341	...	...	0.341
Liu and Lindsay[63]	1970	12	379–574	0.064	0.091	...	0.089
Miles and Menzies[64]	1936	10	298–502	0.314	0.104	...	0.188
Niwa and Shimazaki[42]	1939	6	277–287	0.785	...	...	0.785
*Oliver and Grisard[27]	1956	36	481–645	...	0.010	0.053	0.017
Pupezin *et al.*[40]	1972	96	273–372	0.163	...	...	0.163
Quitzsch *et al.*[65]	1963	4	293–324	0.267	...	...	0.267
*Rivkin and Ahkundov[21]	1962	8	548–639	...	0.015	0.027	0.019
*Zieborak[66]	1966	15	354–494	0.014	0.006	...	0.008
Saturated liquid density ρ'							
Costello and Bowden[67]	1958	10	293–474	0.072	0.241	...	0.157
Grossmann-Doerth[68]	1955	14	368–434	...	0.007	...	0.005
Grossmann-Doerth[69]	1956	9	333–373	0.001	...	...	0.001
Hebert *et al.*[70]	1958	21	448–645	...	0.230	3.183	0.511
Mursalov *et al.*[71]	1999	14	294–644	0.055	0.163	0.656	0.246
Saturated vapor density ρ''							
Hebert *et al.*[70]	1958	21	448–645	...	13.406	8.222	12.913
Mursalov *et al.*[71]	1999	9	572–644	...	1.019	2.948	2.305

[a]Sources preceded by * were used for fitting the EOS.
[b]LT: $T/T_c \leq 0.6$; MT: $0.6 < T/T_c \leq 0.98$; and HT: $T/T_c > 0.98$.
[c]Reference 41 presents differences between the vapor pressure of the metastable subcooled liquid and the sublimation pressure. The vapor pressures were recalculated from Eq. (9).
[d]The reference provides vapor pressures of the metastable subcooled liquid. The deviations were calculated by calculating the vapor pressure with the EOS extrapolated to temperatures below the triple-point temperature.
[e]Reference 57 does not provide the experimental values for pure D_2O. These were given later by Harvey and Lemmon[72] within an article presenting a vapor-pressure correlation for D_2O.

for very few data points, the EOS represents all the data within their estimated experimental uncertainty. The AAD of the dataset from the equation is 0.024%. We conservatively estimate the relative uncertainty of calculated vapor pressures to be 0.05% at temperatures up to 300 K. As a further reliability check, the vapor pressures for H_2O provided by Besley and Bottomley[54] were compared to the reference equation of Wagner and Pruß[32] (IAPWS-95). Although the data were not used in the fitting process of IAPWS-95,[32] they are represented with an AAD of 0.056%.

In the temperature range between 300 K and 350 K, the data situation is less satisfactory than for the rest of the vapor-pressure curve, although the amount of data available is relatively large. However, all of the datasets that exhibit an acceptable level of self-consistency come from the same group of experimentalists, namely, the Central Research Institute for Physics of the Hungarian Academy of Sciences in cooperation with the Chemistry Department of the University of Tennessee.[40,56–58] Although these data were obtained with the same basic experimental setup, they exhibit considerable differences, indicating that the data are not as accurate as the best measurements at lower and higher temperatures. The earliest study from this group was published in 1972 by Pupezin *et al.*[40] As shown in Fig. 8, these data exhibit considerable scatter. However, the EOS of Hill *et al.*[11] was obviously fitted to this dataset, which led to a less reliable description of vapor pressures in this temperature range than with the equation presented here. The later published datasets of Jákli and Illy[56] and Jákli and Van Hook[58] are more consistent, but still exhibit scatter of up to 0.09% and an offset of about 0.08% from the very accurate data of Zieborak[66] at higher temperatures. The newest dataset was published in 1995 by Jákli and Markó[57] within a study of excess properties of ordinary and heavy water solutions of tetrabutylammonium bromide. The vapor pressures of pure heavy water obtained in this work were not provided in the corresponding publication, but were later provided in a personal communication to Harvey and Lemmon who included them in their article.[72] The reproducibility of these data is roughly 0.05%. Considering that the data were published relative to H_2O and that the

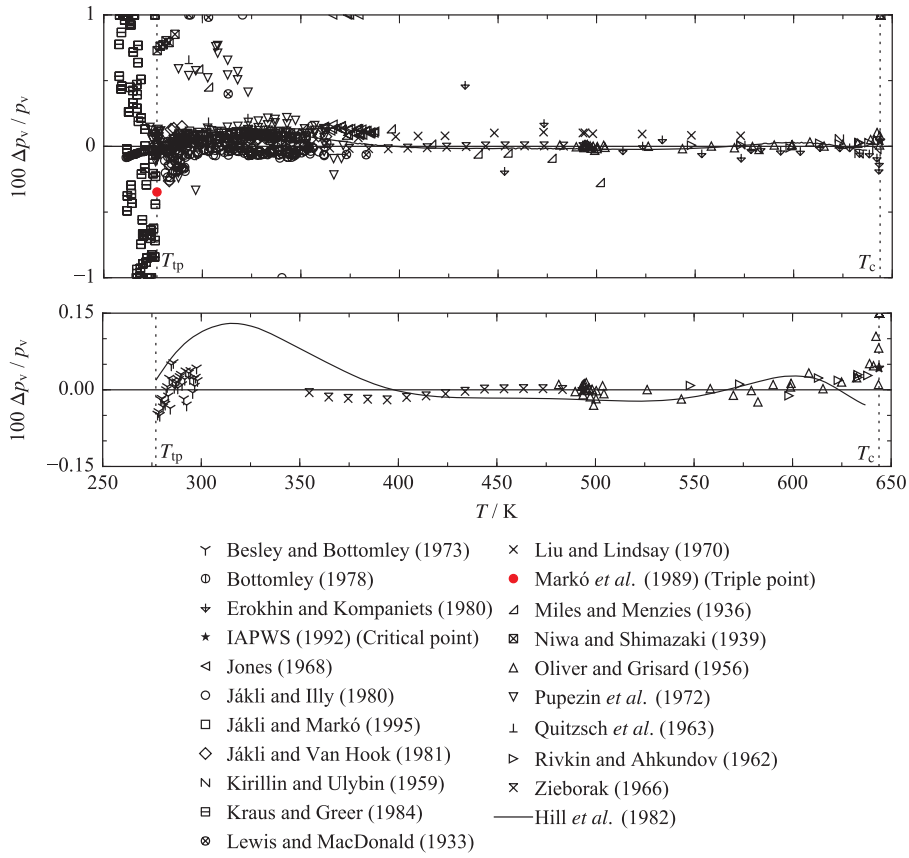

FIG. 8. Top: Relative deviations $\Delta p_v/p_v = (p_{v,exp} - p_{v,calc})/p_{v,exp}$ of the available experimental vapor-pressure data from the new EOS versus temperature. Bottom: Relative deviations of selected experimental data from the new EOS. The equation of Hill *et al.*[11] is plotted for comparison.

uncertainty of vapor pressures calculated from IAPWS-95 is between 0.01% and 0.02% within this temperature range,[32,73] the uncertainty of the data is probably not much less than 0.1%. Summing up the data situation between 300 K and 350 K, the estimated relative uncertainty of calculated vapor pressures in this temperature range is 0.1%. However, this estimate is quite conservative. Considering the experimental uncertainty of the data at lower and higher temperatures, the uncertainty of calculated values is probably lower than that estimated here.

At temperatures between 350 K and 495 K, the vapor-pressure curve calculated from the EOS was mostly defined by fitting the equation to the experimental results of Zieborak.[66] The author states an uncertainty in pressure of about 2.7 Pa but does not provide comparably clear information about the uncertainty in temperature. Nevertheless, azeotropic temperatures of the $H_2O + D_2O$ mixture are reported with an accuracy of 3 mK. Based on this information, we estimated combined expanded ($k = 2$) uncertainties in vapor pressure ranging from 0.01% to 0.03%. The maximum deviation of these data from the EOS is 0.02% and their overall AAD is 0.008%. Considering these deviations and the experimental uncertainty of the data, the estimated relative expanded uncertainty of calculated vapor pressures in this range is 0.03%.

Between 495 K and the critical temperature ($T_c = 643.847$ K), the most reliable data were published by Oliver and Grisard.[27] Above 548 K, the data overlap with the vapor pressures of Rivkin and Akhundov,[21] who provided no clear information about experimental uncertainties. However, the data confirm the vapor pressures of Oliver and Grisard[27] within about 0.03%. Oliver and Grisard[27] measured the saturation temperature relative to ordinary water within 0.01 K. The reported pressures were obtained with the H_2O vapor-pressure correlation of Osborne and Meyers,[74] which is negligibly different from IAPWS-95 in this region. Since the uncertainty of IAPWS-95 in this region is 0.02%,[32,73] we consider this as a good estimate for the uncertainty in saturation pressure of the data by Oliver and Grisard.[27] The estimated relative combined expanded ($k = 2$) uncertainties of these data are thus within 0.06%. However, at temperatures up to 642 K, deviations between these data and the EOS are below 0.05%, and the data are confirmed by the values of Rivkin and Akhundov.[21] Very close to the critical temperature, the deviations of the data increase up to 0.1%, but the critical pressure recommended by IAPWS[17] is represented within 0.05%. As discussed in Sec. 2, for a fixed critical temperature, the uncertainty of the IAPWS value is 0.01 MPa, which corresponds to a relative uncertainty of 0.05%. The EOS consequently represents the critical pressure within its uncertainty. We therefore estimate an expanded relative uncertainty in calculated vapor pressures at temperatures between 495 K and T_c of 0.05%.

A complete overview of the estimated relative uncertainties of calculated vapor pressures as discussed in this section is provided in Fig. 9.

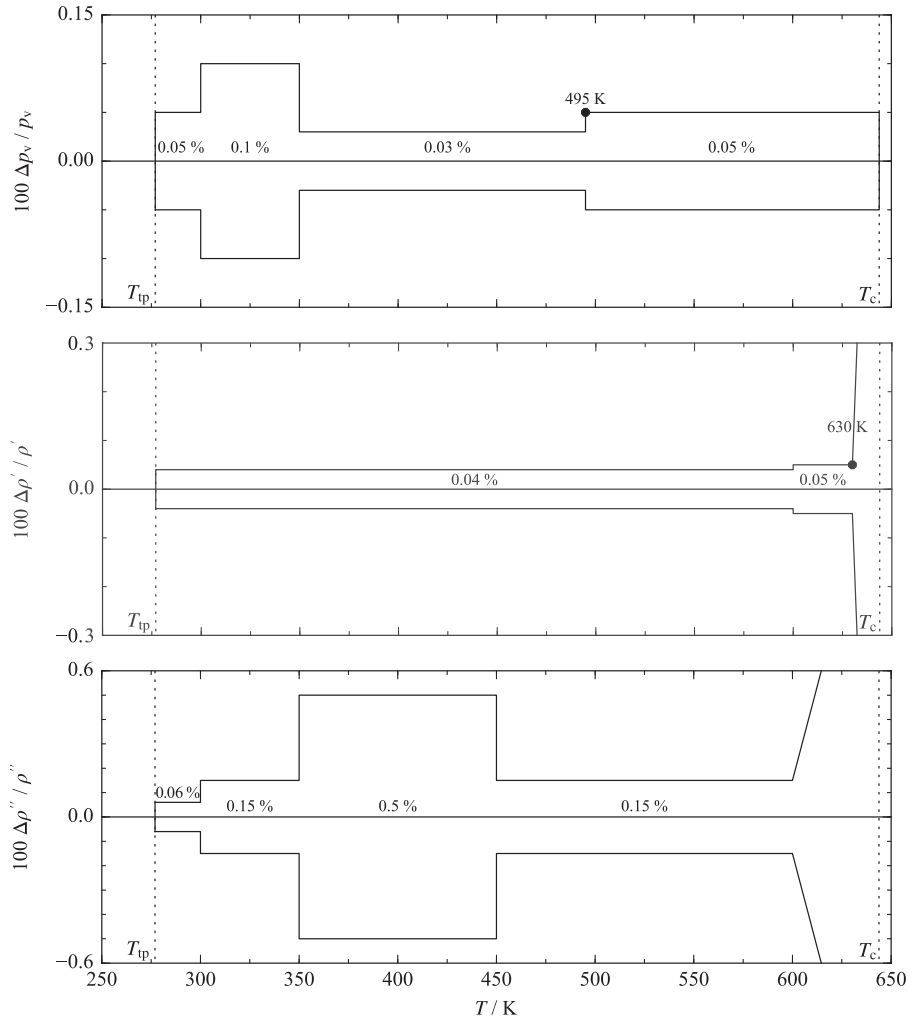

FIG. 9. Expanded uncertainties in vapor pressure, $\Delta p_v/p_v$, in saturated liquid density, $\Delta\rho'/\rho'$, and in saturated vapor density, $\Delta\rho''/\rho''$, estimated for the EOS. The uncertainties for the saturated densities increase linearly to 1.5% at the critical temperature.

Figure 8 shows that the new EOS enables a better description of the vapor-pressure curve than the EOS of Hill *et al.*[11] The most significant improvements were obtained at temperatures below 400 K, where the equation of Hill *et al.*[11] was obviously fitted to the less reliable data of Pupezin *et al.*[40] Furthermore, Hill *et al.* did not consider the very accurate data of Besley and Bottomley.[54] Figure 8 also highlights that the previous standard EOS should not be used in the critical region. In fact, numerical issues with the EOS of Hill *et al.*[11] prevented us from calculating vapor pressures at temperatures higher than approximately 638 K.

5.1.2. Saturated-density data

In comparison to the previously discussed situation for vapor pressures, the data for saturated-liquid and saturated-vapor densities are quantitatively and qualitatively quite limited. Thus, none of the available datasets was used to fit the EOS. Deviations of the data for both properties are shown in Fig. 10.

The saturated-liquid density data cover almost the entire phase boundary from the triple point up to the critical temperature. The new EOS represents most of these experimental data within 0.5%, except for some points close to the critical temperature. The newest reference was published by Mursalov *et al.*,[71] covering the complete temperature range of vapor–liquid equilibrium. The authors state an uncertainty of 0.05% in temperature and 0.04% in volume. Based on this information, the estimated combined uncertainties of these data range from 0.1% to 0.4% for temperatures up to 640 K and increase closer to the critical temperature. Except for one point, our EOS represents this dataset within its experimental uncertainty. The most valuable experimental results were measured by Grossmann-Doerth, who published two remarkably accurate datasets in 1955 and 1956.[68,69] The measurements were carried out relative to H_2O. The author states an uncertainty in the ratio between the mass density of D_2O and H_2O of 3×10^{-5}. The saturation temperature is reported with an uncertainty of 0.1 K. Hence, the combined expanded ($k = 2$) uncertainty of the saturated density is estimated to be below 0.03%. Although the EOS was not fitted to these data, all points exhibit deviations less than 0.02%, which underlines the high accuracy of the data and their consistency with the vapor pressures and the homogeneous-

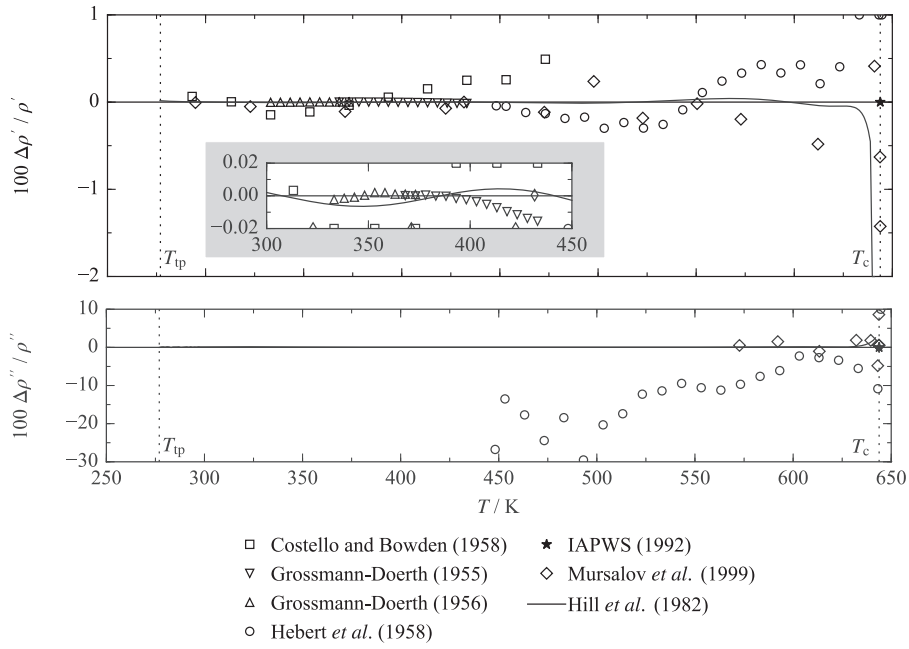

FIG. 10. Top: Relative deviations $\Delta\rho'/\rho' = (\rho'_{exp} - \rho'_{calc})/\rho'_{exp}$ of experimental saturated-liquid density data from the new EOS versus temperature. The EOS of Hill *et al.*[11] is plotted for comparison. Bottom: Relative deviations $\Delta\rho''/\rho'' = (\rho''_{exp} - \rho''_{calc})/\rho''_{exp}$ of experimental saturated-vapor density data from the new EOS. The EOS of Hill *et al.*[11] is again plotted for comparison, but on this scale, deviations from our EOS are only visible close to the critical temperature.

density data used to fit the EOS. Hebert *et al.*[70] published their saturated-liquid data with an uncertainty estimate of 1%, which seems too pessimistic. Although none of the data points was used for fitting the EOS, all deviations are within 0.5% (except close to the critical temperature). The publication of Costello and Bowden[67] does not provide any statement on the experimental uncertainty. The maximum deviation of the data is 0.5%.

Aside from the data of Grossmann-Doerth,[68,69] none of the available datasets is accurate enough to yield appropriate uncertainty estimates for saturated-liquid densities calculated from the EOS. It is, therefore, important to consider that the density at saturation is not a completely independent property, but a subset of the homogeneous density close to the phase boundary $\rho(T, p)$. This implies that fitting the EOS to accurate homogeneous densities leads to an accurate description of saturated densities if high-quality saturation pressures $p_v(T)$ are available. Hence, the combined expanded uncertainty in saturated density can be estimated reasonably by adding in quadrature the uncertainty in homogeneous density $u_c(\rho)$ near the phase boundary and the uncertainty contribution of the vapor pressure. The latter can be determined from the relative uncertainty in vapor pressure estimated in Sec. 5.1.1 [$U_r(p_v) = \Delta p_v/p_v$ in Fig. 9] multiplied by p_v and the isothermal sensitivity coefficient $(\partial\rho/\partial p)_{T\text{sat}}$ calculated from the EOS for the homogeneous phase in the limit of the saturation boundary. The uncertainty of the homogeneous density close to the phase boundary can be reasonably estimated by multiplying the relative uncertainty of the homogeneous density by the saturated density. The final combined uncertainty in saturated density $u_c(\rho_{sat})$ is then

$$u_c(\rho_{sat}) \approx \sqrt{[U_r(p_v) \times p_v]^2 \left(\frac{\partial\rho}{\partial p}\right)^2_{T_{sat}} + [U_r(\rho) \times \rho_{sat}]^2}. \quad (18)$$

Over most of the temperature range, the liquid density is not very sensitive to the pressure, and the uncertainty in saturation pressure can be neglected; thus, the uncertainty in the saturated-liquid density should, to a good approximation, be no larger than the uncertainty in the homogeneous-liquid density. An uncertainty analysis for this property is discussed in detail in Sec. 5.2. Between the triple-point temperature and 315 K, the uncertainty in liquid density is 0.04%, which we adopt as the uncertainty of the saturated-liquid density in this temperature range. The data of Grossmann-Doerth[68,69] cover a temperature range from 333 K up to 434 K. Due to the high quality of these data, the relative uncertainty of calculated saturated-liquid densities in this region is estimated to be 0.04%. We therefore define the uncertainty from the triple-point temperature up to 435 K to be 0.04%. We can reasonably extend the 0.04% uncertainty region up to 600 K, corresponding to the uncertainty in liquid density (see Sec. 5.2). At higher temperatures, the sensitivity coefficient $(\partial\rho/\partial p)_{T\text{sat}}$ becomes larger, which leads to slightly higher combined uncertainties. Our estimated uncertainty is therefore increased to 0.05% between 600 K and 630 K. The phase boundary at temperatures above 630 K is within the critical region (discussed in Sec. 5.2), where the uncertainty in density increases considerably. The uncertainty of the critical density recommended by IAPWS[17] and given in Sec. 2 is about 1.5%. Because the EOS represents this value with a negligible deviation, the uncertainties in calculated saturated-liquid densities are estimated to increase linearly from 0.05% at 630 K to 1.5% at the critical temperature. The

results of the uncertainty analyses for calculated saturated-liquid densities over the entire temperature range of the phase boundary are summarized in Fig. 9.

The saturated-vapor density was measured by Hebert *et al.*[70] at temperatures above 448 K. At lower temperatures, no experimental data are available. Hebert *et al.*[70] state that between 200 °C and 370 °C their data for light water deviate by about 10% from previous literature values. At higher and lower temperatures, these deviations are even larger. Consequently, comparisons of their data for heavy water provide no valuable information on the uncertainty of the EOS. The above-discussed publication by Mursalov *et al.*[71] contains densities of the saturated vapor at temperatures above 572 K. Considering the given information on their accuracy in temperature and volume, the relative expanded ($k = 2$) uncertainties of their data are within 2% below 630 K. At higher temperatures, the experimental uncertainties increase significantly. The EOS represents almost all data points within their uncertainty. Analogous to the experimental saturated-liquid data, the overall data situation for the saturated-vapor density does not allow for reasonable uncertainty estimates for values calculated from the EOS. Therefore, our uncertainty estimates are based on Eq. (18). Unlike for the saturated-liquid density, the uncertainty of the saturation pressure is essential for the accuracy of calculated saturated-vapor densities. We considered the estimated uncertainties in homogeneous vapor density (see Sec. 5.2), the uncertainty in vapor pressure (summarized in Fig. 9), and the sensitivity coefficient $(\partial\rho/\partial p)_{T\mathrm{sat}}$ calculated from the EOS. The uncertainties in saturated-vapor densities calculated in this way are 0.06% between the triple-point temperature and 300 K [where $U_\mathrm{r}(p_\mathrm{v}) = \Delta p/p = 0.05\%$ and $U_\mathrm{r}(\rho) = \Delta\rho/\rho = 0.03\%$], 0.15% between 300 K and 350 K [$U_\mathrm{r}(p_\mathrm{v}) = U_\mathrm{r}(\rho) = 0.1\%$], 0.5% between 350 K and 450 K [$U_\mathrm{r}(p_\mathrm{v}) = 0.03\%$, $U_\mathrm{r}(\rho) = 0.5\%$], and 0.15% between 450 K and 600 K [$U_\mathrm{r}(p_\mathrm{v}) = 0.05\%$, $U_\mathrm{r}(\rho) = 0.1\%$]. At temperatures above 600 K, the sensitivity of the saturated-vapor density to the vapor pressure, $(\partial\rho/\partial p)_{T\mathrm{sat}}$, and the total uncertainty in density, $U_\mathrm{r}(\rho) \times \rho$, increase significantly. Therefore, we estimate a linear increase in the uncertainties of calculated saturated-vapor densities from 0.15% at 600 K to 1.5% at the critical temperature. All results of the uncertainty analysis for calculated saturated-vapor densities are illustrated in Fig. 9.

For the EOS of Hill *et al.*,[11] no uncertainty analysis for saturated densities was published. Due to the poor data situation, a clear statement about the accuracy of that equation for these properties is difficult; however, the calculated saturated densities from both EOS agree within our estimated uncertainties. But the new EOS allows for a reliable description of saturated densities in the critical region where it is not recommended to calculate state properties from the previous standard EOS.

5.2. Homogeneous density data

In Table 10, the available experimental data for homogeneous densities are summarized. In addition to the overall AAD, Table 10 provides separate AAD for the vapor, liquid, critical, and supercritical state regions. The supercritical region is subdivided into three areas: the region of low densities ($\rho/\rho_\mathrm{c} < 0.6$), of medium densities ($0.6 \le \rho/\rho_\mathrm{c} \le 1.5$), and of high densities ($\rho/\rho_\mathrm{c} > 1.5$).

Aside from speed-of-sound measurements, homogeneous density data, also called "*pvT* data," are often the most accurate experimental data available. The majority of the experimental values included in fitting the EOS are *pvT* measurements, and comparisons of the available *pvT* data and calculated values are important to evaluate the EOS. Due to the large amount of experimental data, only the most important datasets can be discussed here. An overview of the database and deviations from the new EOS and from the EOS by Hill *et al.*[11] is given in Fig. 11. The most obvious improvements in accuracy are shown in color, namely, the description of the two accurate and comprehensive vapor and liquid-phase datasets of Kell *et al.*[88,89] and the high-pressure data of Bridgman.[34]

In the homogeneous vapor phase, the EOS was exclusively fitted to the experimental data of Kell *et al.*[89] This dataset comprises the largest number of data points (more than 600) and is considered to be one of the most reliable experimental studies on heavy water. The data range from 423 K to 774 K at pressures up to 37 MPa. Deviations of the data from the new EOS versus temperature and pressure are shown in Fig. 12.

Despite the overall high quality of these data, the corresponding publication has few details about experimental uncertainties. The authors state their uncertainties in density to be between 0.1 mol m^{-3} and 0.3 mol m^{-3},[89] which we interpret as standard uncertainties in the density measurement, not including any effects of temperature or pressure uncertainty. Earlier papers of Kell and co-workers,[105–107] in which their experimental apparatus is discussed in detail, state uncertainties of 2 mK in temperature and 100 Pa in pressure. Considering this information, we calculated combined expanded ($k = 2$) uncertainties for every state point that range from 0.0006 mol dm^{-3} to 0.0010 mol dm^{-3}. Except for a few points, the EOS represents the data within their experimental uncertainties. Since the data cover a wide range of densities (0.03 mol dm^{-3} to 8.8 mol dm^{-3}), their relative uncertainties as well as the deviations from the EOS vary considerably. However, excluding the two lowest isotherms, the EOS represents more than 95% of the data within 0.1%, which we adopt as an uncertainty estimate for the calculated vapor densities between 450 K and 775 K including the supercritical gas-like fluid at pressures up to 30 MPa. The measurements of the two lowest isotherms (423 K and 448 K) are known to be less accurate, as discussed in detail in the IAPWS-95 publication for ordinary water.[32] Based on the deviations of these data, the estimated uncertainty of calculated vapor densities in this temperature range is 0.5%. At temperatures lower than the temperature range investigated by Kell and co-workers, there are no experimental vapor density data available. However, we can still obtain a reasonable estimate of the uncertainty of the EOS in this region. Because the pressure in this region does not exceed 0.5 MPa [$p_\mathrm{v}(423\ \mathrm{K}) = 0.46$ MPa], the vapor density can be described by a virial equation truncated after the second virial coefficient. The EOS accurately

TABLE 10. Data summary and average absolute relative deviations of experimental data for homogeneous densities from the EOS. Clear outliers were not considered in the calculation of the AAD

Reference[a]	Year	No. of data	T (K)	p (MPa)	Average absolute relative deviations in %						
								Supercritical fluid			
					Gas	Liquid	Critical region	LD[b]	MD[b]	HD[b]	Overall
pvT data											
Aleksandrov *et al.*[75]	1976	143	673–824	4.5–101	...	...	0.048[c]	0.088	0.316	0.030	0.126
Aleksandrov *et al.*[76]	1976	65	270–286	3.7–101	...	0.019	...	...	...	...	0.019
Bridgman[34 d]	1935	130	253–374	0.1–1189	...	0.208	...	...	...	...	0.208
Ceccaldi *et al.*[77]	1975	1	295.4	0.1	...	0.021	...	...	...	...	0.021
*Chang and Tung[78 e]	1949	23	276–375	0.1	...	0.005	...	...	...	...	0.005
*Duška *et al.*[79]	2018	242	254–294	0.1–101	...	0.006	...	...	...	...	0.006
*Emmet and Millero[80]	1975	129	275–314	0.1–101	...	0.007	...	...	...	...	0.007
Hare and Sorensen[81]	1986	11	253–313	0.1	...	0.023	...	...	...	...	0.023
Ivanov and Lebedeva[82]	2011	5	278–319	0.1	...	0.007	...	...	...	...	0.007
Ivanov *et al.*[83]	2010	5	278–319	0.1	...	0.010	...	...	...	...	0.010
Ivanov *et al.*[84]	2011	6	278–319	0.1	...	0.005	...	...	...	...	0.005
Jancsó[85]	2007	5	298–319	0.1	...	0.045	...	...	...	...	0.045
Juza *et al.*[86]	1966	36	353–624	50–351	...	0.302	...	...	...	...	0.302
*Kanno and Angell[87]	1980	32	247–294	0.1–148	...	0.052	...	...	...	...	0.052
*Kell *et al.*[88]	1985	415	423–774	0.1–103	...	0.009	0.011[c]	...	0.048	0.024	0.013
*Kell *et al.*[89]	1989	631	423–774	0.1–37	0.065	...	...	0.039	...	...	0.051
Kirillin and Ulybin[60]	1959	124	523–774	7.3–50	0.602	0.299	0.366[c]	0.090	0.615	0.214	0.301
Kudryavtsev *et al.*[90]	1986	5	278–319	0.1	...	0.006	...	...	...	...	0.006
Lewis and MacDonald[62]	1933	9	277–314	0.1	...	0.264	...	...	...	...	0.264
Marczak[91]	1999	5	293–314	0.1	...	0.082	...	...	...	...	0.082
Millero *et al.*[92 f]	1971	14	278–344	0.1	...	0.009	...	...	...	...	0.009
Nevolina and Seifer[93]	1973	6	293.1	0.1–101	...	0.016	...	...	...	...	0.016
Rasmussen and MacKenzie[94]	1973	11	244–274	0.1	...	0.217	...	...	...	...	0.217
Reisler and Eisenberg[95]	1965	7	278–309	0.1	...	0.005	...	...	...	...	0.005
*Rivkin and Ahkundov[21]	1962	43	663–699	4.7–29	...	...	0.027[c]	0.056	0.120	...	0.056
Scharlin and Steinby[96]	2003	6	277–319	0.1	...	0.017	...	...	...	...	0.017
Schrader and Wirtz[97 g]	1951	17	293–374	0.1	...	0.015	...	...	...	...	0.015
*Steckel and Szapiro[98]	1963	61	276–351	0.1	...	0.004	...	...	...	...	0.004
Stokland *et al.*[99]	1939	51	283–301	0.1	...	0.003	...	...	...	...	0.003
Tsederberg *et al.*[100]	1972	71	293–474	1.5–100	...	0.044	...	...	...	...	0.044
Tsederberg *et al.*[101]	1973	173	473–699	1.8–101	0.102	0.058	0.032[c]	0.066	0.057	0.061	0.061
Zheleznyi[102]	1969	20	244–278	0.1	...	0.176	...	...	...	...	0.176

[a]Sources preceded by * were used for fitting the EOS.
[b]LD: $\rho/\rho_c < 0.6$; MD: $0.6 \leq \rho/\rho_c \leq 1.5$; and HD: $\rho/\rho_c > 1.5$.
[c]The AAD of *pvT* data in the critical region is given with respect to pressure instead of density.
[d]All pressures reported by Bridgman[34] were multiplied by 1.0102 (see Sec. 3.4).
[e]The data supersede the data of Chang and Chien,[103] which were consequently omitted.
[f]The article presents two datasets with a D_2O purity of 99.88 mol. % and 98.35 mol. %. The latter data were omitted.
[g]The data supersede the data of Wirtz,[104] which were consequently omitted.

reproduces the values of the second virial coefficient $B(T)$ obtained from first principles (see Sec. 5.3). Any uncertainty in $B(T)$ translates directly into a relative uncertainty in $Z - 1$, where Z is the compressibility factor $p/\rho RT$. A conservative estimate of a 10% expanded uncertainty in $B(T)$, taken at the maximum pressure p_v where the nonideality is greatest, produces the uncertainty estimates shown in Fig. 13. Between 350 K and 425 K, this estimate conveniently matches the uncertainty estimated based on the two lowest isotherms measured by Kell *et al.*[89] Thus, the estimate of a 0.5% uncertainty of calculated vapor densities is extended to the temperature range from 350 K to 450 K. At lower temperatures down to 300 K, the uncertainty is within 0.1%, and at temperatures below 300 K, it does not exceed 0.03%. In fact, the real uncertainties in density are even smaller at the lowest pressures shown in Fig. 13, because in the low-pressure limit the density approaches that of the ideal gas, which is known almost exactly. In Fig. 14, selected experimental data including the vapor-phase data of Kell *et al.*[89] are shown along various (quasi-)isotherms. The solid lines represent the results of the previous standard EOS of Hill *et al.*[11] Comparing the representation of the vapor-phase data of Kell *et al.*[89] with the new EOS and the EOS of Hill *et al.*[11] shows that the previous EOS enables a comparably accurate description of the data for the lowest three isotherms (423 K to 473 K). At higher temperatures, values calculated from the EOS of Hill *et al.*[11] exhibit larger deviations from this dataset. The new EOS yields considerably more accurate results (see also Fig. 11), especially at elevated pressures and densities. We consequently note that the description of densities in the homogeneous vapor phase is improved by the EOS presented here.

Highly accurate densities of liquid heavy water from its melting curve up to 315 K and at pressures up to 100 MPa were recently measured by Duška *et al.*[79] at the Institute of

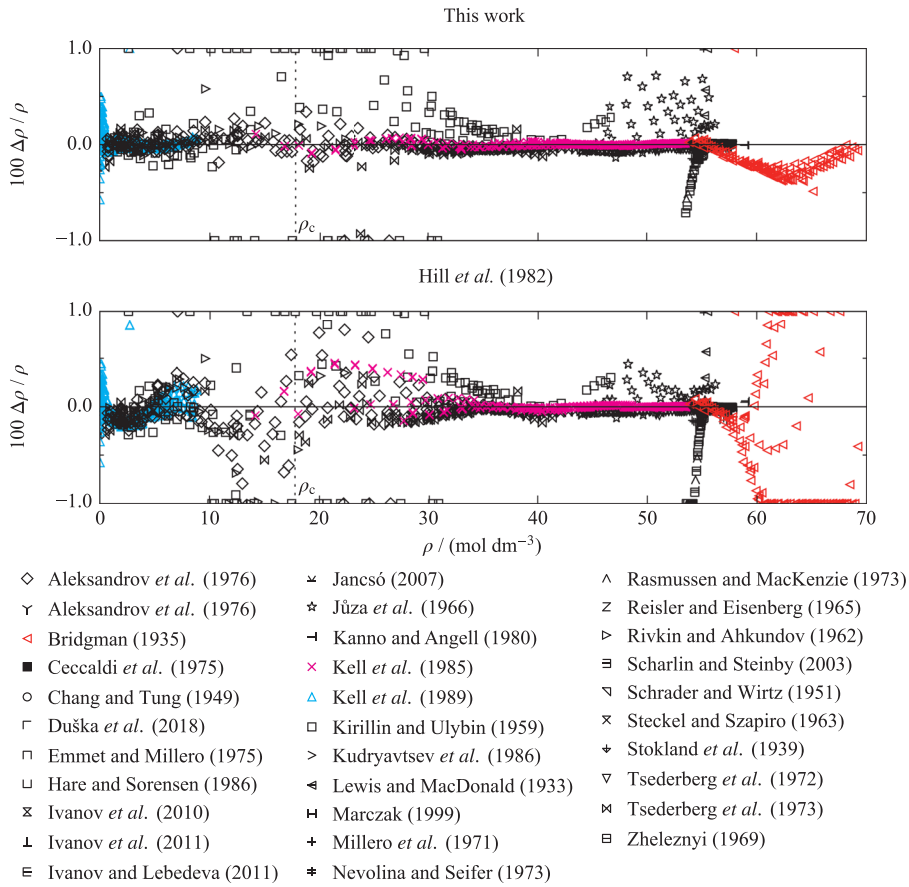

FIG. 11. Top: Relative deviations $\Delta\rho/\rho = (\rho_{exp} - \rho_{calc})/\rho_{exp}$ of the experimental density data from the new EOS versus density. Bottom: Relative deviations of the experimental density data from the equation of Hill *et al.*[11]

Thermomechanics in Prague. The dataset also includes measurements in the metastable subcooled-liquid region that are discussed in Sec. 5.5. In personal communications, the experimentalists estimated the so-far unpublished data to be accurate within an expanded ($k = 2$) uncertainty of 0.04%.

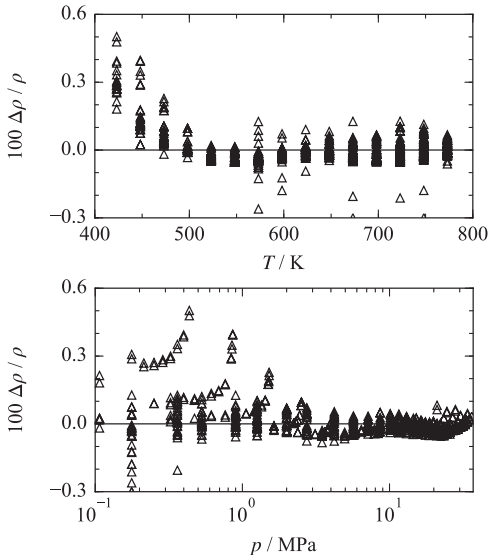

FIG. 12. Top: Relative deviations $\Delta\rho/\rho = (\rho_{exp} - \rho_{calc})/\rho_{exp}$ of the experimental vapor density data of Kell *et al.*[89] from the EOS versus temperature. Bottom: Relative deviations of the experimental vapor-phase data of Kell *et al.*[89] from the EOS versus pressure.

Figure 14 shows that this uncertainty is confirmed by the accurate datasets of Emmet and Millero[80] and Aleksandrov *et al.*[76] Since the EOS describes all the data of Duška *et al.*[79] within their experimental uncertainty, the estimated uncertainty of liquid densities calculated from the present EOS is 0.04% at temperatures up to 315 K and pressures up to 100 MPa. At temperatures between 315 K and 423 K, the most reliable liquid densities at pressures exceeding 1 atm (0.101 325 MPa) were published by Tsederberg *et al.*[100] The authors state an accuracy in specific volume of 0.0015 $cm^3\,g^{-1}$, which we interpret as the standard uncertainty of their results. The corresponding relative uncertainties are between 0.05% and 0.06%, which would be equivalent to an expanded uncertainty of about 0.1%. However, although the EOS was not fitted to these data, all data points between 315 K and 423 K are represented within 0.06%. Thus, we estimate the expanded uncertainty of calculated liquid densities between 315 K and 425 K at pressures up to 100 MPa to be 0.07%.

Figure 14 shows that liquid densities calculated from the present EOS and the previous standard EOS are in quite good agreement within the region from the melting curve up to 425 K and pressures up to 100 MPa. In fact, deviations between the two EOS are within the uncertainties of the data.

A particularly detailed evaluation of the EOS should be made for liquid densities at atmospheric pressure, and thus at temperatures between the normal-melting-point temperature $T_m \approx 276.961$ K as calculated from Eq. (4) and the

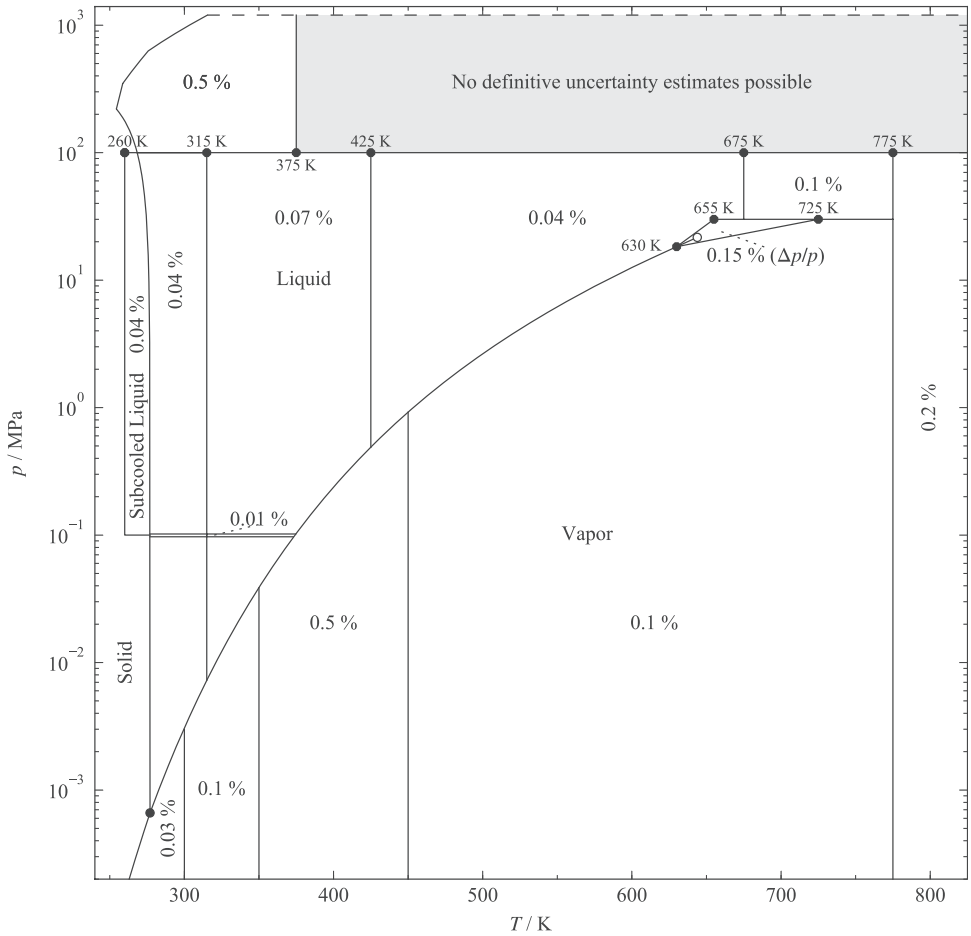

FIG. 13. Expanded relative uncertainties in density, $\Delta\rho/\rho$, estimated for the EOS. In the enlarged critical region (triangle), the uncertainty is given as a percentage uncertainty in pressure, $\Delta p/p$. This region is bordered by the two isochores 8 mol dm^{-3} and 29 mol dm^{-3} and by the 30 MPa isobar. The positions of the lines separating the uncertainty regions are approximate. At low pressures for the vapor, the uncertainties become much smaller than indicated because the vapor is nearly an ideal gas.

normal-boiling-point temperature $T_{nbp} \approx 374.549$ K. For H_2O, there are extremely accurate experimental data at these conditions. In fact, the expanded relative uncertainty of these metrological measurements is within 10^{-6} (1 ppm).[32,108] For D_2O, the available data are of clearly lower quality, but there are still some very accurate datasets. Deviations of the most reliable data from the new EOS and the EOS of Hill *et al.*[11] are shown in Fig. 15.

The only dataset covering the entire temperature range from the freezing to the boiling point was published by Chang and Tung[78] in 1949. Despite the age of this work, the data are of remarkably high quality. Over the complete temperature range, the data exhibit deviations below 85 ppm. The authors corrected their data to 100% D_2O and provide an experimental uncertainty of 0.05 g dm^{-3}, which corresponds to about 2.5 mol m^{-3} and which we interpret as a standard uncertainty. The resulting relative expanded uncertainties are within 94 ppm. Accordingly, the EOS represents every state point within its experimental uncertainty. The publication additionally includes measurements of H_2O at identical temperatures. In this state region, liquid densities calculated from IAPWS-95 are accurate to 1 ppm. The H_2O densities of Chang and Tung[78] deviate from IAPWS-95 by less than 31 ppm, which confirms the high quality of the data. The D_2O data of Stokland *et al.*[99] are in remarkably good agreement with the measurements of Chang and Tung.[78] The experimentalists involved in the work of Stokland and co-workers were among the pioneers of heavy water research. Nevertheless, the claimed experimental uncertainty of 10^{-5} kg dm^{-3}, which is equivalent to an expanded relative uncertainty of about 18 ppm, seems somewhat underestimated, although the data are obviously quite accurate, with deviations below 76 ppm.

Aside from these datasets, the most accurate measurements covering a range of temperature were published by Steckel and Szapiro.[98] The reliability of the data was verified by comparing their measurements of H_2O with IAPWS-95. The calculated deviations are nowhere larger than 18 ppm. The D_2O dataset includes a result for the maximum density of heavy water that is reported with an uncertainty of 3×10^{-5} g ml^{-1} (1.5 mol m^{-3}). Adopting this value as the experimental uncertainty of the density measurement over the entire range of the data, and adding the uncertainty contribution of the D_2O purity of the sample in quadrature, yields a relative expanded uncertainty of approximately 60 ppm. We estimated the uncertainty contribution of the D_2O purity by calculating the deviation of the reported density ρ_{sample} (for 99.78 mol. %

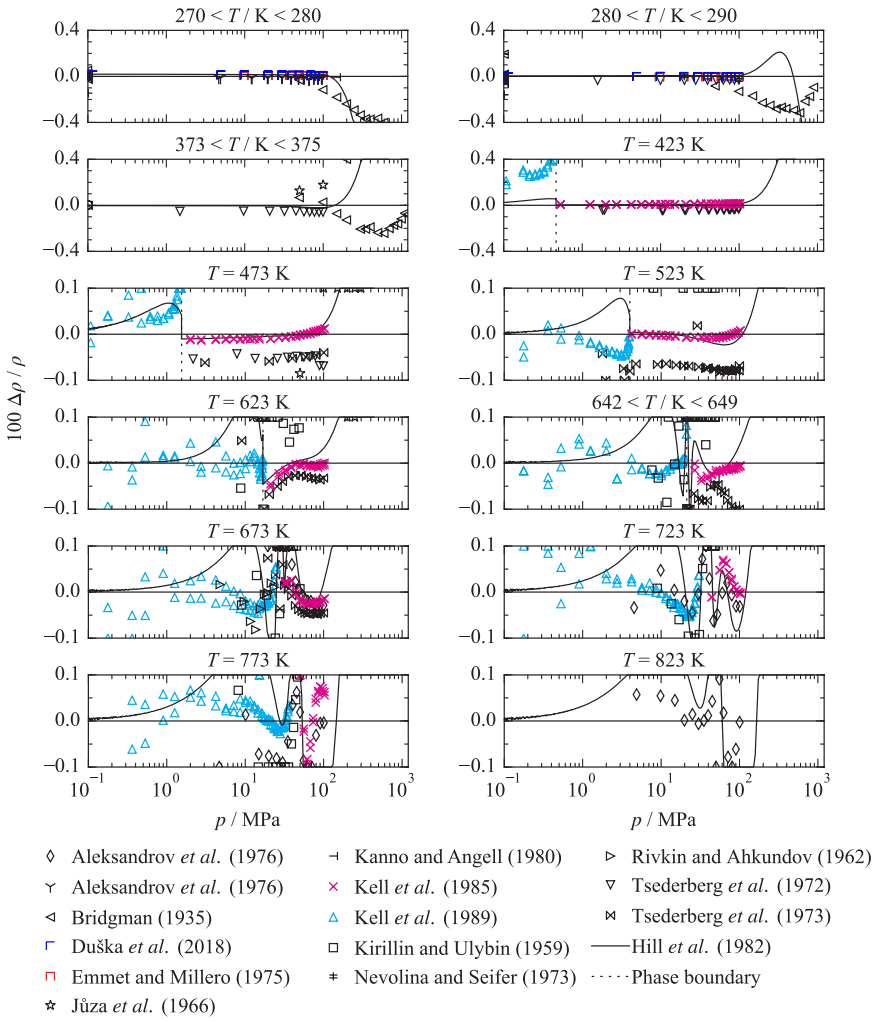

FIG. 14. Relative deviations $\Delta\rho/\rho = (\rho_{exp} - \rho_{calc})/\rho_{exp}$ of selected experimental density data along (quasi-)isotherms from the new EOS. The EOS of Hill *et al.*[11] is plotted for comparison. For plots showing a temperature range, the EOS of Hill *et al.*[11] was calculated at the average temperature. The first four diagrams have a larger deviation scale than the other diagrams.

D_2O, meaning that 99.78% of the hydrogen atoms are deuterium, D) from the value corrected to 100% D_2O. The corrected density ρ_{D2O} is defined as

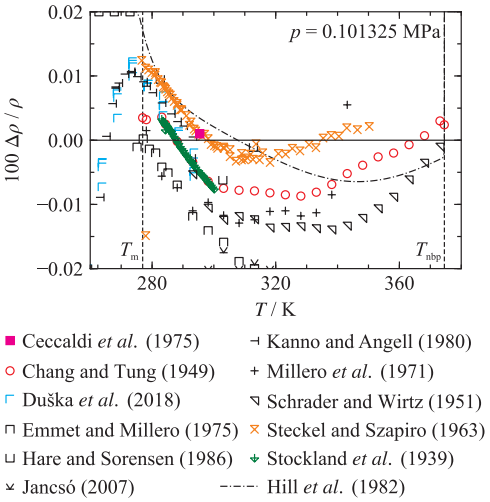

FIG. 15. Relative deviations $\Delta\rho/\rho = (\rho_{exp} - \rho_{calc})/\rho_{exp}$ of the most accurate experimental density data in the liquid phase at atmospheric pressure from the new EOS. The EOS of Hill *et al.*[11] is plotted for comparison.

$$\rho_{D_2O} = \frac{x_{D_2O}}{\left(\rho_{sample}^{-1} - (1 - x_{D_2O})\rho_{H_2O}^{-1}\right)}, \tag{19}$$

where x_{D_2O} is the molar D fraction of the investigated sample and ρ_{H_2O} is the density of ordinary water as calculated from IAPWS-95 at the given temperature and pressure. At temperatures above 287 K, the EOS represents all data points of Steckel and Szapiro[98] within their uncertainty. At lower temperatures, the deviations are within 0.01%, except for the last two points that exhibit slightly higher deviations. More intensive fitting of the EOS to the data at temperatures below 287 K led to lower deviations but worsened the representation of the data in the metastable subcooled-liquid region (see Sec. 5.5). The already discussed work of Duška *et al.*[79] includes some measurements at atmospheric pressure and temperatures up to 294 K. The investigated sample contained 99.993 mol. % D. The uncertainty contribution of the remaining H content is below 1 ppm as estimated from Eq. (19), and thus is negligible. Since the main focus of this experimental investigation was metastable subcooled heavy water, the provided expanded uncertainty of 0.04% is a conservative

estimate for the densities of the stable liquid phase. In fact, above the freezing point, all data are represented within a maximum deviation of 85 ppm. The data confirm the measurements of Steckel and Szapiro[98] and Chang and Tung,[78] with slightly better agreement with the latter dataset. Considering the deviations of these accurate datasets, we estimate the uncertainty of liquid densities at atmospheric pressure to be 0.01% at temperatures from the freezing point to the normal boiling point. Figure 15 shows that the EOS agrees with the previous standard EOS within this estimated uncertainty, except in a small temperature range from the melting-point temperature to 282 K. There, the EOS of Hill *et al.*[11] provides a more accurate description of the data of Steckel and Szapiro.[98]

Some additional comments should be made about the experiments of Ceccaldi *et al.*[77] carried out at the Bureau International des Poids et Mesures (BIPM), Paris, and published in 1975. This extremely thorough work presents the density of D_2O at 22.3 °C and 1 atm with metrological accuracy. The authors claim a precision on the order of 10^{-3} kg m^{-3}, which corresponds to 0.05 mol m^{-3}. This precision is equivalent to a relative expanded ($k = 2$) uncertainty of approximately 2 ppm. The isotopic composition of the sample was carefully studied (with regard to both hydrogen and oxygen isotopes), and the density was then corrected to isotopically pure D_2O with all oxygen atoms being ordinary oxygen ^{16}O. Since "standard" heavy water also contains the heavier oxygen isotopes ^{17}O and ^{18}O (see Sec. 1), the mass-based density of Ceccaldi *et al.*[77] must be converted to a molar value not by means of the molar mass given in Table 1 but instead by $M = 20.023\ 118$ g mol^{-1}, which is the molar mass of isotopically pure $D_2{}^{16}O$. The so-obtained molar density deviates from the new EOS by 10 ppm (and by about 25 ppm from the previous standard EOS). Thus, it is not represented within its experimental uncertainty. Nevertheless, its small deviation underscores the high accuracy of both the new EOS and the other accurate experimental data at atmospheric pressure (see Fig. 15).

When discussing the representation of liquid densities, the description of the maximum density of heavy water is of special interest. For ordinary water, the maximum density at atmospheric pressure is widely known to occur at approximately 4 °C, or to more digits 3.983 °C, as recommended by Tanaka *et al.*[108] Heavy water exhibits a similar density maximum, but the values of the density and temperature at the maximum are less accurately investigated. An overview of parameters taken from the literature and calculated from the new EOS as well as from the EOS of Hill *et al.*[11] is given in Table 11. All temperatures were converted to ITS-90.

Table 11 shows that the temperature of maximum density at 1 atm is reported in various publications, but only two of them also present the corresponding density. The new EOS deviates from the maximum density of Stokland *et al.*[99] by about 18 ppm, which is within the claimed (but questioned) experimental uncertainty of this value. The result of Steckel and Szapiro[98] is represented within 73 ppm and thus not within the estimated experimental uncertainty of 60 ppm. However, the calculated value agrees with both experimental results within the estimated uncertainty of the EOS, which is 0.01% as discussed above. The temperature of the maximum density calculated from the EOS is 284.748 K (about 11.6 °C), which is slightly higher than all experimentally based results and not within the temperature uncertainty given by Stokland *et al.*[99] (0.02 K) and Steckel and Szapiro[98] (0.03 K). This shift in temperature can be seen in Fig. 16, which shows the shape of the 1 atm isobar in the vicinity of the maximum density as calculated from the new EOS and the EOS of Hill *et al.*[11] together with the most accurate experimental data.

TABLE 11. Maximum density of D_2O at atmospheric pressure and its corresponding temperature as taken from the literature and calculated from the new EOS and the EOS of Hill *et al.*[11]

Reference	Year	$T_{\rho max,atm}$ (K)	$\rho_{max,atm}$ (mol dm^{-3})
Lewis and MacDonald[62]	1933	284.742	...
Takéuchi and Inai[109]	1936	284.542	...
Stokland *et al.*[99]	1939	284.373	55.222
Steckel and Szapiro[98]	1963	284.383	55.225
Aleksandrov *et al.*[110]	1977	284.329	...
Kanno and Angell[87]	1980	284.417	...
Hill *et al.*[11]	1982	284.321	55.225
This work	2018	284.748	55.221

In the vicinity of the maximum density, neither EOS performs obviously better than the other; the difference between the two formulations is within the estimated uncertainty of our EOS. The maximum density at 1 atm is defined not only by the experimental data that were fitted in this region but also by other liquid-phase data at higher pressures, where the maximum density occurs at lower temperatures. Also, the maximum in density is related to other characteristics of water such as the maximum in speed of sound (see Sec. 5.6). Thus, the representation of the maximum density is additionally influenced by the speed-of-sound data used to fit the EOS.

The high-pressure liquid phase was investigated by Bridgman.[34] His data cover temperatures from the melting

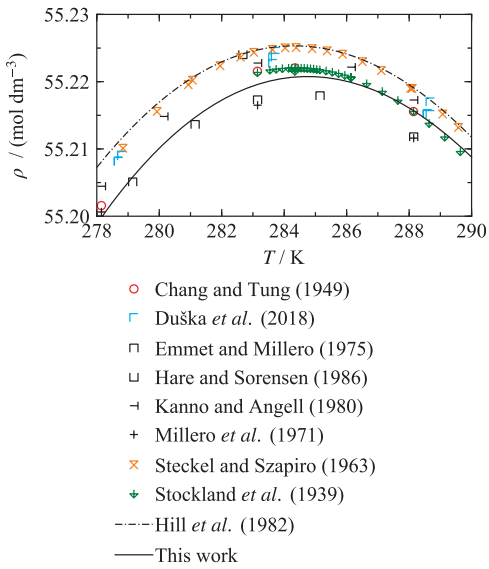

FIG. 16. Liquid densities calculated from the new EOS and the EOS of Hill *et al.*[11] versus temperature at atmospheric pressure. The diagram is focused on the vicinity of the maximum density of heavy water. Selected experimental data are shown for comparison.

curve up to 373 K at pressures to approximately 1200 MPa, which defines the upper pressure limit of the new EOS (p_{max} = 1200 MPa). As discussed in Sec. 3.4, all pressures specified in this dataset were multiplied by 1.0102 in order to compensate for an obsolete calibration. Because Bridgman's publication does not provide clear information about uncertainties, his data were not used to fit the EOS. However, their representation was continuously evaluated during fitting. Except for one outlier, all data points are represented within 0.4%. Thus, we estimate the expanded uncertainty of calculated liquid densities to be 0.5% in the high-pressure range from 100 MPa to 1200 MPa and at temperatures from the melting curve to 375 K. Apart from Bridgman's data, the only other high-pressure dataset available was published by Jůza *et al.*[86] While fitting the EOS, these data were found to be less reliable and thus were not considered in the estimation of the uncertainty of calculated values. Therefore, no definitive uncertainty estimates are possible in the high-pressure region at temperatures above 375 K. The EOS of Hill *et al.*[11] is not valid at pressures above 100 MPa. The results illustrated in Figs. 11 and 14 were calculated by extrapolating the EOS to higher pressures. These calculated densities deviate considerably from Bridgman's data.

At pressures up to 100 MPa and temperatures above 423 K, the EOS was fitted to the very accurate liquid-phase data of Kell *et al.*[88] that range from 423 K to 773 K. As "a good approximation," the authors estimated the error of their measurements to be within 0.01%, which at least needs to be expanded (k = 2) to 0.02%. In fact, for temperatures up to 673 K, the EOS represents more than 95% of the data within 0.02%. Some higher deviations occur at moderate pressures and thus lower densities. Because all of the data up to 673 K are represented within 0.04% (see Fig. 14), we conservatively estimate the expanded uncertainty of calculated liquid densities to be 0.04% at temperatures between 425 K and 675 K and pressures up to 100 MPa. This uncertainty estimate is not valid in the critical region, which is discussed later in this section. The two highest isotherms measured by Kell *et al.*[111] (723 K and 773 K) exhibit maximum deviations of 0.07% and 0.09%, respectively. Hence, we estimate the uncertainty of calculated supercritical liquid-like densities to be 0.1% in the temperature range from 675 K to 775 K. More intensive fitting of the EOS to the data on these isotherms did not significantly improve these deviations, but led to an unreasonable description of the physical behavior of the fluid. Thus, we assume that at these temperatures, the experimental uncertainty of the data is considerably higher than stated in the publication. This assumption is supported by reviewing the H_2O measurements by Kell *et al.*[111] that were published in the same year as the D_2O data. At 723 K and 773 K, the H_2O densities deviate by up to 0.1% from IAPWS-95.[32] As already noted in the discussion of vapor densities, the EOS of Hill *et al.*[11] is remarkably accurate in representing the experimental data of Kell and co-workers, although the data were published in 1985 and 1989, and thus some years after the publication of the previous reference EOS. However, the publication of Hill *et al.*[11] refers to some then-unpublished data provided by Kell. The later published article of Kell *et al.*[111] stated that preliminary values of the liquid density up to 400 °C were contributed to the correlating work of Hill and co-workers. This explains why the previous EOS is in very good agreement with these data for temperatures up to 673 K (see Fig. 14) but exhibits larger deviations from the data at higher temperatures. The measurements at 723 K and 773 K correspond to the lowest densities in the dataset. As is apparent from Fig. 11, within this state region, at densities below approximately 35 mol dm^{-3}, the new EOS clearly better represents the data.

The upper temperature limit of the new EOS (T_{max} = 825 K) is defined by the data of Aleksandrov *et al.*[75] ranging from 673 K to 823 K. This dataset is a correction and extension of the high-temperature study carried out by the same group of experimentalists and published by Tsederberg *et al.*[101] Considering the given information about the uncertainties in temperature, pressure, and volume, we calculated combined expanded (k = 2) uncertainties for every state point. At the two highest isotherms, which exceed the temperature range experimentally investigated by Kell *et al.*,[88] these uncertainties range from about 0.1% to 0.16%. Figure 14 shows that, except for some outliers, our EOS represents these data within 0.2%, which is consequently a reasonable estimate for the expanded uncertainty of calculated supercritical densities between 775 K and 825 K. Like all other estimated uncertainties in densities calculated from the EOS, this estimate is illustrated in Fig. 13. Since the discussion of the experimental data that lead to the uncertainty estimates in the liquid and supercritical state region has been quite comprehensive, the representation of these datasets is additionally summarized in Fig. 17.

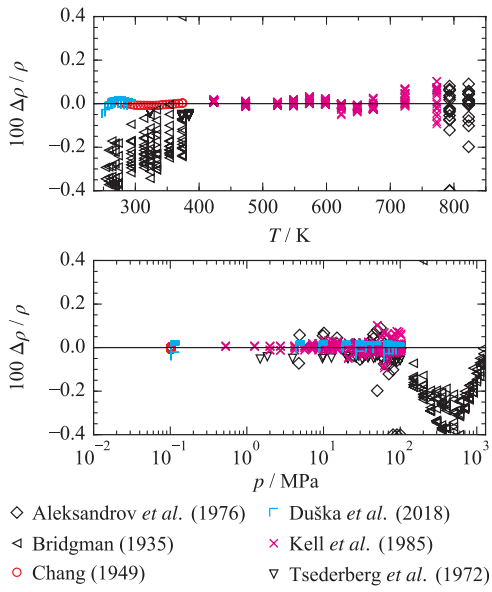

FIG. 17. Top: Relative deviations $\Delta\rho/\rho = (\rho_{exp} - \rho_{calc})/\rho_{exp}$ of selected experimental liquid and supercritical density data from the EOS versus temperature. Bottom: Relative deviations of the selected experimental data from the EOS versus pressure. Depicted are the datasets that lead to the uncertainty estimates for calculated density data in the liquid and supercritical state region as summarized in Fig. 13. Only selected points of the datasets of Bridgman,[34] Tsederberg *et al.*,[100] and Aleksandrov *et al.*[75] are depicted.

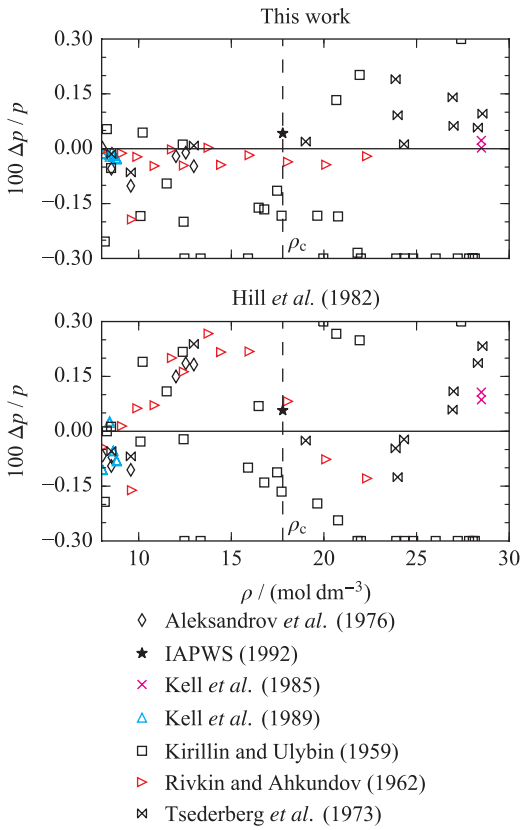

FIG. 18. Top: Relative deviations $\Delta p/p = (p_{exp} - p_{calc})/p_{exp}$ of experimental pvT data in the critical region from the new EOS versus density. The temperature and pressure ranges of the depicted data are $633 < T/K < 724$ and $18.8 < p/MPa < 29.7$. Bottom: Relative deviations of the experimental data from the EOS of Hill *et al.*[11]

For a complete discussion of the homogeneous pvT data, some statements should be made about the accuracy of the EOS in the critical region. In the IAPWS-95 Release for the thermodynamic properties of H_2O, the critical region is bordered by the two isochores 144 kg m^{-3} and 527 kg dm^{-3} and by the 30 MPa isobar.[73] In order to define the critical region of heavy water, we adopted the 30 MPa isobar as the upper pressure limit and transferred the density limits by means of the corresponding-states principle. Thereby, the critical region is bordered by the two isochores 8 mol dm^{-3} and 29 mol dm^{-3}, which yields the triangular temperature and pressure range shown in Fig. 13. The experimental database in this region is quite limited. The available data and their representation by means of the new EOS and the EOS of Hill *et al.*[11] are illustrated in Fig. 18. Within the critical region, very large values of $(\partial\rho/\partial p)_T$ lead to less meaningful deviations in density. Therefore, the deviations shown in Fig. 18 are calculated in terms of pressure at the given temperature and density.

In the critical region, the data of Rivkin and Akhundov[21] and Kell *et al.*[88,89] are considered to be the most reliable, but only the dataset of Rivkin and Akhundov[21] covers densities close to ρ_c. Except for one clear outlier, the entire dataset deviates from the new EOS by less than 0.05% in pressure. The two "high-density" measurements and several "low-density" data points of Kell *et al.*[88,89] are represented within 0.03%. As discussed in Sec. 5.1.1, the new EOS represents the critical pressure recommended by IAPWS[17] within its given uncertainty of about 0.05%. Since this uncertainty is the same order of magnitude as the deviations discussed above, it emphasizes the reliability of these datasets. Based on these deviations, and because the experimental uncertainty of the data is not clearly stated, we conservatively estimate the expanded uncertainty of calculated pvT data to be 0.15% in pressure. In addition to the three datasets discussed above, this estimate also includes the results of Aleksandrov *et al.*[75] that deviate by up to 0.1% in pressure from the new EOS. As mentioned in Secs. 1 and 5.1, IAPWS does not recommend using the previous standard EOS in the vicinity of the critical point.[13] In fact, the data of Rivkin and Akhundov[21] deviate by up to 0.27% from the EOS of Hill *et al.*[11] (see Fig. 18). We therefore conclude that the EOS presented here enables far more reliable calculations of critical-region pvT data than the previous EOS.

5.3. Virial-coefficient data

An overview of the available data for the second virial coefficient B and the third virial coefficient C is given in Table 12. The AAD are calculated for the complete temperature range. Since percentage deviations are less meaningful for virial coefficients, the AAD are given as absolute instead

TABLE 12. Data summary and average absolute deviations of data for the second and third virial coefficients from the EOS

Reference[a]	Year	No. of data	T (K)	Average absolute deviations
Second virial coefficient B (cm³ mol^{-1})				
*Garberoglio *et al.*[112 b]	2018	19	250–2000	1.648
Kell *et al.*[89 c]	1989	31	423–774	1.162
Third virial coefficient C (dm^6 mol^{-2})				
Garberoglio *et al.*[112 d]	2018	4	500–1000	0.002
Kell *et al.*[89 c]	1989	31	423–774	0.0169

[a]Source preceded by * was used for fitting the EOS.
[b]The AAD excludes two data points at 200 K and 225 K where the magnitude of B becomes large. The AAD for all 21 data points is 3.629 cm³ mol^{-1}.
[c]The data supersede the data of Kell *et al.*,[113] which were consequently omitted.
[d]The AAD excludes one data point at 300 K where the magnitude of C is much larger than for other points. The AAD for all 5 data points is 1.785 dm^6 mol^{-2}.

of relative values; these AAD are dominated by the values at the lowest temperatures where the magnitude of the virial coefficients is large.

In most cases, EOS that accurately represent *pvT* data and particularly homogeneous vapor densities also provide reliable values for the virial coefficients. This is logical, since most virial-coefficient data are determined from gas-phase *pvT* measurements that are subsequently described with a virial expansion truncated after the third coefficient. Therefore, most virial-coefficient data are redundant with the underlying *pvT* data and thus not independently valuable for fitting an EOS. For D_2O, experimentally based data for the second and third virial coefficients, B and C, were published by Kell *et al.*[89] The data were determined from the corresponding vapor densities discussed in Sec. 5.2. Because our EOS was extensively fitted to these densities, the virial-coefficient data were not considered additionally in the fit. Instead, the EOS was fitted to the theoretically obtained second virial-coefficient data of Garberoglio *et al.*[112] These $B(T)$ were calculated from a high-quality flexible pair potential[114] with full accounting for quantum effects, agreeing with the available experimental data for both D_2O and H_2O but covering a much wider temperature range. The $B(T)$ data are depicted in the top panel of Fig. 19, which also shows the second virial coefficient calculated from the new EOS and the previous standard EOS as a function of temperature. At high temperatures, the second virial coefficient should become positive and eventually exhibit a maximum before gradually decreasing while remaining positive. At low temperatures, the EOS should yield large negative virial coefficients, corresponding to an attraction-dominated interaction between the molecules. Both the new EOS and the previous EOS exhibit qualitatively correct low-temperature behavior, but the EOS of Hill *et al.*[11] incorrectly produces negative $B(T)$ at high temperatures. The new EOS is in excellent agreement with the recently established theoretical data of Garberoglio *et al.*[112] throughout the temperature range, meaning that its vapor densities can be trusted even at temperatures where no experimental data exist. As discussed in Sec. 4.3, at low temperatures, (heavy) water exhibits a considerably steeper slope of B versus temperature than most other fluids; Fig. 19 shows that the new EOS describes this specific behavior quite accurately.

For the third virial coefficient, values for real fluids become increasingly negative at low temperatures. At higher temperatures, $C(T)$ becomes positive and goes through a maximum before declining but remaining positive. The bottom panel of Fig. 19 shows that the new EOS exhibits the correct qualitative behavior, but the EOS of Hill *et al.*[11] exhibits qualitatively wrong behavior at both low and high

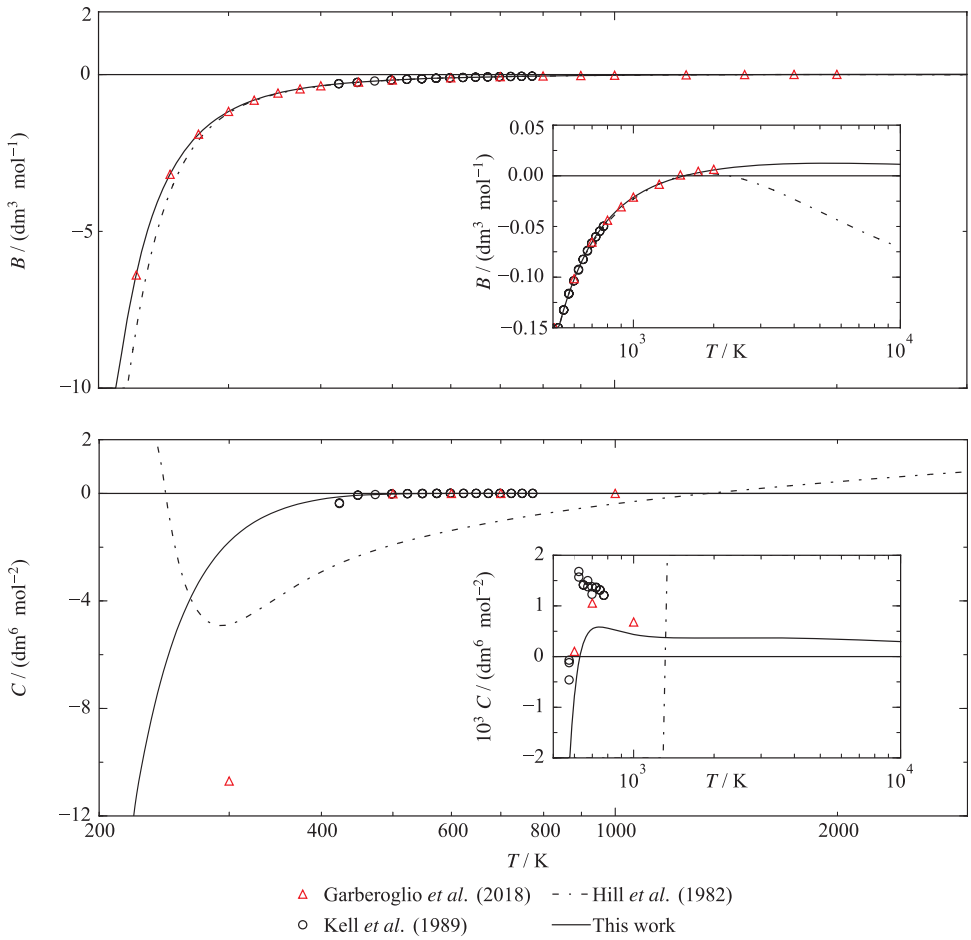

FIG. 19. Top: Second virial coefficient B as a function of temperature as calculated from the new EOS and the EOS of Hill *et al.*[11] The available data are plotted for comparison. Bottom: Third virial coefficient C as a function of temperature as calculated from both EOS; the available data are included for comparison.

temperatures. The only experimental $C(T)$ data for heavy water were again taken from Kell *et al.*,[89] but their uncertainty was not stated. We also plot five points given by Garberoglio *et al.*[112] which were based on high-quality pair[114] and three-body[115] potentials. Unlike with $B(T)$, these theoretical $C(T)$ values are not considered to be highly accurate. Garberoglio *et al.*[112] concluded that the available three-body potentials were inadequate to produce quantitatively accurate $C(T)$. From the bottom panel of Fig. 19, it is apparent that the new EOS is in qualitative agreement with the available data, but there are systematic differences. Since we do not have uncertainty information about either data source, it is not possible to say if these differences are significant.

The accurate representation of the second virial coefficient, including its steep slope at low temperatures, and the qualitatively correct description of C, underscore the exceptionally good extrapolation behavior of our EOS, which is strongly connected to the representation of the so-called ''ideal curves'' as discussed in Sec. 5.6.

5.4. Caloric property data

Caloric property data such as speed of sound or isobaric heat capacity are of special interest in the development and validation of a fundamental EOS. Whereas pvT data only depend on the first derivative of the residual Helmholtz energy with respect to density, caloric properties depend on higher-order derivatives, including temperature derivatives, of both the ideal and residual parts of the Helmholtz energy. Thus, fitting the EOS to such data is essential for the overall functional form including the ideal-gas correlation (see Sec. 4.1). This aspect is particularly interesting with regard to speed-of-sound data, which can be measured with quite low uncertainties. The available caloric property data for heavy water are summarized in Table 13. The given AAD are reported following the conventions presented in Sec. 5.2.

5.4.1. Speed-of-sound data

Compared to the previous EOS of Hill *et al.*,[11] by far the greatest improvement was achieved in the representation of speed-of-sound data. This aspect is highlighted in Fig. 20, which shows deviations of values calculated with both equations from the available experimental data.

For the most accurate datasets by Wegge *et al.*,[129] Fehres and Rudtsch,[121] Aleksandrov and Larkin,[116] and Wilson,[130] the previous EOS deviates from the data by up to 1%, whereas the new EOS describes all relevant data within 0.1% or better. Because the description of the available data by means of the new EOS is so much better than with the EOS of Hill *et al.*,[11] no further discussion of the old EOS is given in this section. Nevertheless, the results of the old EOS are included in Fig. 21.

A highly accurate experimental study of the speed of sound in liquid heavy water was carried out by Wegge *et al.*[129] at Ruhr-Universität Bochum (RUB). The data were specifically obtained to enhance the fitting process of the new EOS. The experimentalists applied the double-path-length pulse-echo technique with a relative combined expanded ($k = 2$) uncertainty of 0.011%. The data range from 278 K to 354 K at pressures up to approximately 20 MPa. The EOS describes all data points within the given uncertainty. Based on these data, we conservatively estimate the combined expanded ($k = 2$) uncertainty of speeds of sound calculated from the EOS to be 0.015% at temperatures from the melting curve up to 355 K and pressures up to 20 MPa. Selected isotherms of the data of Wegge *et al.*[129] are included in Fig. 21, while the complete dataset is shown on a more suitable deviation scale in Fig. 22. Figures 21 and 22 emphasize that the data from RUB are in very good agreement with the most recent and so-far unpublished results of Fehres and Rudtsch.[121] This work was performed at Physikalisch-Technische Bundesanstalt (PTB), Berlin, also applying the pulse-echo technique. The data cover pressures up to about 60 MPa, which exceeds the pressure range investigated by Wegge *et al.*,[129] and temperatures up to 314 K, which is lower than the upper temperature limit in Ref. 129.

The EOS describes all data points of Fehres and Rudtsch within 0.02%. Because the data are unpublished, no concrete results of an uncertainty analysis are available. With regard to their deviations from the EOS, our uncertainty estimate for calculated speeds of sound is 0.02% for temperatures up to 315 K and pressures between 20 MPa and 60 MPa.

At higher pressure, our uncertainty estimate is based on the data of Wilson[130] that cover temperatures and pressures up to 365 K and 97 MPa. The maximum deviation of these data is 0.1% (see Fig. 21). No detailed statement about the uncertainty of the data is given in the corresponding publication. In an earlier work, Wilson studied the speed of sound in ordinary water.[144] In the IAPWS-95 publication, the uncertainty of those data was estimated to be 0.05%.[32] The D_2O data exhibit a maximum offset of about 0.08% from the very accurate data of Fehres and Rudtsch.[121] We therefore assume that an uncertainty estimate of 0.1% is reasonable for Wilson's data and adopt this as the estimated uncertainty of sound speeds calculated from the EOS at temperatures from the melting curve up to 365 K and pressures between 60 MPa and 100 MPa. All estimated uncertainties in calculated sound speeds are summarized in Fig. 23.

After this work was completed, we learned of new sound-speed measurements of Lago and Giuliano Albo[126] at temperatures from 277 K to 363 K and pressures up to 210 MPa. Comparisons to these data are shown in Figs. 20 and 21. At and below 100 MPa, these data confirm our uncertainty estimates and the data sources on which we based those estimates. At higher pressures, where there were previously no experimental data that we could use in fitting, there is a small systematic deviation between our EOS and these new data, with the EOS sound speeds higher than the data by up to 0.36% at the highest pressure.

Figure 23 shows that for the rest of the liquid phase, excluding the critical region, the uncertainty estimate is 0.1%. This estimate is based on the representation of the 1977 data of Aleksandrov and Larkin.[116] The data range from the melting curve up to 649 K at pressures up to 72 MPa. Deviations between the EOS and almost all data points are below 0.1%, except for some measurements close to the phase

TABLE 13. Data summary and average absolute relative deviations of experimental data for caloric properties from the EOS. Clear outliers were not considered in the AAD

					Average absolute relative deviations in %						
								Supercritical fluid			
Reference[a]	Year	No. of data	T (K)	p (MPa)	Gas	Liquid	Crit. Reg.	LD[b]	MD[b]	HD[b]	Overall
Speed of sound w											
*Aleksandrov and Larkin[116]	1977	176	271–649	0.1–72	...	0.057	1.878	1.281	1.453	0.041	0.091
Aleksandrov and Larkin[117]	1978	15	277–374	0.1	...	0.011	...	...	...	...	0.011
*Chen and Millero[118]	1977	132	277–334	0.1–100	...	0.024	...	...	...	0.051	0.041
Conde *et al.*[119]	1982	32	259–357	0.1	...	0.651	...	...	...	...	0.651
Erokhin and Kompaniets[55]	1980	38	433–644	Sat.	0.290	1.048	...	...	...	...	0.689
Evsteefev *et al.*[120]	1979	139	423–574	0.1–12	...	0.600	...	...	...	...	0.600
*Fehres and Rudtsch[121]	2017	100	278–314	0.1–60	...	0.011	...	...	...	0.008	0.010
Fine and Millero[122]	1975	18	277–364	0.1	...	0.037	...	...	...	...	0.037
Gupta *et al.*[123]	1976	15	280–354	0.1	...	0.307	...	...	...	...	0.307
Heusinger[124]	1949	10	278–364	0.1	...	0.236	...	...	...	...	0.236
Ivanov *et al.*[125]	2009	4	283–339	0.1	...	0.050	...	...	...	...	0.050
Lago and Giuliano Albo[126]	2018	72	276–364	0.2–211	...	0.036	...	...	...	0.112	0.097
Marczak[91]	1999	5	293–314	0.1	...	0.031	...	...	...	...	0.031
McMillan and Lagemann[127]	1947	9	278–334	0.1	...	0.282	...	...	...	...	0.282
Pancholy[128]	1953	14	278–364	0.1	...	0.716	...	...	...	...	0.716
*Wegge *et al.*[129]	2016	72	278–354	0.1–21	...	0.006	...	...	...	...	0.006
*Wilson[130]	1961	136	277–365	0.1–97	...	0.031	...	...	...	0.051	0.046
Isobaric heat capacity c_p											
*Angell *et al.*[131]	1982	30	240–291	0.1	...	1.484	...	...	...	...	1.484
*Eucken and Eigen[132]	1951	12	292–398	Sat.	...	0.457	...	...	...	...	0.457
Long and Kemp[38]	1936	4	279–296	0.1	...	0.996	...	...	...	...	0.996
Rivkin and Egorov[133 c]	1959	28	293–574	4.9-10	...	0.184	...	...	...	...	0.184
Rivkin and Egorov[134]	1962	133	530–728	22.1-30	...	...	3.010	1.257	2.183	0.584	1.931
Rivkin and Egorov[135]	1963	100	464–729	9.8–25	1.106	0.539	3.993	1.741	1.894	0.708	1.194
*Rivkin and Egorov[136 d]	1963	293	293–724	4.9–30	1.086	0.348	2.425	1.484	2.046	0.353	0.668
*Smirnova *et al.*[137]	2006	34	274–351	0.1	...	0.649	...	...	...	...	0.649
Isochoric heat capacity c_v											
Amirkhanov *et al.*[138]	1975	275	294-743	0.002-77	...	2.474	4.731	...	1.813	5.274	3.261
*Mursalov *et al.*[71]	1999	636	294-747	0.002-76	3.377	2.497	5.091	3.396	1.728	4.984	3.543
Mursalov *et al.*[71]	1999	23	294-644	Sat.	11.228	5.390	...	...	...	...	7.674
*Polikhronidi *et al.*[139 e]	2002	115	639-672	20.5-31	...	6.069	8.089	...	...	...	7.931
Joule-Thomson coefficient μ_{JT}											
Jůza *et al.*[86 f]	1966	27	423-444	0.11-0.17	3.727	...	...	...	...	...	3.727

[a]Sources preceded by * were used for fitting the EOS.
[b]LD: $\rho/\rho_c < 0.6$; MD: $0.6 \leq \rho/\rho_c \leq 1.5$; and HD: $\rho/\rho_c > 1.5$.
[c]A translated version was published in 1961 by Rivkin and Egorov.[140]
[d]A translated version was published in 1964 by Rivkin and Egorov.[141]
[e]The data supersede the earlier data of Polikhronidi *et al.*[142]
[f]As shown by Ertle[143] for H_2O, the data of Jůza *et al.*[86] are missing a correction for a "heat leakage" of the experimental setup. The data were not relevant for fitting the EOS and thus are not further discussed in this article.

boundary, where the experiment might have been carried out in the two-phase region, and a few data points in the critical region. The data are shown in Figs. 20 and 21; the critical-region data are also depicted separately in Fig. 24.

Figure 24 shows that the critical-region data of Aleksandrov and Larkin[116] are represented within 3%, which we adopt as the uncertainty of calculated sound speeds in the critical region (as defined in Sec. 5.2). However, in the vicinity of the critical point, the speed of sound decreases steeply and should, in theory, be zero at the critical point. Since the EOS does not allow for the description of this phenomenon, the uncertainty of calculated sound speeds is larger than 3% in the vicinity of the critical point (see Fig. 23). The description of the physical behavior in the critical region is discussed in more detail in Sec. 5.6. Figure 24 also includes the data of Erokhin and Kompaniets[55] that were measured along the dew and bubble curves. This dataset is the only experimental investigation of the speed of sound at saturation. In the critical region, the data deviate by about 4% from the EOS, whereas Fig. 20 illustrates that the majority of the data down to 433 K is represented within 0.5%, which is also the approximate scatter of the data. Due to the lack of comparative data from other sources, no definitive uncertainty estimate for calculated sound speeds at saturation is possible. As discussed for density in Sec. 5.1.2, the uncertainty in sound speed for the saturated liquid should be similar to that in the

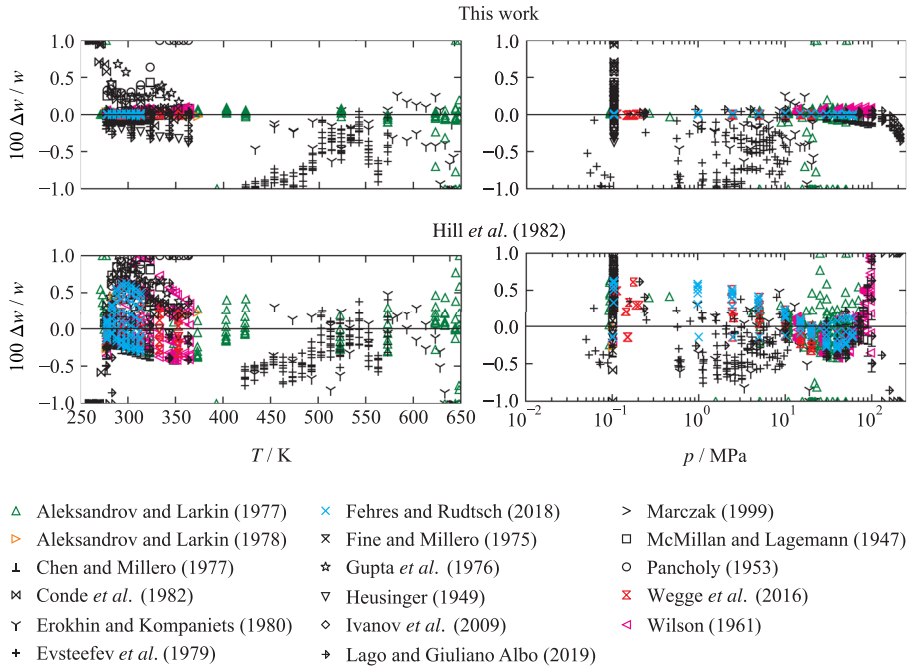

FIG. 20. Top: Relative deviations $\Delta w/w = (w_{exp} - w_{calc})/w_{exp}$ of experimental speed-of-sound data from the new EOS versus temperature (left) and pressure (right). Bottom: Relative deviations of experimental speed-of-sound data from the equation of Hill *et al.*[11]

adjacent homogeneous liquid region. No experimental data for the speed of sound in heavy water vapor are available, and therefore Fig. 23 shows that no definitive estimate of uncertainty can be made in this region. However, we note that, at low pressures, the uncertainty of calculated values is small, since the vapor approaches the ideal-gas state that is described accurately (see Sec. 4.1) due to the high-accuracy c_p^o data.

5.4.2. Heat-capacity data

The experimental database for other caloric properties is much less satisfactory than for the speed of sound. Aside from one dataset with Joule-Thomson coefficients, which is not accurate enough to contribute to the fitting process, some data on the isochoric and isobaric heat capacities are available. Since the isochoric heat-capacity data exhibit relatively large uncertainties and inconsistencies, only the isobaric heat-capacity data were relevant during the fitting of the present EOS. Nevertheless, these data also have higher uncertainties than desired. Consequently, the equation was fitted only to a careful selection of low-weighted data points in order to reach at least a representation of the data within their estimated experimental uncertainties.

5.4.2.1. Isobaric heat-capacity data

An overview of the experimental isobaric heat capacities and their deviations from values calculated from the new EOS and the previous standard EOS is shown in Fig. 25.

The data cover almost the entire temperature range of validity of the EOS. The high-temperature data range up to approximately 730 K. The lowest isotherms were investigated below the triple point and thus within the metastable subcooled liquid region (see Sec. 5.5). Most of the measurements were carried out in the liquid phase at pressures up to 30 MPa. The vapor phase was only investigated at pressures above 15 MPa and temperatures higher than 620 K. The large majority of the experimental data was obtained by Rivkin and Egorov between 1959 and 1963.[133–136] The first dataset published in 1959 contains measurements of the liquid phase at temperatures between 293 K and 574 K at pressures up to 10 MPa,[133] whereas the publication from 1962 presents measurements of the critical and supercritical regions between 530 K and 728 K and higher pressures between 22.1 MPa and 30 MPa.[134] In 1963, Rivkin and Egorov published two further articles: one presenting new data at temperatures between 464 K and 729 K and pressures between 9.8 MPa and 25 MPa[135] and another one that seems to supersede all prior publications.[136] Reference 136 presents data at temperatures from 293 K to 723 K at pressures between 4.9 MPa and 30 MPa, and it also includes a few vapor-phase data points at pressures starting at approximately 15 MPa. We could not clarify the chronological order of the two publications from 1963, since neither of them is cited by the other. However, we assume that the values in Ref. 136, which also presents the most comprehensive dataset, can be considered as Rivkin's and Egorov's final values of the isobaric heat capacity of heavy water. In this publication, the authors claim that the maximum error of their measurements is 0.35% for the liquid and vapor at a certain distance from the saturation curve and within 1% or 2% close to saturation or near the maximum heat capacity along the supercritical isobars. We assume that these error estimates are underestimated and also not equivalent to combined expanded uncertainties. The EOS clearly represents all liquid-phase data within 1%, excluding the critical region. We adopt this as the estimated uncertainty of

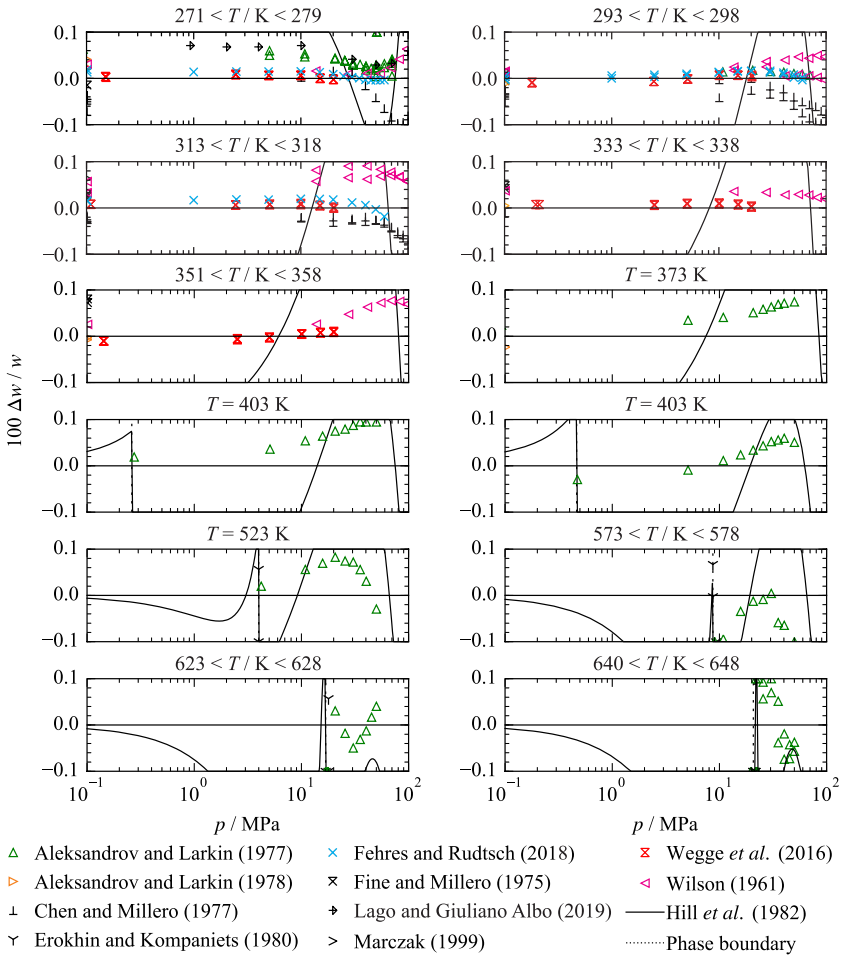

FIG. 21. Relative deviations $\Delta w/w = (w_{exp} - w_{calc})/w_{exp}$ of selected experimental speed-of-sound data along (quasi-)isotherms from the new EOS. The EOS of Hill *et al.*[11] is plotted for comparison. For plots showing a temperature range, the EOS of Hill *et al.*[11] was calculated at the average temperature.

calculated isobaric heat capacities in the liquid phase at pressures up to 30 MPa. Although this uncertainty estimate might be conservative with regard to the deviations of the data, it is reasonable because no experimental data from other sources are available. The 1% uncertainty estimate can be extended to temperatures below 293 K as investigated by Rivkin and Egorov, since the EOS was fitted to extremely accurate speed-of-sound data in this state region (see Sec. 5.4.1). The available experimental heat-capacity data at temperatures below 293 K are of lower accuracy and limited to atmospheric pressure.[38,131,137]

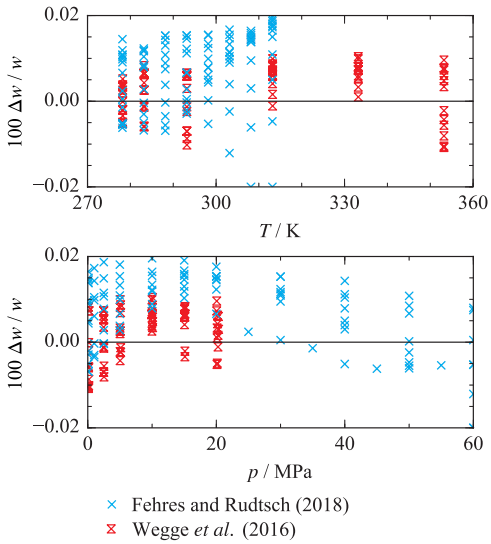

FIG. 22. Top: Relative deviations $\Delta w/w = (w_{exp} - w_{calc})/w_{exp}$ of the experimental speed-of-sound data of Wegge *et al.*[129] and Fehres and Rudtsch[121] from the EOS versus temperature. Bottom: Relative deviations of the experimental data from the EOS versus pressure.

The EOS represents the few vapor-phase measurements of Rivkin and Egorov[135,136] within maximum deviations of approximately 3% (AAD of 1.1%), which we adopt as the estimated uncertainty of calculated isobaric heat capacities of the vapor phase at pressures above 15 MPa and temperatures between T_{sat}(15 MPa) ≈ 614 K and 730 K. At lower pressures and temperatures, no definitive uncertainty estimates for calculated isobaric heat capacities are possible because no experimental data are available. Nevertheless, we note that with decreasing pressures the uncertainty approaches the uncertainty of the ideal-gas heat capacity, which is less than 0.02% as discussed in Sec. 4.1.

The critical-region data of Rivkin and Egorov[134–136] are shown in Fig. 26. The EOS describes the majority of the data within about 5%. In fact, the two newer datasets from 1963 are mainly represented within about 3%. However, we define 5% as a reasonable uncertainty estimate for calculated

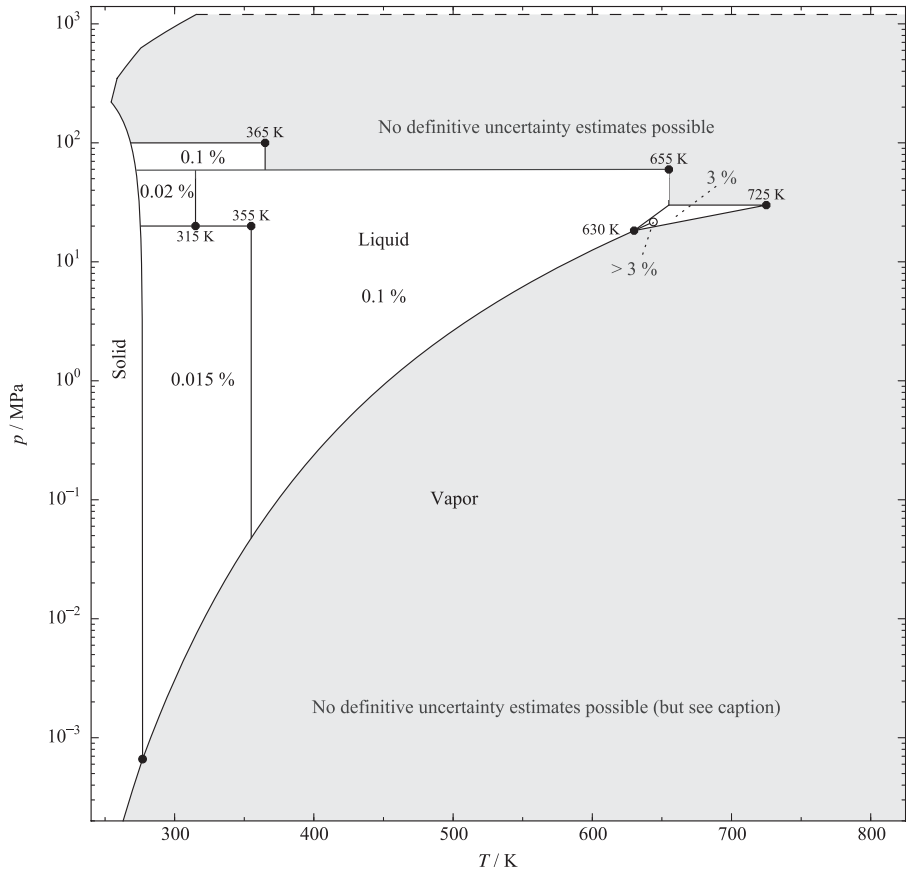

FIG. 23. Expanded relative uncertainties in speed of sound, $\Delta w/w$, estimated for the EOS. For the definition of the triangle around the critical point, see the caption of Fig. 13. The positions of the lines separating the uncertainty regions are approximate. At low pressures for the vapor, the uncertainty becomes small because the vapor approaches the ideal-gas limit.

isobaric heat capacities in the critical region. The uncertainty will be larger in the immediate vicinity of the critical point, where c_p increases toward infinity.

Isobaric heat capacities of the saturated liquid were published by Eucken and Eigen,[132] who claim a relative experimental uncertainty of 0.15%. However, this uncertainty seems to be underestimated. The EOS describes the data within a maximum deviation of 0.76%. Further fitting of the data led to a worse description of some homogeneous liquid-phase data such as the highly accurate speed-of-sound data (see Sec. 5.4.1)

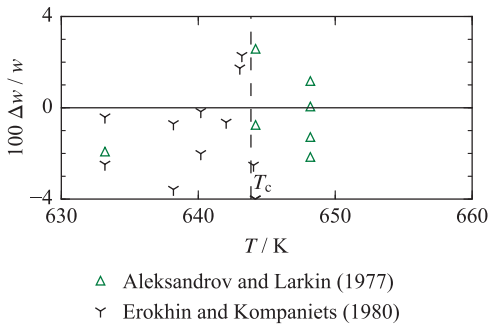

FIG. 24. Relative deviations $\Delta w/w = (w_{exp} - w_{calc})/w_{exp}$ of the available experimental speed-of-sound data in the critical region from the EOS versus temperature. The density and pressure range of the depicted data is $8.5 < \rho/(\text{mol dm}^{-3}) < 28.4$ and $19.0 < p/\text{MPa} < 25.6$.

or the density data at atmospheric pressure. Since no comparative data are available, we do not provide a concrete uncertainty estimate for isobaric heat capacities at saturation, but the uncertainties should be similar to that in the adjacent single-phase region. All other results of the uncertainty analysis discussed in this section are illustrated in Fig. 27.

Some comments should be made on comparisons between isobaric heat capacities calculated from the new EOS and from the previous standard EOS of Hill *et al.*[11] Figure 25 shows that the new EOS represents the stable liquid-phase data at temperatures up to about 500 K more consistently than the old EOS. However, the differences between calculated values are mostly within the 1% uncertainty estimate. The same applies for the gas phase, where calculated values agree within our uncertainty estimate of 3%. In the critical region, as shown in Fig. 26, the new EOS represents a better compromise among all available data. In addition, considerably more data points exhibit deviations above 5% from the old EOS than from the one presented in this work.

5.4.2.2. Isochoric heat-capacity data

Figure 28 shows that there is a considerable amount of experimental data for the isochoric heat capacity, covering the liquid phase as well as the critical and supercritical regions. The complete database was measured at the Dagestan

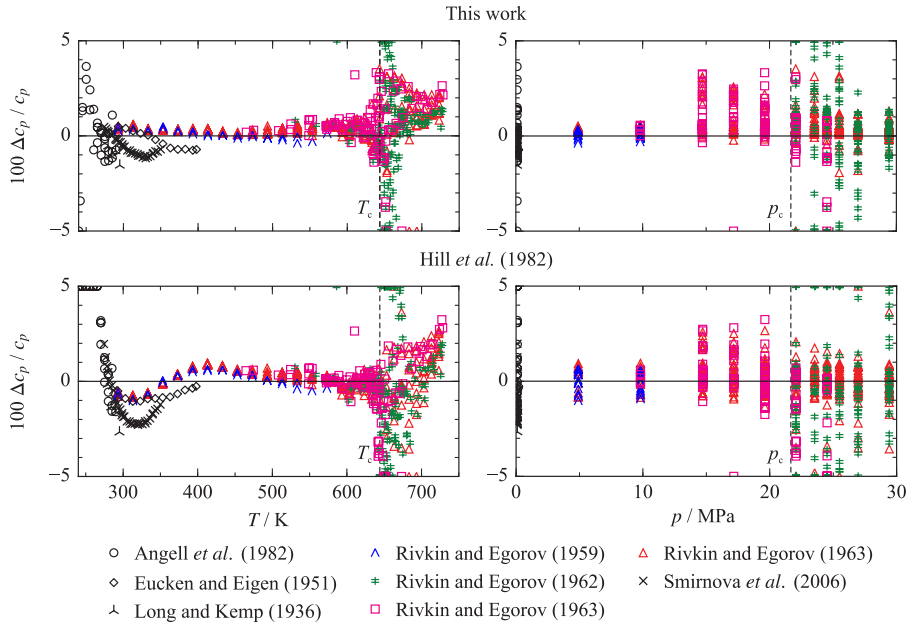

FIG. 25. Top: Relative deviations $\Delta c_p/c_p = (c_{p,\mathrm{exp}} - c_{p,\mathrm{calc}})/c_{p,\mathrm{exp}}$ of experimental isobaric heat-capacity data from the new EOS versus temperature (left) and pressure (right). Bottom: Relative deviations of experimental isobaric heat-capacity data from the equation of Hill *et al.*[11]

Scientific Center of the Russian Academy of Sciences. The earliest study of Amirkhanov *et al.*[138] was superseded and extended by the work of Mursalov *et al.*[71] Subsequently, Polikhronidi *et al.*[139] investigated the critical region more intensively. Figure 28 shows that Ref. 139 also presents some data points in the vapor–liquid equilibrium region. These are results for the overall heat capacity of the two-phase system in the measuring cell instead of separate results for the coexisting saturated liquid and vapor states. During the fitting process, these data always exhibited quite large deviations from the EOS. We therefore assumed relatively high experimental uncertainties and thus omitted these data. Deviations of the single-phase isochoric heat-capacity data are shown in Fig. 29, and the two-phase data are shown in Fig. 30.

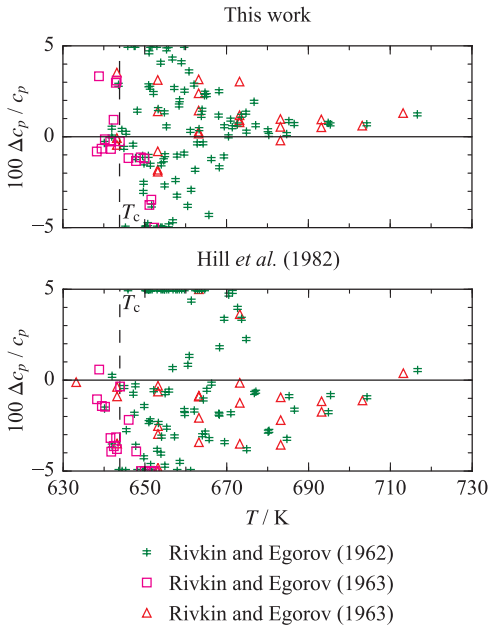

FIG. 26. Top: Relative deviations $\Delta c_p/c_p = (c_{p,\mathrm{exp}} - c_{p,\mathrm{calc}})/c_{p,\mathrm{exp}}$ of experimental isobaric heat-capacity data in the critical region from the new EOS versus temperature. The density and pressure range of the depicted data is $8.1 < \rho/(\mathrm{mol\ dm^{-3}}) < 29.0$ and $19.6 < p/\mathrm{MPa} < 29.5$ MPa. Bottom: Relative deviations of experimental isobaric heat-capacity data from the equation of Hill *et al.*[11]

The top panel of Fig. 29 shows that the available experimental data exhibit fairly large deviations from the new EOS, which could never be significantly reduced during the fitting process. In order to get an impression of the quality of the available data, we compared the experimental results of Amirkhanov *et al.*[145] for ordinary water with the IAPWS-95 formulation. The results are shown in the bottom panel of Fig. 29. At temperatures up to about 525 K, the data agree with IAPWS-95 within about 5%. With increasing temperatures, these deviations increase to 10% or even higher in the critical region. In the IAPWS-95 publication, Wagner and Pruß[32] stated that, due to the relatively large uncertainties and inconsistencies in the data measured at the Dagestan Scientific Center, none of these points was used to develop the IAPWS-95 formulation. Instead, the EOS was fitted to limited data from other sources. This statement agrees with our findings. The new EOS for D_2O was therefore only fitted with low weight to a small number of data points taken from the work of Mursalov *et al.*[71] and Polikhronidi *et al.*[139]

At temperatures up to about 550 K, the new EOS represents the available liquid-phase data mostly within 5%. As discussed in Secs. 5.4.1 and 5.4.2.1, the EOS is clearly more accurate in the representation of the available speed-of-sound and isobaric heat-capacity data in this region. Therefore, we assume that the uncertainty of calculated isochoric heat capacities in the liquid phase is less than 5% at temperatures up to 550 K. Over the rest of the fluid surface, the quality of the experimental data does not allow any uncertainty estimates. Nevertheless, we once again note that in the vapor phase and

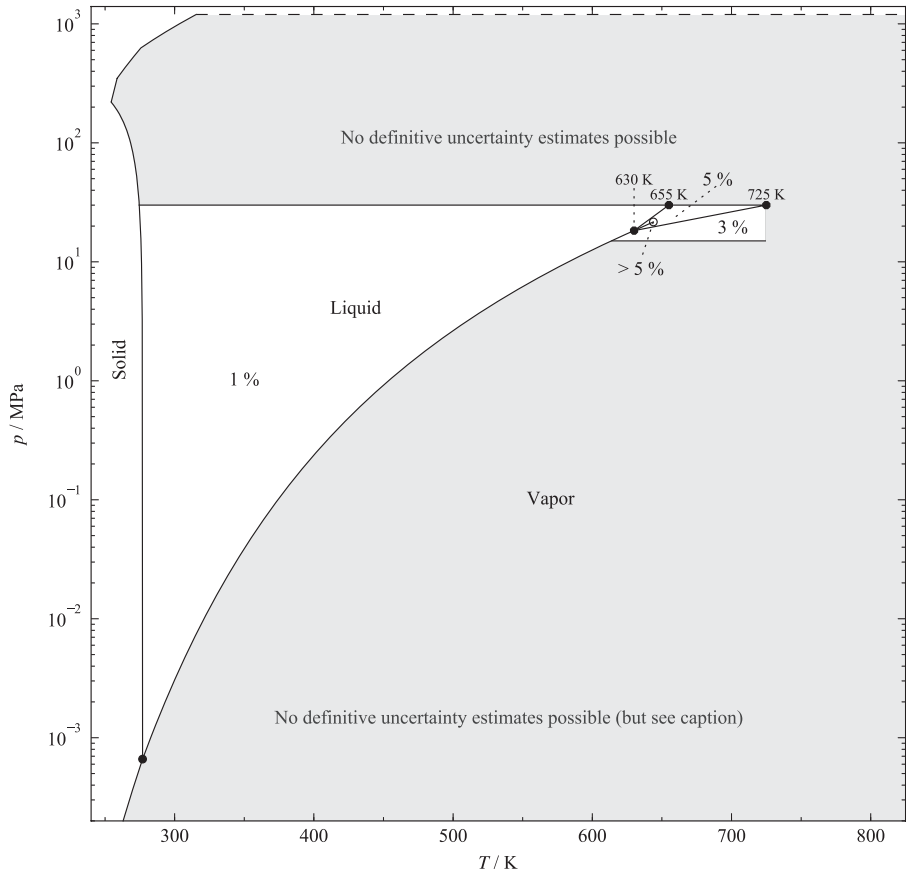

FIG. 27. Expanded relative uncertainties in isobaric heat capacity, $\Delta c_p/c_p$, estimated for the EOS. For the definition of the triangle around the critical point, see the caption of Fig. 13. The positions of the lines separating the uncertainty regions are approximate. The uncertainty in the vapor phase at low pressures approaches the uncertainty of the ideal-gas heat capacity, which is less than 0.02% as discussed in Sec. 4.1.

at low pressures the uncertainty becomes small, since the EOS is essentially defined by the ideal-gas part α^o (see Sec. 4.1).

As previously mentioned, the two-phase data of Polikhronidi *et al.*[139] deviate considerably from our EOS (see Fig. 30),

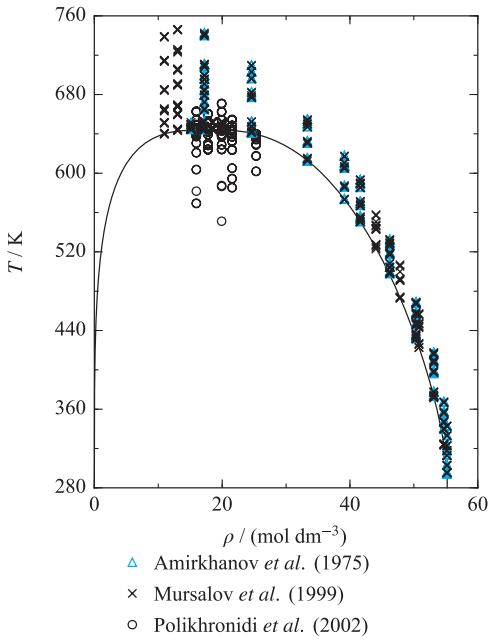

FIG. 28. Distribution of the available experimental isochoric heat-capacity data in a T, ρ diagram.

which we explain by potentially higher uncertainties of these data. Thus, we do not provide an uncertainty estimate for the calculated overall isochoric heat capacities of the two-phase system.

Deviations of the isochoric heat capacity of the saturated liquid and vapor as measured by Mursalov *et al.*[71] from the EOS are shown in Fig. 31. The saturated-vapor data exhibit maximum deviations of about 5% at temperatures below 640 K, whereas the saturated-liquid data are represented within about 1.8% for temperatures up to 612 K. At higher temperatures, the deviations for the saturated-liquid data increase to almost 40%. These extremely high deviations result from critical phenomena that are only qualitatively described by the EOS. In theory, the isochoric heat capacity should become infinite at the critical point. Because the functional form of the EOS does not include special provisions for incorporating nonclassical critical phenomena, it does not represent the nonanalytic effects at the critical point (see Sec. 5.6).

Due to the large deviations between the experimental isochoric heat capacities and calculated values, comparisons between the new EOS and the EOS of Hill *et al.*[11] are less meaningful and are consequently not presented in this section. We note that the deviations of the data from the old EOS are largely comparable to those presented here. In their publication, Hill *et al.* discuss the same limitations of describing critical phenomena with the use of an analytical functional form as we did above.

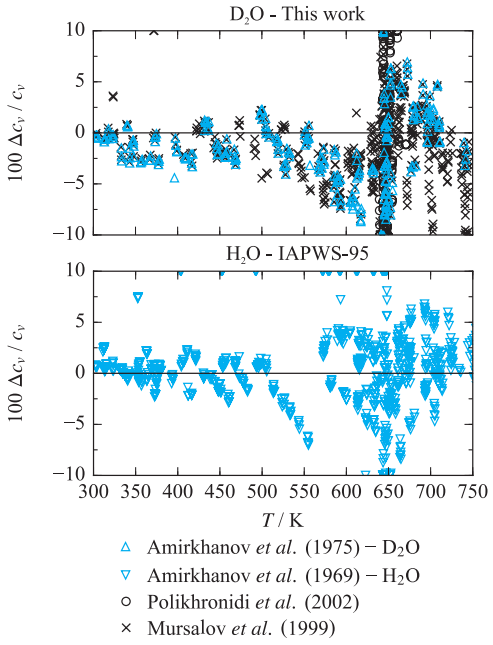

FIG. 29. Top: Relative deviations $\Delta c_v/c_v = (c_{v,\mathrm{exp}} - c_{v,\mathrm{calc}})/c_{v,\mathrm{exp}}$ of experimental isochoric heat-capacity data for D_2O from the new EOS versus temperature. Bottom: Relative deviations of experimental isochoric heat-capacity data for H_2O from the IAPWS-95 formulation.[32,73]

5.5. Data at metastable states

The fluid surface includes three metastable regions: the subcooled liquid (metastable with respect to the solid), the superheated liquid (metastable with respect to the vapor), and the subcooled vapor (metastable with respect to the liquid or solid). Except for one dataset for the speed of sound in the superheated liquid,[120] all experimental studies are focused on the subcooled liquid. To our knowledge, there are no experimental data in the subcooled vapor region, although at low and moderate pressures it should be described accurately if the second and third virial coefficients (see Sec. 5.3) are accurate.

The speed of sound in the superheated liquid region was investigated by Evstefeev *et al.*[120] in the temperature range from 423 K to 573 K. Unfortunately, these data are only graphically given in the corresponding publication and the underlying experimental results are no longer available. Thus, we extracted the data from the figure in the article.

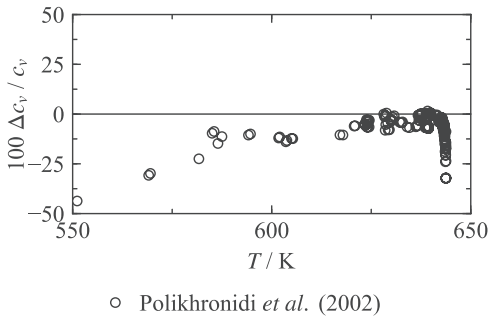

FIG. 30. Relative deviations $\Delta c_v/c_v = (c_{v,\mathrm{exp}} - c_{v,\mathrm{calc}})/c_{v,\mathrm{exp}}$ of the experimental isochoric heat-capacity data of Polikhronidi *et al.*[139] in the two-phase region from the EOS versus temperature.

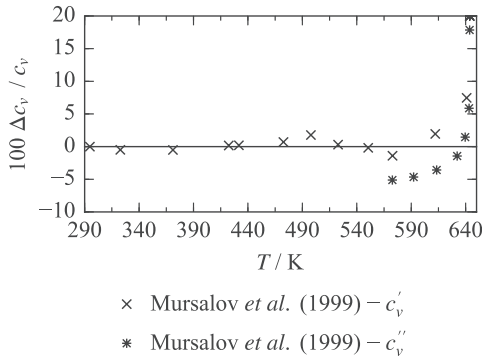

FIG. 31. Relative deviations $\Delta c_v/c_v = (c_{v,\mathrm{exp}} - c_{v,\mathrm{calc}})/c_{v,\mathrm{exp}}$ of the experimental isochoric heat-capacity data of Mursalov *et al.*[71] at saturation from the EOS versus temperature.

Comparisons between the experimental uncertainty of these data and their deviations from our EOS are consequently of limited value because considerable additional uncertainty was added by the graphical determination. Nevertheless, the authors state a "total error" of approximately 0.2%, which we assume should not be equated with the combined expanded uncertainty of the data. Deviations of the data from the EOS are shown in Fig. 20. The EOS represents the majority of the graphically determined data within 1%. The data at temperatures above 493 K are in better agreement with the EOS than the results along the lower isotherms. The distribution of the data in relation to the saturation curve is illustrated in Fig. 32. Since the measurements were carried out along isotherms, the degree of superheating is not obvious. The largest difference between the saturation pressure and the pressure investigated occurs at 503 K and is equivalent to a superheating of approximately 130 K.

At lower temperatures, the offset between the data of Evstefeev *et al.*[120] and sound speeds calculated from the EOS is quite evident. In the stable liquid region at temperatures between 423 K and 523 K, the EOS was fitted to the accurate data of Aleksandrov and Larkin,[116] which are represented

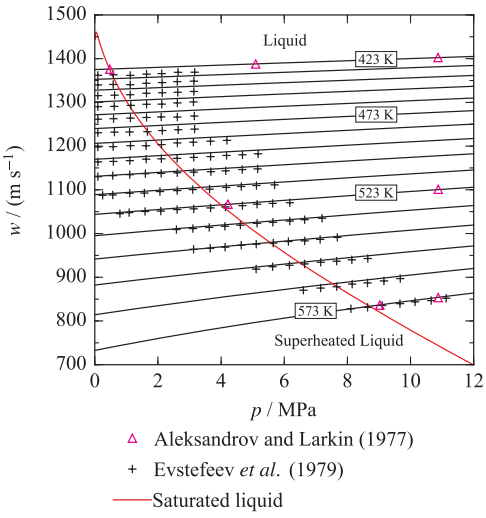

FIG. 32. Speed of sound along isotherms as a function of pressure in the metastable superheated and stable liquid region as calculated from the EOS. The experimental data of Evstefeev *et al.*[120] and Aleksandrov and Larkin[116] are plotted for comparisons.

within 0.1% (see Sec. 5.4.1). For comparison, some of these data points are included in Fig. 32. At 423 K, they deviate considerably from the results of Evstefeev *et al.*[120] We cannot clarify whether the results presented in Ref. 120 are of significantly less accuracy or whether these deviations are a result of the graphical determination of the data. Nevertheless, Fig. 32 indicates that the EOS allows for a qualitatively and, to a certain extent, also quantitatively correct description of the metastable superheated liquid region. Figure 20 shows that the previous reference EOS of Hill *et al.*[11] is in surprisingly good agreement with Evstefeev's data. The data deviate by less than 0.8% from values calculated from Hill's EOS. However, Hill did not discuss or cite the data of Evstefeev *et al.*[120] in his publication. In addition to this, and as discussed in Sec. 5.4.1, our EOS enables a significantly more accurate description of the speed-of-sound data in the stable liquid. Thus, we assume that the good agreement between the old EOS and the superheated-liquid data is coincidental.

In recent years, the thermodynamics of metastable subcooled (also referred to as "supercooled") water has been a very active scientific subject. Aside from its relevance for the understanding of meteorological phenomena such as cloud formation, its thermodynamic properties are important for the modeling of seawater and other aqueous mixtures, where the employed models for water are often evaluated below the pure-water freezing temperature. The most important IAPWS-associated work in this field is the EOS for supercooled water published by Holten *et al.*,[146] which also led to an IAPWS Guideline on this topic.[147] This guideline is for the thermodynamic properties of H_2O and does not include any information on D_2O. Nevertheless, an EOS for subcooled heavy water was published by Holten *et al.*[148] within the supplement of an article presenting a preliminary version of the EOS for ordinary water. Because the range of validity of our new EOS is officially limited to stable states at temperatures above the minimum temperature along the melting curve, we do not present detailed comparisons with the EOS of Holten *et al.*,[148] which was exclusively developed for the small temperature range of the subcooled liquid. Nevertheless, we carefully studied their work in order to identify the most reliable datasets that enabled a reasonable extrapolation of our EOS below its lower temperature limit.

In addition to the theoretical work of Holten and collaborators, there are some experimental activities on subcooled light and heavy water within IAPWS. In Sec. 5.2, we discussed the highly accurate density measurements of Duška *et al.*,[79] which cover both the stable liquid at low temperatures and the metastable subcooled liquid at pressures up to 100 MPa. Measurements of the vapor pressure of subcooled heavy water are currently being carried out at the Italian National Institute of Metrological Research (INRiM), Turin, but were not completed prior to the development of our EOS. Thus, the most recent and [with an expanded ($k = 2$) uncertainty of 0.04%] also most accurate experimental data are the densities of Duška *et al.*[79] Deviations of these data from the values calculated from the EOS are shown in Fig. 33, which additionally presents data from other sources. In order to get a better impression of the accuracy of these experimental studies, Fig. 33 presents the data in not only the metastable but, if investigated, also in the stable liquid region. Due to the negative slope of the melting-pressure curve of (heavy) water (see Sec. 3.4), it can be difficult to see the magnitude of subcooling of the data when plotted against absolute temperature. Therefore, we have calculated the corresponding melting temperature for every data point at its investigated pressure from Eq. (4). This allows us to plot the deviations in

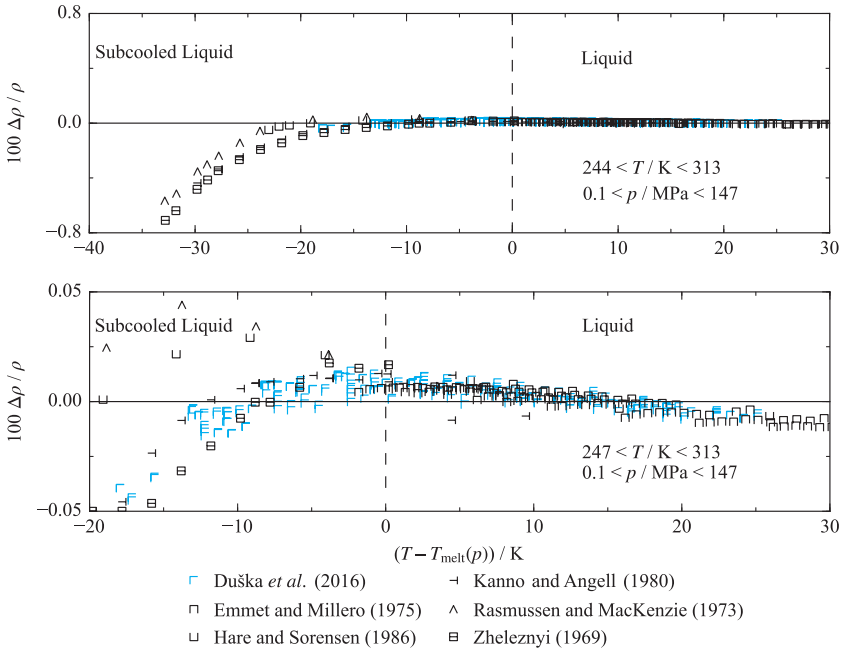

FIG. 33. Top: Relative deviations $\Delta\rho/\rho = (\rho_{exp} - \rho_{calc})/\rho_{exp}$ of the experimental density data in the metastable subcooled liquid and in the stable liquid region from the EOS. The deviations are plotted versus the difference between the measured temperature and the melting temperature at the given pressure calculated from Eq. (4). Bottom: Relative deviations of the most accurate experimental data from the EOS on a much smaller scale.

Fig. 33 against the difference between the measured temperature and the melting temperature.

Except for two data points at a subcooling of about 17 K (absolute temperature of 255 K), our EOS represents the complete dataset of Duška *et al.*[79] within its experimental uncertainty of 0.04%. Thus, we estimate that the uncertainty of calculated densities of the subcooled liquid at temperatures from the melting curve down to 260 K and at pressures up to 100 MPa is 0.04%. This temperature range is equivalent to a maximum subcooling of about 18 K. Due to the high reliability of Duška's data, we include the 0.04% uncertainty estimate in Fig. 13, although the data are beyond the official range of validity of the EOS. As is evident from the top panel of Fig. 33, three experimental studies investigated even deeper states of subcooling. Kanno and Angell[87] measured densities down to 247 K (subcooling of 30 K), whereas Zheleznyi[102] and Rasmussen and MacKenzie[94] made measurements at about 244 K (subcooling of 33 K), which is stated to be close to the homogeneous nucleation temperature, which is the natural limit of subcooling. All these experiments were carried out at atmospheric pressure. The corresponding publications do not provide any useful information about experimental uncertainties. Thus, we can only state that the new EOS describes all these data within 0.8%, which is not necessarily equivalent to the uncertainty of calculated densities in this temperature range. The EOS of Hill *et al.*[11] is not valid at temperatures below the triple point. Nevertheless, we could reasonably extrapolate the EOS and calculate densities of the subcooled liquid. At 260 K, these calculated densities deviate by about 0.25% from the data of Duška *et al.*;[79] the data at deeper states of subcooling exhibit deviations of up to 2.2%.

The vapor pressure of the subcooled liquid is reported in two experimental studies by Bottomley[41] and Kraus and Greer.[61] The data were already mentioned briefly in Sec. 5.1.1 and are included in Fig. 8, which shows deviations of all available vapor-pressure data from the EOS. A more detailed presentation of these two datasets is given in Fig. 34.

The top panel of Fig. 34 shows the distribution of the experimental vapor pressures of the subcooled liquid in relation to the phase boundaries that separate liquid, vapor, and solid states. It might be difficult to imagine the vapor pressure of a subcooled liquid. Thus, the experimental procedure for measuring this property is worth summarizing. A measuring cell is filled with an extremely pure water sample and then repeatedly frozen, degassed in vacuum, and re-liquefied. After this preparation, the water sample is in vapor–liquid equilibrium and thus at its saturation pressure. The sample can be subcooled below the triple-point temperature while the corresponding pressure is always equivalent to the vapor pressure. The pressures thus obtained follow the vapor-pressure curve extended to temperatures below the triple-point temperature. As is apparent from the top panel of Fig. 34, this "extrapolation" of the vapor-pressure curve exhibits a considerable difference from the sublimation-pressure curve; the difference in slope is related to the difference between the enthalpy of vaporization of the liquid and the enthalpy of sublimation of the solid. Bottomley[41] reported

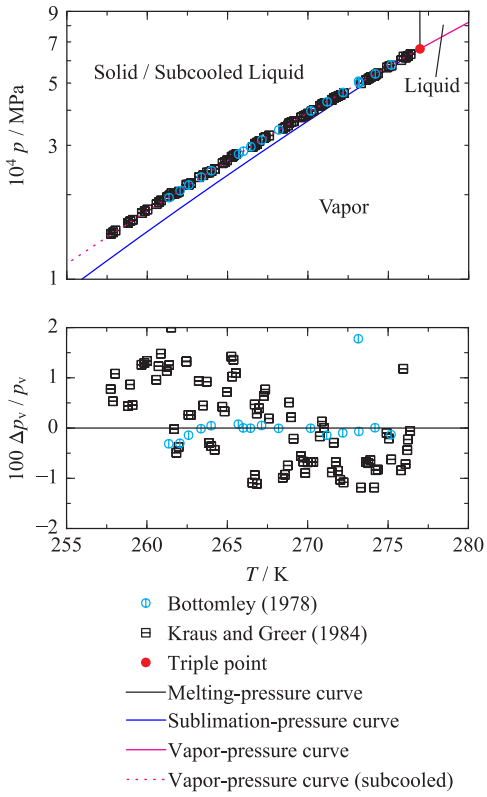

FIG. 34. Top: Available experimental data for the vapor pressure of the metastable subcooled liquid in a p, T diagram. The vapor-pressure curve is calculated with the EOS. The sublimation- and melting-pressure curves are obtained from Eqs. (4) and (9), respectively. Bottom: Relative deviations $\Delta p_v/p_v = (p_{v,exp} - p_{v,calc})/p_{v,exp}$ of the experimental data from the EOS.

experimental results for this difference between vapor and sublimation pressures. We obtained the corresponding sublimation pressures from Eq. (9). Because the data determined in this way are dependent on our sublimation-pressure correlation, they were not used for fitting the new EOS. Nevertheless, all deviations between the data and calculated values are below 0.15% at temperatures down to about 263 K except for one outlier; at the two lowest temperatures (261 K and 262 K), the deviations increase up to 0.32%. The data of Kraus and Greer[61] range to slightly lower temperatures, down to 257 K, but they also exhibit considerably larger deviations of up to 1.5% and a scatter of at least 1%. Thus, the data do not allow for a reasonable uncertainty analysis of the EOS. Our uncertainty estimate for calculated vapor pressures of the subcooled liquid is consequently based on comparisons to the data of Bottomley. From the triple-point temperature down to 260 K, this uncertainty estimate is 0.5%. This estimate is conservative with regard to the deviations, but reasonable considering that the experimental uncertainty of Bottomley's data is not clearly specified and that no comparative data are available. We did not carry out comparisons between subcooled-liquid p_v data calculated from our EOS and the EOS of Hill *et al.*,[11] since numerical issues prevented us from evaluating the old EOS at temperatures below the triple point.

The isobaric heat capacity of the subcooled liquid was comprehensively investigated by Angell *et al.*[131] The work of Smirnova *et al.*[137] only includes two data points at

a maximum subcooling of about 2.5 K and is thus of little relevance for our discussion. Both datasets are limited to atmospheric pressure. Figure 35 shows that Angell's data range to extremely low temperatures, down to 240 K (about 37 K of subcooling). The authors of Ref. 131 state a reproducibility of 1%, which is not equivalent to the experimental uncertainty of the data. In the IAPWS-95 publication,[32] the uncertainty of the light-water data from the same reference is estimated to be 3%, which is consistent with the deviations between the D_2O data and our EOS (see the bottom panel of Fig. 35). In fact, down to 242 K, the maximum deviation between the data and the EOS is 3.65%. We can consequently conclude that the EOS represents the majority of the data within their estimated experimental uncertainty. Only the data point at the lowest temperature exhibits a quite large deviation of 13.8%. The reason for this is evident in the top panel of Fig. 35: the EOS overestimates the anomalous increase in c_p with decreasing temperature. The EOS of Holten *et al.*[148] is shown for comparison. Since that model is based on the existence of a liquid–liquid critical point in subcooled water, the calculated isobaric heat capacity exhibits a maximum that comes along with a change in curvature allowing for a more accurate description of Angell's data. During the development of our EOS, we did not consider any critical-like phenomena in the subcooled liquid region. However, at temperatures above 242 K, the EOS provides a quantitatively correct description of c_p in the subcooled liquid. So far no experimental evidence for the peak of c_p at lower temperatures has been published, either for H_2O or D_2O. Extrapolating the EOS of Hill *et al.*[11] to temperatures below its lower limit yields quantitatively reasonable results for the isobaric heat capacity down to 265 K (deviations from Angell's data within 6.3%). At lower temperatures, the deviations from Angell's data increase significantly with decreasing temperature. The maximum deviation is almost 62% at 240 K. Furthermore, the top panel of Fig. 35 shows that Hill's EOS does not reproduce the anomalous increase in c_p with decreasing temperature; instead, c_p becomes smaller at higher magnitudes of subcooling.

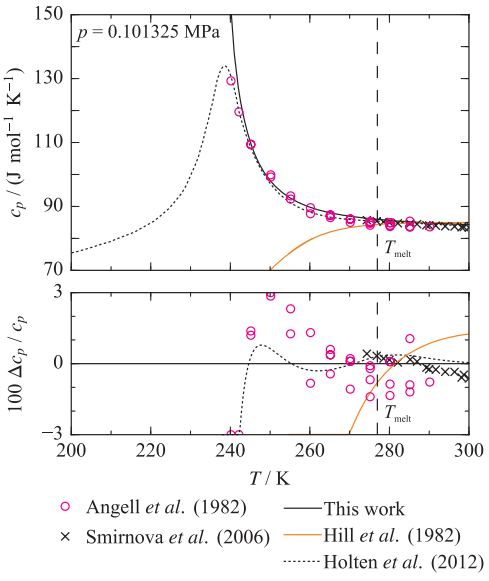

FIG. 35. Top: Isobaric heat capacity at atmospheric pressure as a function of temperature in the metastable subcooled and stable liquid region as calculated from the new EOS, the EOS of Hill *et al.*,[11] and the EOS of Holten *et al.*[148] The available experimental data are plotted for comparisons. Bottom: Relative deviations $\Delta c_p/c_p = (c_{p,\mathrm{exp}} - c_{p,\mathrm{calc}})/c_{p,\mathrm{exp}}$ of the experimental data from the new EOS. The EOS of Hill *et al.*[11] and of Holten *et al.*[148] are shown for comparisons.

For the sake of completeness, the speed-of-sound data of Conde *et al.*[119] should be mentioned. The measurements were carried out at atmospheric pressure at temperatures ranging down to 259 K. The data are only graphically presented in the corresponding publication. Personal communications with Conde clarified that the raw experimental data are no longer available. In the stable liquid region, the graphically determined data agree with the most accurate data within 0.5% (see Fig. 20). In the subcooled liquid region, the deviations increase with decreasing temperatures and reach a maximum of 3.2% at 259 K. Because no comparative data are available, we could not clarify the accuracy of either our graphical determination of the data or of the underlying experiments in the subcooled liquid. We consequently do not provide an uncertainty estimate for calculated sound speeds in this region.

5.6. Representation of physical behavior and extrapolation

One of the main targets in the development of EOS is that the final solution should not only exhibit the lowest possible deviations from the available experimental data, but also should provide a correct representation of the physical behavior of the fluid. The physical behavior of (heavy) water includes some characteristic features such as the density maximum, the sharp decrease of the second virial coefficient with decreasing temperature, and the anomalous steep slope of the isobaric heat capacity with temperature in the subcooled liquid. We already showed that the EOS accurately describes these characteristics (see Secs. 5.2, 5.3, and 5.5). As mentioned in Sec. 5.2, the density maximum also leads to a maximum speed of sound in the liquid phase. Figure 36 shows that our EOS excellently reproduces this characteristic behavior. The most accurate experimental data are included in order to highlight that the maximum sound speed in liquid (heavy) water is experimentally proven.

Figure 36 also shows the distinct minimum of the speed of sound at the critical point. In Sec. 5.4.1, we already discussed that, in theory, the speed of sound should be zero at the critical point, which cannot be reproduced by the functional form of our EOS. There are no experimental data close enough to the critical point to give such extremely low values of the speed of sound. However, Fig. 36 shows that our EOS yields a steep decrease in the sound speed in the critical region.

Comparisons between the EOS and the available pvT data in the critical region were discussed in Sec. 5.2 (see also Fig. 18). A p, ρ diagram showing the behavior of our EOS in the critical region is presented in Fig. 37. The diagram includes the phase boundaries, the rectilinear diameter, and the critical isotherm as calculated from the EOS. As required, the critical isotherm shows a horizontal inflection point at the critical point. Moreover, the rectilinear diameter (the average of saturated-liquid

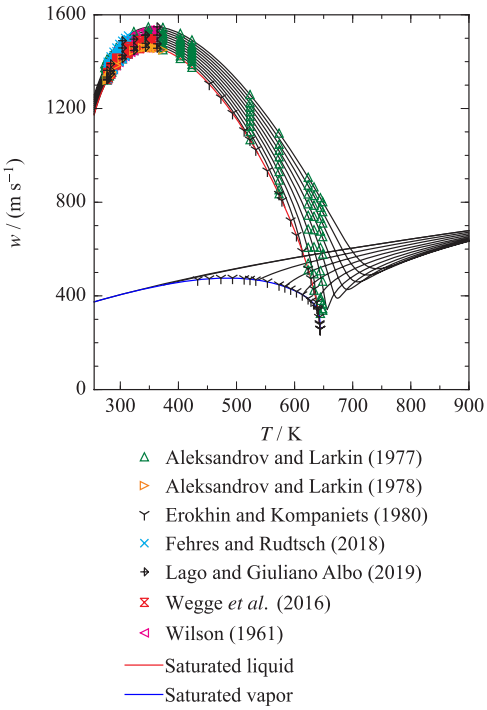

FIG. 36. Speed of sound along isobars up to 50 MPa (in steps of 5 MPa) as a function of temperature as calculated from the EOS. The most accurate experimental data are plotted for comparison.

and -vapor densities) exhibits a smooth behavior up to the critical point without any unphysical bends.

As important as the validation of the EOS within its range of validity is the evaluation of its extrapolation behavior into regions beyond the experimental data defining the range of validity. In general, this aspect is particularly important for the use of EOS in mixture models that can often access regions outside the range of validity of their pure components. However, since mixtures with heavy water are probably of low technical interest, it is more important to consider that correct extrapolation behavior also leads to a more accurate representation of state points in technically relevant regions.[29] A standard procedure to validate the extrapolation behavior of an EOS is the calculation and discussion of various diagrams showing the behavior of properties at extreme values of temperature and pressure. Figure 38 illustrates a p, ρ diagram along isotherms up to 10 000 K, which leads to pressures up to

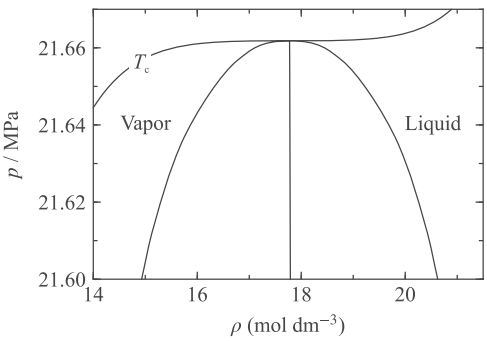

FIG. 37. Critical region in a p, ρ diagram showing the phase boundaries, the rectilinear diameter, and the critical isotherm as calculated from the EOS.

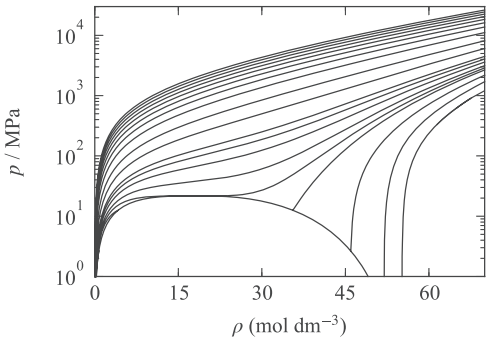

FIG. 38. p, ρ diagram along isotherms up to 10 000 K as calculated from the EOS.

about 30 GPa. The isotherms exhibit the desired converging behavior without crossing each other.

Another important criterion to judge the extrapolation behavior is the shape of the "ideal curves." These are curves along which one specific property of the real fluid is equivalent to the corresponding property of the hypothetical ideal gas at the same temperature and density.[51,149] The ideal curves are usually defined for the compressibility factor Z and its derivatives. The most commonly discussed ideal curves are the ideal curve (where $Z = 1$), the Boyle curve [where $(\partial Z/\partial \rho)_T = 0$], the Joule-Thomson inversion curve [where $(\partial Z/\partial T)_p = 0$], and the Joule inversion curve [where $(\partial Z/\partial T)_\rho = 0$]. In Fig. 39, these curves are shown in a (p/p_c) versus (T/T_c) diagram as calculated from the new EOS and the previous reference EOS of Hill *et al.*[11]

The ideal curves calculated from our EOS are smooth over the entire temperature and pressure range plotted in Fig. 39 and do not exhibit any unreasonable bumps or discontinuities. The gap between the y-axis and the Joule inversion curve occurs where this curve would theoretically intersect with the melting-pressure curve of the ice structure VII that could not be correlated for heavy water (see Sec. 3.4). The EOS of Hill *et al.*[11] does not allow for reasonable calculations of the ideal curves; these are not even qualitatively correct except for the

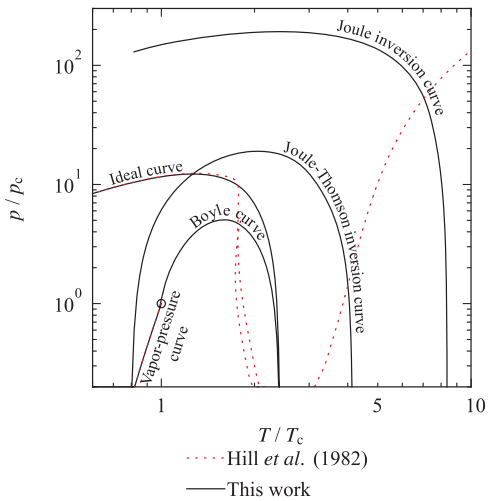

FIG. 39. Ideal curves as calculated from the new EOS and the EOS of Hill *et al.*[11]

ideal curve at low reduced temperature. This emphasizes the numerical problems of this EOS, which are among the main reasons for developing the new EOS for heavy water.

Aside from the examples shown in this section, we have carefully evaluated a large number of other property plots at technically relevant conditions as well as at extreme values of temperature, pressure, and density. We can conclude that the new EOS allows for the correct representation of the physical behavior of heavy water and that it can be extrapolated reasonably into regions beyond the experimentally investigated states.

6. Conclusions

We have developed a new fundamental EOS for heavy water (D_2O) that is explicit in the reduced Helmholtz energy. The EOS will replace the previous standard formulation of IAPWS developed by Hill *et al.*[11] in 1982. Our new EOS enables calculations of all thermodynamic properties over the whole fluid surface from the melting-pressure curve up to a temperature of 825 K at pressures up to 1200 MPa. The development of the EOS was based on a comprehensive evaluation of the available experimental data, including the most recent studies. We showed that the EOS describes the most accurate experimental results and almost all other available data within their uncertainties (see Sec. 5). Furthermore, we presented detailed uncertainty estimates for the calculated values of the most important thermophysical properties, namely, thermal saturation data (see Fig. 9), density (Fig. 13), speed of sound (Fig. 23), and isobaric heat capacity (Fig. 27). The most accurate experimental data were published for homogeneous liquid densities at atmospheric pressure from the triple-point to the normal-boiling-point temperature; the EOS represents these data with an uncertainty of 0.01%. Compared to the previous EOS of Hill *et al.*, the new EOS allows for a significantly more accurate representation of sound speeds in the liquid phase (matching the most accurate data with an expanded uncertainty between 0.015% and 0.02%), liquid densities at pressures above 100 MPa, second and third virial coefficients, and also the available experimental data in the critical region and the metastable subcooled liquid. In fact, the description of the metastable subcooled liquid was carefully fitted, although we limited the official range of validity of the EOS to temperatures above the melting-pressure curve. Considering the entire fluid surface, we showed that the EOS not only matches the experimental data but also enables a correct representation of the physical behavior of the fluid including various specific characteristics of (heavy) water. Furthermore, the EOS has a more compact and well-behaved functional form than its predecessor and can be reasonably extrapolated to extreme values of temperature and pressure.

The structure of the EOS contains an ideal-gas part that results from a newly developed correlation for the ideal-gas isobaric heat capacity. This correlation was fitted to the recent data of Simkó *et al.*[47] (see Sec. 4.1). In addition to this ideal-gas correlation, we developed auxiliary equations for the melting-pressure curves of the ice structures Ih, III, V, and VI, as well as the sublimation-pressure curve of ice Ih (see Secs. 3.4 and 3.5).

During the fitting process, we revealed some gaps in the available experimental database. If a further improved EOS were to be developed, accurate *pvT* data at pressures above 100 MPa and speed-of-sound data at pressures higher than 60 MPa would be extremely valuable. Between 300 K and 350 K, the experimental database on vapor pressures was found to be less accurate than for lower and higher temperatures. New accurate data would improve the description of vapor–liquid equilibria, which would also benefit from accurate saturated-density data that are so far not available in the literature. In general, the homogeneous vapor phase is experimentally less investigated; densities are only available at temperatures above 423 K and no data have been published for vapor-phase sound speeds. To our knowledge, no reliable experimental data are available for metastable superheated-liquid and subcooled-vapor states, although these state regions are of significant relevance for energy applications.

Our EOS has already been implemented into the software package REFPROP 10[150] of NIST and will also be available in the upcoming version 4.0 of TREND developed at RUB[151] as well as in version 6.2 of CoolProp.[152]

Acknowledgments

We thank the International Association for the Properties of Water and Steam (IAPWS) for funding Stefan Herrig's research stay at NIST, Boulder, in 2013 that began this project. Moreover, we would like to thank the members of the IAPWS working group ''Thermophysical Properties of Water and Steam'' for continuous thoughtful discussions of this work and for various other valuable contributions. We are particularly indebted to the IAPWS evaluation group of this project, namely, Hans-Joachim Kretzschmar, Matthias Kunick, Sebastian Herrmann, Vincent Holten, Michal Duška, Jan Hrubý, Rainer Feistel, and Frédéric Caupin. This work was greatly supported by Roland Span, who facilitated the research on the thermodynamic properties of D_2O at RUB. We also thank Robin Wegge and Markus Richter for many important inputs to the evaluation of the experimental data available in the literature and especially for providing extremely accurate new speed-of-sound measurements that significantly enhanced the quality of the new EOS. These measurements were also enabled by the work of Christian Scholz to whom we address our warmest thanks. The algorithms used to prepare the figures in this article result from the long-time work of Sebastian Hielscher; we highly appreciate his generous assistance while using these. Special thanks go to Christopher Tietz for taking and providing the photograph used in Fig. 1. We are grateful to Gergana Tsankova for helping with translations of many Russian publications. We also appreciate the support of Ryo Akasaka in collecting and understanding some old Japanese publications. We are very thankful for the important contributions of the following student co-workers at RUB: Tobias Neumann for setting up very useful software tools to validate the new EOS, Judith Rohde for developing preliminary correlations for the melting- and sublimation-pressure curves,

and especially Matthias Körber for editing many of the presented figures. PTB, Berlin, provided very accurate new speed-of-sound measurements prior to publication; we especially acknowledge the collaboration with Felix Fehres, who carried out these measurements. We also thank Simona Lago for sharing additional speed-of-sound data that were measured at INRiM, Turin, at the same time as this article was finalized. Finally, we would like to thank the following scientists for many essential contributions to this project as well as for their constant interest and motivation: Ian Bell, Mark McLinden, Arno Laesecke, Andreas Jäger, Theresa Eckermann, Olaf Hellmuth, Vaclav Vinš, and especially Wolfgang Wagner, who repeatedly gave important advice and generously shared his experience and comprehensive literature about the thermophysical properties of water.

Finally, we acknowledge and remember Phil Hill (1932-2016), whose thorough work on the thermodynamics of heavy water has remained useful for decades. Professor Hill, who was named an IAPWS Honorary Fellow in 1997, will be remembered in the IAPWS community not only for his excellent work but also for his kind and generous nature that made him a valued colleague.

7. References

[1]G. S. Kell, J. Phys. Chem. Ref. Data **6**, 1109 (1977).
[2]International Association for the Properties of Water and Steam, IAPWS G5-01(2016), Guideline on the Use of Fundamental Physical Constants and Basic Constants of Water, 2001.
[3]H. C. Urey, F. G. Brickwedde, and G. M. Murphy, Phys. Rev. **40**, 1 (1932).
[4]C. Waltham, e-print arXiv:physics/0206076v2 [physics.hist-ph] (2011).
[5]J. R. Dunning, G. B. Pegram, G. A. Fink, and D. P. Mitchell, Phys. Rev. **48**, 265 (1935).
[6]N. Lifson, G. B. Gordon, and R. McClintock, J. Appl. Physiol. **7**, 704 (1955).
[7]D. A. Schoeller and E. van Santen, J. Appl. Physiol. **53**, 955 (1982).
[8]R. G. Fairchild, D. N. Slatkin, J. A. Coderre, P. L. Micca, B. H. Laster, S. B. Kahl, P. Som, I. Fand, and F. Wheeler, Pigm. Cell Res. **2**, 309 (1989).
[9]G. Czakó, E. Mátyus, and A. G. Császár, J. Phys. Chem. A **113**, 11665 (2009).
[10]M. Ceriotti, W. Fang, P. G. Kusalik, R. H. McKenzie, A. Michaelides, M. A. Morales, and T. E. Markland, Chem. Rev. **116**, 7529 (2016).
[11]P. G. Hill, R. D. C. MacMillan, and V. Lee, J. Phys. Chem. Ref. Data **11**, 1 (1982).
[12]H. Preston-Thomas, Metrologia **27**, 3 (1990).
[13]International Association for the Properties of Water and Steam, IAPWS R3-84(2005), Revised Release on the IAPS Formulation 1984 for the Thermodynamic Properties of Heavy Water Substance, 2005.
[14]A. Kostrowicka Wyczalkowska, K. S. Abdulkadirova, M. A. Anisimov, and J. V. Sengers, J. Chem. Phys. **113**, 4985 (2000).
[15]International Association for the Properties of Water and Steam, IAPWS R16-17, Release on the IAPWS Formulation 2017 for the Thermodynamic Properties of Heavy Water, 2017.
[16]P. J. Mohr, D. B. Newell, and B. N. Taylor, J. Phys. Chem. Ref. Data **45**, 043102 (2016).
[17]International Association for the Properties of Water and Steam, IAPWS R2-83(1992), IAPWS Release on the Values of Temperature, Pressure and Density of Ordinary and Heavy Water Substances at their Respective Critical Points, 1992.
[18]L. Markó, G. Jákli, and G. Jancsó, J. Chem. Thermodyn. **21**, 437 (1989).
[19]G. Blank, Wärme- Stoffübertragung **2**, 53 (1969).
[20]J. M. H. Levelt Sengers, J. Straub, K. Watanabe, and P. G. Hill, J. Phys. Chem. Ref. Data **14**, 193 (1985).
[21]S. L. Rivkin and T. S. Akhundov, Teploenergetika **9**(5), 62 (1962).
[22]L. A. Guildner, D. P. Johnson, and F. E. Jones, Science **191**, 1261 (1976).
[23]W. M. Jones, J. Am. Chem. Soc. **74**, 6065 (1952).
[24]E. Bartholomé and K. Clusius, Z. Phys. Chem. **28B**, 167 (1935).
[25]E. H. Riesenfeld and T. L. Chang, Z. Phys. Chem. **30B**, 61 (1935).
[26]H. Eck, Phys. Z. **40**, 3 (1939).
[27]G. D. Oliver and J. W. Grisard, J. Am. Chem. Soc. **78**, 561 (1956).
[28]E. W. Lemmon and A. R. H. Goodwin, J. Phys. Chem. Ref. Data **29**, 1 (2000).
[29]E. W. Lemmon, M. O. McLinden, and W. Wagner, J. Chem. Eng. Data **54**, 3141 (2009).
[30]K. Gao, J. Wu, P. Zhang, and E. W. Lemmon, J. Chem. Eng. Data **61**, 2859 (2016).
[31]W. Wagner, A. Saul, and A. Pruß, J. Phys. Chem. Ref. Data **23**, 515 (1994).
[32]W. Wagner and A. Pruß, J. Phys. Chem. Ref. Data **31**, 387 (2002).
[33]W. Wagner, T. Riethmann, R. Feistel, and A. H. Harvey, J. Phys. Chem. Ref. Data **40**, 043103 (2011).
[34]P. W. Bridgman, J. Chem. Phys. **3**, 597 (1935).
[35]S. J. Henderson and R. J. Speedy, J. Phys. Chem. **91**, 3069 (1987).
[36]P. W. Bridgman, Proc. Am. Acad. Arts Sci. **47**, 347 (1911).
[37]G. F. Molinar, V. Bean, J. Houck, and B. Welch, Metrologia **16**, 21 (1980).
[38]E. A. Long and J. D. Kemp, J. Am. Chem. Soc. **58**, 1829 (1936).
[39]J. Timmermans, M. Hennaut-Roland, and D. Rozental, C. R. Acad. Sci. **202**, 1061 (1936).
[40]J. D. Pupezin, G. Jákli, G. Jancsó, and W. A. Van Hook, J. Phys. Chem. **76**, 743 (1972).
[41]G. A. Bottomley, Aust. J. Chem. **31**, 1177 (1978).
[42]K. Niwa and E. Shimazaki, J. Chem. Soc. Jpn. **60**, 985 (1939).
[43]G. Jancsó, J. Pupezin, and W. A. Van Hook, J. Phys. Chem. **74**, 2984 (1970).
[44]International Association for the Properties of Water and Steam, IAPWS R14-08(2011), Revised Release on the Pressure along the Melting and Sublimation Curves of Ordinary Water Substance, 2011.
[45]E. W. Lemmon and R. T. Jacobsen, J. Phys. Chem. Ref. Data **34**, 69 (2005).
[46]M. Thol and E. W. Lemmon, Int. J. Thermophys. **37**, 28 (2016).
[47]I. Simkó, T. Furtenbacher, J. Hrubý, N. F. Zobov, O. L. Polyansky, J. Tennyson, R. R. Gamache, T. Szidarovszky, N. Dénes, and A. G. Császár, J. Phys. Chem. Ref. Data **46**, 023104 (2017).
[48]T. Furtenbacher, T. Szidarovszky, J. Hrubý, A. A. Kyuberis, N. F. Zobov, O. L. Polyansky, J. Tennyson, and A. G. Császár, J. Phys. Chem. Ref. Data **45**, 043104 (2016).
[49]A. S. Friedman and L. Haar, J. Chem. Phys. **22**, 2051 (1954).
[50]J. M. L. Martin, J. P. François, and R. Gijbels, J. Chem. Phys. **96**, 7633 (1992).
[51]R. Span, *Multiparameter Equations of State: An Accurate Source of Thermodynamic Property Data* (Springer, Berlin, 2000).
[52]R. Span and W. Wagner, J. Phys. Chem. Ref. Data **25**, 1509 (1996).
[53]R. Span, E. W. Lemmon, R. T. Jacobsen, W. Wagner, and A. Yokozeki, J. Phys. Chem. Ref. Data **29**, 1361 (2000).
[54]L. Besley and G. A. Bottomley, J. Chem. Thermodyn. **5**, 397 (1973).
[55]H. I. Erokhin and B. H. Kompaniets, Teplofiz. Vys. Temp. **18**, 1172 (1980).
[56]G. Jákli and H. Illy, *Vapour Pressure Isotope Effect of the Equimolar H_2O-D_2O Mixture* (Hungarian Academy of Sciences, Budapest, Hungary, 1980).
[57]G. Jákli and L. Markó, ACH Models Chem. **132**, 226 (1995).
[58]G. Jákli and W. A. Van Hook, J. Chem. Eng. Data **26**, 243 (1981).
[59]W. M. Jones, J. Chem. Phys. **48**, 207 (1968).
[60]V. A. Kirillin and S. A. Ulybin, Teploenergetika **8**(4), 67 (1959).
[61]G. F. Kraus and S. C. Greer, J. Phys. Chem. **88**, 4781 (1984).
[62]G. N. Lewis and R. T. MacDonald, J. Am. Chem. Soc. **55**, 3057 (1933).
[63]C.-T. Liu and W. T. Lindsay, J. Chem. Eng. Data **15**, 510 (1970).
[64]F. T. Miles and A. W. C. Menzies, J. Am. Chem. Soc. **58**, 1067 (1936).
[65]K. Quitzsch, R. Hüttig, H.-G. Vogel, H.-J. Gesemann, and G. Geiseler, Z. Phys. Chem. **223O**, 225 (1963).
[66]K. Zieborak, Z. Phys. Chem. **231O**, 248 (1966).
[67]J. M. Costello and S. T. Bowden, Recl. Trav. Chim. Pays-Bas **77**, 32 (1958).
[68]U. Grossmann-Doerth, Z. Naturforsch., A **10**, 799 (1955).
[69]U. Grossmann-Doerth, Z. Naturforsch., A **11**, 254 (1956).
[70]G. M. Hebert, H. F. McDuffie, and C. H. Secoy, J. Phys. Chem. **62**, 431 (1958).
[71]B. A. Mursalov, I. M. Abdulagatov, V. I. Dvoryanchikov, A. N. Kamalov, and S. B. Kiselev, Int. J. Thermophys. **20**, 1497 (1999).
[72]A. H. Harvey and E. W. Lemmon, J. Phys. Chem. Ref. Data **31**, 173 (2002).

[73]International Association for the Properties of Water and Steam, IAPWS R6-95(2016), Revised Release on the IAPWS Formulation 1995 for the Thermodynamic Properties of Ordinary Water Substance for General and Scientific Use, 2016.
[74]N. S. Osborne and C. H. Meyers, J. Res. Natl. Bur. Stand. **13**, 1 (1934).
[75]A. A. Aleksandrov, T. S. Khasanshin, and D. K. Larkin, *Specific Volumes of Ordinary and Heavy Water at High Pressures and Temperatures*, Report to Working Group I (IAPS, 1976).
[76]A. A. Aleksandrov, T. S. Khasanshin, and D. K. Larkin, Zh. Fiz. Khim. **50**, 394 (1976).
[77]M. Ceccaldi, G. Girard, M. Menaché, and M. Riedinger, Metrologia **11**, 53 (1975).
[78]T.-L. Chang and L.-H. Tung, Nature **163**, 737 (1949).
[79]M. Duška, J. Hykl, P. Peukert, A. Blahut, V. Vinš, and J. Hrubý, "Relative density and isobaric expansivity of cold and supercooled heavy water from 254 to 298 K and up to 100 MPa," (to be published).
[80]R. T. Emmet and F. J. Millero, J. Chem. Eng. Data **20**, 351 (1975).
[81]D. E. Hare and C. M. Sorensen, J. Chem. Phys. **84**, 5085 (1986).
[82]E. V. Ivanov and E. Y. Lebedeva, J. Mol. Liq. **159**, 124 (2011).
[83]E. V. Ivanov, E. Y. Lebedeva, and V. K. Abrosimov, Thermochim. Acta **500**, 38 (2010).
[84]E. V. Ivanov, E. Y. Lebedeva, and V. K. Abrosimov, Thermochim. Acta **513**, 26 (2011).
[85]G. Jancsó, J. Solution Chem. **35**, 991 (2006).
[86]J. Jůza, V. Kmoníček, O. Šifner, and K. Schovanec, Physica **32**, 362 (1966).
[87]H. Kanno and C. A. Angell, J. Chem. Phys. **73**, 1940 (1980).
[88]G. S. Kell, G. E. McLaurin, and E. Whalley, Philos. Trans. R. Soc., A **315**, 247 (1985).
[89]G. S. Kell, G. E. McLaurin, and E. Whalley, Philos. Trans. R. Soc., A **425**, 49 (1989).
[90]S. G. Kudryavtsev, A. N. Strakhov, O. V. Ershova, and G. A. Krestov, Zh. Fiz. Khim. **60**, 2202 (1986).
[91]W. Marczak, J. Chem. Eng. Data **44**, 621 (1999).
[92]F. J. Millero, R. Dexter, and E. Hoff, J. Chem. Eng. Data **16**, 85 (1971).
[93]N. A. Nevolina and A. L. Seifer, J. Struct. Chem. **14**, 501 (1973).
[94]D. H. Rasmussen and A. P. MacKenzie, J. Chem. Phys. **59**, 5003 (1973).
[95]E. Reisler and H. Eisenberg, J. Chem. Phys. **43**, 3875 (1965).
[96]P. Scharlin and K. Steinby, J. Chem. Thermodyn. **35**, 279 (2003).
[97]R. Schrader and K. Wirtz, Z. Naturforsch., A **6**, 220 (1951).
[98]F. Steckel and S. Szapiro, Trans. Faraday Soc. **59**, 331 (1963).
[99]K. Stokland, E. RonŁss, and L. Tronstad, Trans. Faraday Soc. **35**, 312 (1939).
[100]N. V. Tsederberg, A. A. Aleksandrov, and T. S. Khasanshin, Therm. Eng. **19**(10), 96 (1972).
[101]N. V. Tsederberg, A. A. Aleksandrov, T. S. Khasanshin, and D. K. Larkin, Therm. Eng. **20**(8), 17 (1973).
[102]B. V. Zheleznyi, Russ. J. Phys. Chem. **41**, 1311 (1969).
[103]T. L. Chang and J. Y. Chien, J. Am. Chem. Soc. **63**, 1709 (1941).
[104]K. Wirtz, Phys. Z. **43**, 465 (1942).
[105]G. S. Kell and E. Whalley, Philos. Trans. R. Soc., A **258**, 565 (1965).
[106]G. S. Kell, G. E. McLaurin, and E. Whalley, Philos. Trans. R. Soc., A **360**, 389 (1978).
[107]G. S. Kell, G. E. McLaurin, and E. Whalley, J. Chem. Phys. **48**, 3805 (1968).
[108]M. Tanaka, G. Girard, R. Davis, A. Peuto, and N. Bignell, Metrologia **38**, 301 (2001).
[109]T. Takéuchi and T. Inai, Jpn. J. Phys. **11**, 67 (1936).
[110]A. A. Aleksandrov, D. K. Larkin, A. B. Matveev, and Z. A. Ershova, Izv. Vyss. Ucheb. Zaved. Energ. **11**, 84 (1977).
[111]G. S. Kell, G. E. McLaurin, and E. Whalley, Philos. Trans. R. Soc., A **315**, 235 (1985).
[112]G. Garberoglio, P. Jankowski, K. Szalewicz, and A. H. Harvey, "Fully quantum calculation of the second and third virial coefficients of water and its isotopologues from *ab initio* potentials," Faraday Discuss (to be published).
[113]G. S. Kell, G. E. McLaurin, and E. Whalley, J. Chem. Phys. **49**, 2839 (1968).
[114]P. Jankowski, G. Murdachaew, R. Bukowski, O. Akin-Ojo, C. Leforestier, and K. Szalewicz, J. Phys. Chem. A **119**, 2940 (2015).
[115]U. Góra, W. Cencek, R. Podeszwa, A. van der Avoid, and K. Szalewicz, J. Chem. Phys. **140**, 194101 (2014).
[116]A. A. Aleksandrov and D. K. Larkin, Teploenergetika **24**(1), 73 (1977).
[117]A. A. Aleksandrov and D. K. Larkin, Inzh.-Fiz. Zh. **34**, 110 (1978).
[118]C.-T. A. Chen and F. J. Millero, J. Acoust. Soc. Am. **62**, 553 (1977).
[119]O. Conde, J. Teixeira, and P. Papon, J. Chem. Phys. **76**, 3747 (1982).
[120]V. N. Evstefeev, V. P. Skripov, and V. N. Chukanov, High Temp. **17**, 252 (1979).
[121]F. Fehres and S. Rudtsch (personal communication, 2018).
[122]R. A. Fine and F. J. Millero, J. Chem. Phys. **63**, 89 (1975).
[123]R. N. Gupta, P. C. Jain, and V. S. Nanda, J. Chem. Thermodyn. **8**, 627 (1976).
[124]P.-P. Heusinger, Naturwissenschaften **36**, 279 (1949).
[125]E. V. Ivanov, E. Y. Lebedeva, and V. K. Abrosimov, J. Chem. Eng. Data **54**, 2777 (2009).
[126]S. Lago and P. A. Giuliano Albo, "Speed of sound measurements in deuterium oxide (D_2O) at temperatures between (276.97 and 363.15) K and at pressures up to 210 MPa" (to be published).
[127]D. R. McMillan and R. T. Lagemann, J. Acoust. Soc. Am. **19**, 956 (1947).
[128]M. Pancholy, J. Acoust. Soc. Am. **25**, 1003 (1953).
[129]R. Wegge, M. Richter, and R. Span, Fluid Phase Equilib. **418**, 175 (2016).
[130]W. D. Wilson, J. Acoust. Soc. Am. **33**, 314 (1961).
[131]C. A. Angell, W. J. Sichina, and M. Oguni, J. Phys. Chem. **86**, 998 (1982).
[132]A. Eucken and M. Eigen, Z. Elektrochem. Angew. Phys. Chem. **55**, 343 (1951).
[133]S. L. Rivkin and B. N. Egorov, At. Energy **7**, 462 (1959).
[134]S. L. Rivkin and B. N. Egorov, Teploenergetika **9**(12), 60 (1962).
[135]S. L. Rivkin and B. N. Egorov, Teploenergetika **10**(7), 75 (1963).
[136]S. L. Rivkin and B. N. Egorov, At. Energy **14**, 416 (1963).
[137]N. N. Smirnova, T. A. Bykova, K. van Durme, and B. van Mele, J. Chem. Thermodyn. **38**, 879 (2006).
[138]K. I. Amirkhanov, G. V. Stepanov, B. A. Mursalov, and O. A. Bui, Teploenergetika **22**(4), 90 (1975).
[139]N. G. Polikhronidi, I. M. Abdulagatov, J. W. Magee, and G. V. Stepanov, Int. J. Thermophys. **23**, 745 (2002).
[140]S. L. Rivkin and B. N. Egorov, Sov. J. At. Energy **7**, 928 (1961).
[141]S. L. Rivkin and B. N. Egorov, Sov. J. At. Energy **14**, 430 (1964).
[142]N. G. Polikhronidi, I. M. Abdulagatov, J. W. Magee, and G. V. Stepanov, Int. J. Thermophys. **22**, 189 (2001).
[143]S. Ertle, Ph.D. thesis, TU München, 1979.
[144]W. D. Wilson, J. Acoust. Soc. Am. **31**, 1067 (1959).
[145]K. I. Amirkhanov, G. V. Stepanov, and B. G. Alibekov, *Isochoric Heat Capacity of Water and Steam* (Akademii Nauk SSSR, Dagestanskii Filial, Makhachkala, Dagestan, 1969).
[146]V. Holten, J. V. Sengers, and M. A. Anisimov, J. Phys. Chem. Ref. Data **43**, 043101 (2014).
[147]International Association for the Properties of Water and Steam, IAPWS G12-15, Guideline on Thermodynamic Properties of Supercooled Water, 2015.
[148]V. Holten, C. E. Bertrand, M. A. Anisimov, and J. V. Sengers, J. Chem. Phys. **136**, 094507 (2012).
[149]E. H. Brown, Annexe Bull. Inst. Int. Froid. **1**, 169 (1960).
[150]E. W. Lemmon, I. H. Bell, M. L. Huber, and M. O. McLinden, *NIST Standard Reference Database 23: Reference Fluid Thermodynamic and Transport Properties-REFPROP, Version 10.0* (National Institute of Standards and Technology, Standard Reference Data Program, Gaithersburg, 2018).
[151]R. Span, R. Beckmüller, T. Eckermann, S. Herrig, S. Hielscher, A. Jäger, T. Neumann, S. Pohl, B. Semrau, and M. Thol, TREND. Thermodynamic Reference and Engineering Data 4.0 (Lehrstuhl für Thermodynamik, Ruhr-Universität Bochum, Bochum, Germany) (to be published).
[152]I. H. Bell, J. Wronski, S. Quoilin, and V. Lemort, Ind. Eng. Chem. Res. **53**, 2498 (2014).